Batch and Flow Synthesis of Inorganic Nanoparticles and Organic Particles

Thesis Submitted to AcSIR

For the Degree of

DOCTOR OF PHILOSOPHY

In Chemical Sciences

AcSIR

By

Arun Vilas Nikam

10CC12J26015

Under guidance of

Dr. Amol A. Kulkarni

and

Dr. B. L. V. Prasad

CSIR-National Chemical Laboratory, Pune-411008, India.

CERTIFICATE

This is to certify that the work incorporated in this Ph.D. thesis entitled **"Batch and Flow Synthesis of Inorganic Nanoparticles and Organic Particles"** submitted by **Mr. Arun Vilas Nikam** to Academy of Scientific and Innovative Research (AcSIR) in fulfillment of the requirements for the award of the degree of **Doctor of Philosophy**, in **Chemical Sciences**, embodies original research work under my supervision. I further certify that this work has not been submitted to any other University or Institution in part or full for the award of any degree or diploma. Research material obtained from other sources has been duly acknowledged in the thesis. Any text, illustration, table etc., used in the thesis from other sources, have been duly cited and acknowledged.

Arun Vilas Nikam

(Student)

Dr. Amol A. Kulkarni

(Supervisor)

Dr. B. L. V. Prasad

(Co-Supervisor)

Declaration

I hereby declare that all experiments embodies in this thesis entitled **"Batch and Flow synthesis of Inorganic Nanoparticles and Organic Particles"** submitted for degree of Doctor of Philosophy in Chemical Sciences, to the Academy of Scientific and Innovative Research, Chennai has been carried out by me at Chemical Engineering & Process Development and Physical & Material Chemistry Divisions, CSIR-National Chemical Laboratory, Pune, India, under guidance of Dr. Amol Kulkarni and co-guidance of Dr. B. L. V. Prasad. Such material as has been obtained by other sources fully acknowledge in this thesis. The work is original and has not been submitted in part or fully by me, for any degree or diploma to this or to any other university.

Date: 29 December 2017

Place: Pune

(Arun Vilas Nikam)

Acknowledgements

I would like to take this opportunity to express my gratitude to some of the people to whom I met at CSIR-NCL, without their help and contribution this work would be highly impossible. First of all, I express my sincere thanks to Dr. Amol Kulkarni and Dr. B. L. V. Prasad for their guidance, encouragement, valuable discussion and patience. I cannot imagine the fate of this thesis without their contribution. They gave me enough freedom to express my views whether they are right or wrong. I am grateful to Prasad sir for his encouragement and enthusiastic discussions. I am very much thankful to Amol sir for bearing me and for his patience to correct my poor written English.

I am thankful to Director of CSIR-NCL, Prof. Ashwini Kumar Nangia, Ex-Head of CEPD Dr. V. V. Ranade for giving me an opportunity to work with CSIR-NCL. I like to thank my DAC members Dr. Nandini Devi, Dr. Sakya Sen, Dr. Sayam Sengupta and Director Nominee Dr. C. J. Gadgil for attending my seminar with patience and for giving valuable suggestions. I am thankful to Council of Scientific and Industrial Research (CSIR, New Delhi) for financial assistance.

I am thankful to Dr. Arulraj, Dr. Vijay Chaudhari and Arun Dadwal for valuable discussion and helping me in application part. I would like to thank Dr. K. Krishnamoorthy, Dr. C. V. Ramana and Dr. P. A. Joy. I am thankful to Technicians of CMC for their contribution to get good quality data. My special thanks to all the lab member, Pravin, Yachita, Sayan, Jaydeep, Gunwant, Mrityunjay, Chinmay, Sourabh, Dr. Atul, Rajashri, Roopashree, Prachi, Jayesh, Poulomi, Abhijit, Shankar, Arivazhagan, Jayshigh, Ketan, PM Jadhav, and Ranjit. I am thankful to past members of lab Dr. Vilas, Dr. Ravi, Dr. Balanagulu, Dr.

Abstract

An explosive growth of nanotechnology innovates existing market products due to outstanding properties of nanomaterial. Nanomaterial has been significantly contributing to cutting-edge nanotechnology which invokes scientist to increase competency for the synthesis of nanomaterials. Strict control over quality (size, shape, phase, and composition) of nanomaterial is prerequisite for any nanotechnology-based application. Surface structures, phase, shape, and size of nanoparticles are the key aspects to get the targeted properties. In this direction, wet chemical synthesis protocols have made significant progress to obtain size and shape selective nanomaterial due to its simple and modular nature. Wet chemical synthesis has provision to tune reaction parameters that offers great control over structure of nanomaterials. These reactions are conducted in a batch reactor, typically, in a flask or a glass vial under magnetic stirring and produce few milligrams and milliliters of nanodispersion. Scaling the batch processes to obtain nanomaterial in large quantity and at high production rate suffers from the limitation of inhomogeneous mass and heat transfer which affects the selectivity of nanoparticles. Discontinuities in batch operations lead to low production rate. Continuous flow synthesis is enabling approach to overcome difficulties associated with scale-up of synthesis of nanomaterials. In continuous flow synthesis, controlled and homogeneous mixing could be achieved by controlling addition rate, using micromixer, microreactors, impellers, and applying an external force such as ultrasound, piezo-electric and magnetic forces, etc. To overcome heat transfer limitation, microreactor has been used because of high surface to volume ratios, the heat transfer is faster in microchannels. Microwave heating is another alternative to conventional heating to achieve homogeneous volumetric heating of the reaction solution.

Microwave heating has been used for rapid homogeneous heating which reduces reaction time and helps in increasing production rate and yield of nanomaterials. The production capacity of flow process could be further enhanced by the integration of microwave with flow process having control over size, shape, and phase and composition of nanomaterials. Ultrafine organic or APIs particles have been obtained using such integrated system of flow and ultrasound by enhancing micromixing. In this thesis, semiconducting copper oxide nanoparticles have been synthesized in continuous microwave assisted synthesis to increase production rate. On other hand, reports on continuous microwave-assisted flow synthesis of the bimetallic nanoparticle is rather scares hence, scale-up of bimetallic nanoparticles using microwave-assisted flow synthesis has been paid much attention in this thesis. In case organic nanoparticles, integration flow, and ultrasound has been realized to prepare small size metformin hydrochloride particles

The thesis has divided into six chapters.

Chapter 1: Introduction

This chapter explains about i) current scenario of applications of nanomaterials and demand for nanomaterials in global market ii) different classes of nanomaterials iii) advantages of flow process over batch process iv) impact of integration of flow process with microwave and ultrasound for the synthesis of inorganic nanoparticles and ultrafine organic particles in a large quantity.

Chapter 2: Microwave-Assisted Batch and Flow Synthesis of CuO and Cu_2O Nanoparticles

A single-step protocol to prepare Cu_2O and CuO nanocrystalline particles from the same precursor by microwave irradiation has been developed using the pH of the solution as the only variable parameter. Effect of variation in reaction parameters in the batch process has

been studied to obtain smaller size (~3.6 nm) CuO nanoparticles. Batch parameters have been considered to adopt continuous microwave-assisted flow synthesis of CuO nanoparticles. Production rate for flow synthesis of CuO nanoparticles is 61 g/ day. The utility of different bivalent Cu-precursors for the synthesis of CuO and Cu_2O nanoparticles was also investigated. Field effect transistors based on CuO nanoparticles showed a hole mobility of 3.5×10^{-2} cm^2 V^{-1} s^{-1}, making them a suitable candidate for sensing applications. The effect of hydrazine vapor exposure on CuO nanoparticles was also investigated. This revealed a decrease in source current with respect to time. Particularly, CuO nanoparticles showed 9% thermal conductivity enhancement at 4% volume fraction of CuO nanoparticles in ethylene glycol as the base fluid.

Chapter 3: Batch and Flow Synthesis of Palladium Supported Nickel Nanoparticles

Palladium nanoparticles supported on nickel nanoparticles (Pd/Ni) were synthesized in a continuous flow manner by the microwave-assisted method in the presence and absence of oleylamine. Parameters optimized for batch experiments were considered while performing continuous flow synthesis. The Pd/Ni nanoparticles synthesized in the presence of oleylamine displayed good catalytic activity for hydrogenation of aromatic nitro compounds, and those bearing alkene and alkyne moieties. The ferromagnetic character of the supporting nickel nanoparticles allowed the recovery of the catalyst, and these recovered catalysts could be reused several times.

Chapter 4: Batch and Flow Synthesis of NiPt Alloy Nanoparticles

NiPt alloy nanoparticles were prepared in shorter reaction time than conventional heating method. The composition of NiPt alloy nanoparticles was systematically tuned by the varying initial molar concentration of Ni-precursor and Pt-precursor in a batch. Batch

parameters were extended for flow synthesis to attain high production rate (140 mg/h). 20 wt % loading of NiPt on carbon was tested for electrocatalytic hydrogen evolution reaction. $Ni_{50}Pt_{50}/C$ electro-catalyst showed (1571 mA/cm^2) highest efficiency for hydrogen evolution reaction than the $Ni_{96}Pt_{04}/C$, $Ni_{83}Pt_{17}/C$, and commercial Pt/C catalyst.

Chapter 5: Batch and Continuous Flow Precipitation of Organic Particles

Formation of small-sized metformin hydrochloride particles is an important for preparing the formulations in the pharmaceutical industry. Small sized metformin hydrochloride particles can be obtained using reprecipitation method. Effect of solute concentration, antisolvent/solvent ratio, the temperature of antisolvent has been investigated to attain a higher degree of supersaturation to obtain small sized metformin particles. Optimized batch process parameters have been extended for continuous flow process. Rapid mixing of antisolvent and solvent was facilitated by using inverted impinging jet reactor and ultrasound in a continuous flow process. Efficient mixing in the inverted impinging jet reactor produces small size (15 μm) metformin hydrochloride particles.

Chapter 6: Conclusions

In this chapter, we have summarized work described in the previous chapter. Highlights and achievement of work are presented in terms development of flow process for material processing.

Table of Contents

List of Figures

List of Tables

Chapter 1

Introduction

1.1 Introduction

In the 21st century, word "NANO" has become familiar to common people. Materials having any one dimension within 1-100 nm range is known as nanomaterial and in such a form it exhibits properties different than their basic building (atoms or molecules) units and bulk counterparts owing to their surface and quantum effect.[1] The properties of nanomaterials are highly sensitive to its dimensions and morphology[2]. Hence, application of nanomaterial is driven by its property resulting from dimension, morphology, and structure. Table 1.1 shows property driven applications of the nanomaterials.

Table 1.1: Property driven applications of the nanomaterials.

Nanomaterials	Properties	Applications
Ag nanocubes	Electronic (Enhanced Raman signal)	Detection[3]
PtNi nano-octahedra	Surface (Structural changes)	Catalysis[4]
Iron oxide Nanoparticles	Magnetic (Superparamagnetic)	Biomedical[5]
B-carotene Nanoparticles	Physical (Dissolution rate)	Animal fodder[6]
Copper oxide Nanoparticles	Electronic (Charge transport)	Sensors[7]
Ni@Pd core-shell Nanoparticles	Surface (Structural changes)	Catalysis[8]

Due to unique properties of nanomaterials, it is being used in consumer products and becomes a daily part of everyone's life. Hence, the nanomaterial becomes important commodities in a global market. Nanomaterials cover a broad spectrum of materials involving inorganic metal and metal oxide nanomaterials, carbon-based nanomaterials,

polymeric particulate materials and organic materials. Nanomaterials have influenced many areas such as healthcare, sporting goods, cosmetics and personal care, automotive, food and beverage, home and garden, coatings in numerous sectors, lubricants and consumer electronics.[9] This makes the nanomaterial industry fall in multi-billion dollar category with continuous growth. Many million tons of nanomaterial are produced every year to meet the industrial requirement. One can easily see future of nanotechnology and predict requirement nanomaterial. Figure 1.1 shows the demand for nanomaterial would be 5 million tons by 2025 from 2014 when the production of nanomaterials was less than 1 million tons.[10] Due to growing demand for nanomaterial, there is need to produce nanomaterial in large quantity which needs to satisfied by scaling-up synthesis of nanomaterial without losing the quality of nanomaterial in term shape, size, and composition. In this thesis, we are focusing on exploring the nanomaterial synthesis methods that can be translated for large scale production to meet industrial requirements.
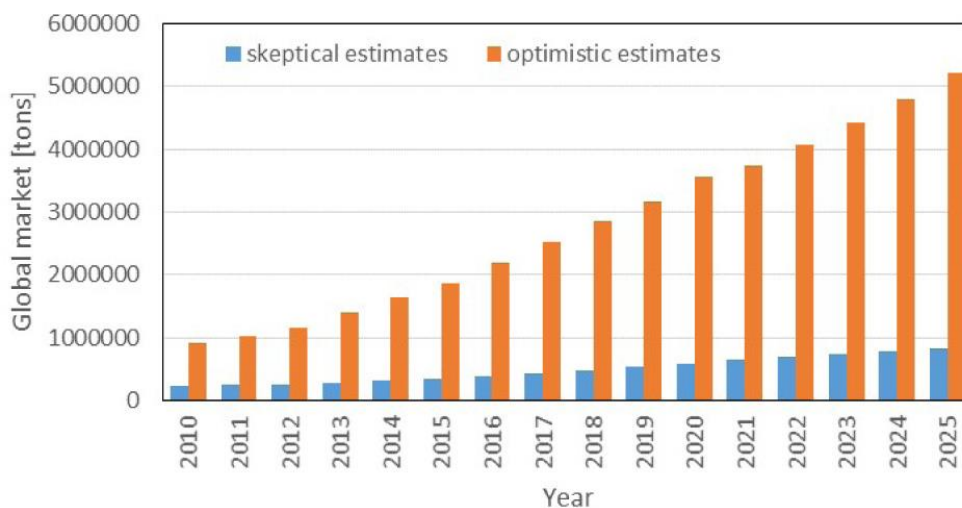
Figure 1.1: The global market for nanomaterials (Image is taken from ref. 9).

1.2 Classification of nanomaterials

Nanomaterials can be classified as inorganic nanomaterial or macromolecular nanomaterial or low molecular weight organic nano-material based on their chemical composition (see Figure 1.2).
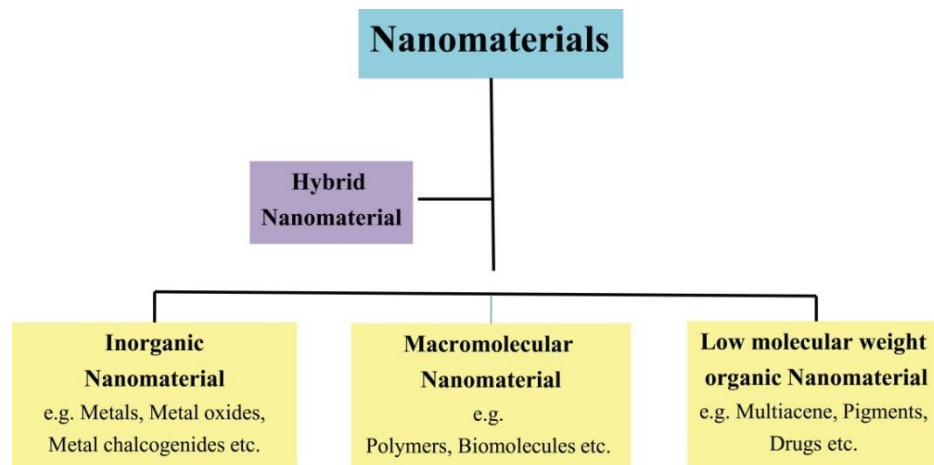
Figure 1.2: Classification of nanomaterial-based on basic building units.

Inorganic nanomaterials involving metallic nanoparticles, metal oxides nanoparticles, metal chalcogenides nanoparticles, etc. are widely pursued. Inorganic nanomaterials formed due to the arrangement of ions and atoms in the extended crystal lattice that can be confined in nanoscale dimensions.[11] Examples of inorganic nanomaterials include nanoparticles such as Au nanoparticles, Ag nanoparticles, Ni nanoparticles, Pt nanoparticles, Pd nanoparticles, iron oxide nanoparticles, cobalt oxide nanoparticles, copper oxide nanoparticles, CdS nanoparticles, and PdSe nanoparticles, etc. On the other hand, macromolecular and organic nanoparticles that include polymers, bio-molecules, drugs, graphene, dendrimers, etc. have been investigated extensively during the past decade. In a polymeric and organic nanomaterials, molecules are arranged

together due to non-covalent interactions such as π-π stacking, hydrogen bonding, van der Waals and electrostatic interaction.[12] Examples of polymeric and organic nanomaterials are polystyrene,[13] polypyrrole,[14] polyaniline,[15] polythiazide, ibuprofen, glyburide, artemisinin,[16] quinacridone,[17] etc.

1.3 Wet chemical synthesis:

Synthesis of nanomaterial needs a different level of expertise to have control over size, shape, and composition. The various method has been invented to produce nanomaterial in a controlled manner since 1980's. Wet chemical synthesis is simplest, modular and scalable method to obtain desire nanomaterial compared wet milling, laser ablation, chemical vapor deposition, and lithography. Wet chemical synthesis does not need any expensive instrumentation or extremely high temperature, and pressure condition. One can easily control size and shape of the nanomaterial by tuning reaction parameters such temperature, concentration, addition rate and sequence of reagents and pH.[18, 19] The wet chemical method includes various approaches such as reduction, precipitation, sol-gel, reverse micelle, thermal decomposition, hydrothermal or solvothermal, and microwave-assisted method.[20] Typically, the wet chemical synthesis of nanomaterial conducted in a batch reactor (reaction flask, see Figure 1.3) and it involves metal precursors with precipitating/reducing agent and ligands, all are heated in a solvent with constant stirring, which produces nanoparticles in the reaction solution (see Figure 1.3). After washing and drying of the product produced in the batch reactor, ends up with 5-50 mg quantity of nanomaterial.[21, 22]

Metal Precursors +
Reducing / Precipitating agent
+ Ligand

Solvent

Metal/ Metal Oxide /
Metal Chalcogenide Nanoparticles
Each batch ~ 5-25 mg
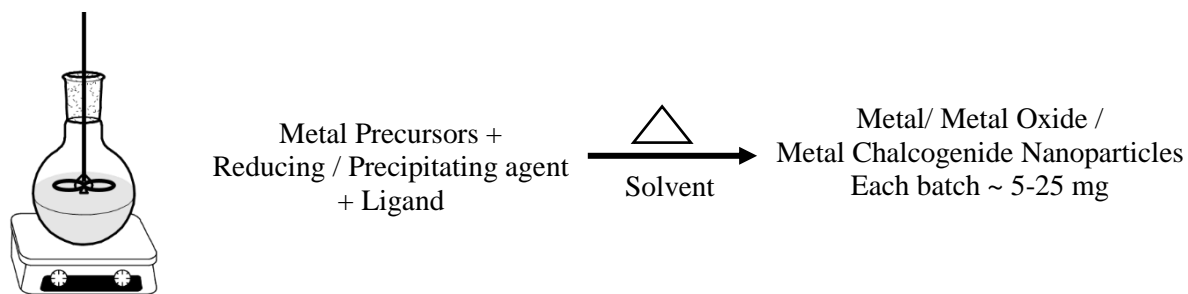
Figure 1.3: Schematics of typical wet chemical synthesis of nanoparticles in a batch reactor.

As mentioned in an earlier section that 5 million tons nanomaterial required by 2025. Hence, satisfying current requirements of nanomaterial by using batch synthesis is quite challenging. Various options have been tried to synthesize nanomaterial in huge volume viz. i) conducting the synthesis in multiple batches, ii) increase reaction volume and iii) conducting the synthesis using continuous flow method. Generally, for the sake of simplicity more quantities of nanomaterials can be synthesized by repeating it in multiple batches or increase the reaction volume. Various efforts have been made for scalable synthesis of mono-disperse nanoparticles in batch. Very few attempts for scale-up using batch reactor were successfully able to maintain the quality of nanomaterial. Park et al. demonstrated thermal decomposition method to synthesize 40 g of monodisperse iron oxide nanoparticles in a single batch.[23] Klinkova et al. developed a highly reproducible synthesis of Pd, Pt, and Ag nanoparticles which produced 350 mg of nanoparticles with great control over size and shape.[24] On the other hand, continuous flow synthesis nanoparticles are attracting tremendous attention due to high through put and highly reproducible. Khan et al. reported the synthesis of monodisperse Pd nanoparticles using segmented flow with the volumetric productivity of 10 L/day.[25] One

can increase production of nanomaterials using wet chemical synthesis to obtain size and shape controlled nanoparticles in batch and flow.

1.4 Batch and flow synthesis of nanoparticles

In general, nanoparticles are prepared in a batch mode which produces 5-50 mg of nanoparticles in a single batch operation. Reproducibility of size and shape of nanoparticles in batch operation is a very difficult task due to batch to batch variation in product quality.[26] Scale-up of batch process involves the use of the large volume of reactor and which has their drawbacks. Although efforts have been taken to produce nanoparticles in grams scale using batch mode, it could not maintain the quality of nanoparticles when reaction volume is increased. One can easily notice that for scale-up of such reactions, mixing and heat management play vital role in deciding conversion, selectivity, yield and quality of the product. Typically, in lab scale operation, mixing is achieved using magnetic bar in the small size of the batch reactor. When such reaction scaled up to 100 times, achieving uniform mixing at large volume is becoming a difficult task. To process large volume, mixing can be carried out by mechanical agitation using impellers but uniform mixing throughout such large-scale synthesis can be expected and the variation in mixing increase with an increase in batch volumes.[27] If in such scale-up attempt in a batch is unsuccessful, consequences are chemical wastage, loss of efforts, and time. On the other hand, increase in batch volume also inhibits homogeneous heat distribution through the reactor. In case of synthesis of nanoparticles, inhomogeneous mixing and heating lead to variation in local nucleation and growth rate which cause variation in size and shape of nanoparticles. Most of the nanoparticle-based applications

are driven by size and shape of nanoparticles. Hence, increasing batch volume cannot be always a reliable practice to obtain consistent product at large scale.

However, continuous flow processes are a more reliable approach than the batch processes as it gives reproducible results due to controlled addition of reagents and the reaction conditions. It is becoming popular and has potential to produce nanomaterials in large quantity to fulfil the industrial requirement. Flow synthesis has an added advantage of high production rate, reproducibility, and can be automated.[28] In a typical flow process, reaction is carried out in a narrow channel (tube, capillary or microfluidic devices) or continuous stirred tank reactor (CSTR). Experimental setup for tube reactor and CSTR is shown in figure 1.4.
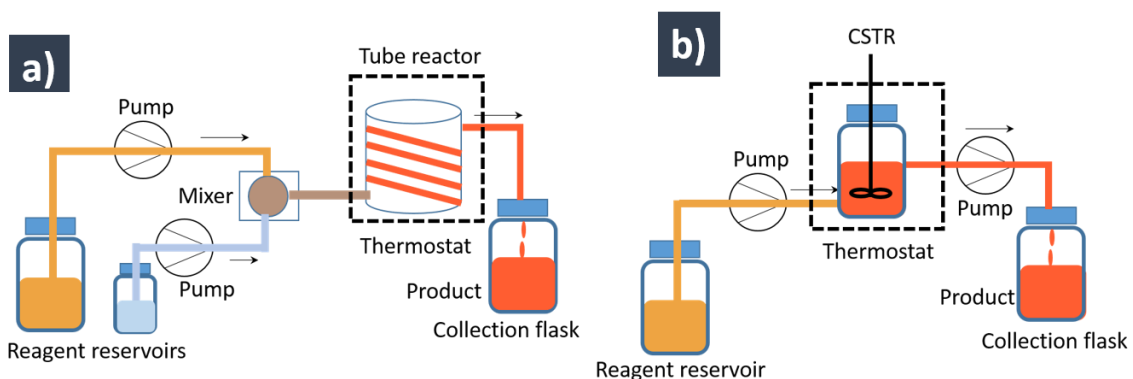
Figure 1.4: Schematics of continuous flow setup for a) tubular reactor and b) continuous stirred tank reactor (CSTR).

Flow synthesis involves various component such as reagent reservoirs, tubings, pumps, mixer or impeller, thermostat, the reactor (tube reactor, see Figure 1.4a, and CSTR, see Figure 1.4b) and collection flask. Typically in flow synthesis, reagents from the reservoir injected through tubing in a reactor and mixing of reagent introduces into

mixers. Once, reaction solution enters into a reactor placed in thermostat where product starts forming. The resulting product is collected at the outlet. When the reaction solution spends necessary residence time in a reactor, the conversion can be maximized. Over last decade, flow synthesis has been practiced in miniature reactors such as small size tubing (I.D., 0.5 -3.0 mm) and capillaries (O.D., 0.1-0.5 mm). Mixing of reagents in capillary and tube size mixer is faster compared to batch reactor due to high surface to volume ratio.[29] This small size reactor is operated in a laminar flow regime where Reynolds number ($R_e = \rho VDh/\mu$) is less than 2000. In a miniaturized reactor, mixing is a diffusion dominated phenomenon and takes places in a short time along the width of the reactor or over the tube diameter. T and Y type simple micromixers have been used to mix the reagents, and these are known to be passive mixer where additional force does not require for mixing other than pumping[30]. However, in active mixers, external energy is used in the form of acoustic waves (i.e. ultrasound), piezoelectric energy, mechanical vibrations and magnetic fields to enhance mixing.[31] Another added advantage of the miniature reactor is fast and uniform heat transfer and homogeneous temperature distribution. Rapid heat transfer and homogeneous temperature distribution is achieved due to the high surface area to volume ratio.[32] Mostly, synthesis of nanomaterial occurs by heating reaction solution in rage 25˚C to 300˚C. In such cases, uniform heating could be achieved using micro or mill-fluidic reactor having a high surface area to volume ratio to attain homogeneous nucleation and growth rate.[28] The homogeneous distribution of nucleation and growth rate throughout the reactor leads to uniform size and shape of nanoparticles with the maximum conversion.

Continuous flow process overcomes inherent discontinuity of batch process which increases the reproducibility and production rate. Hence, flow synthesis of nanoparticles is the solution for large-scale production of nanomaterials to meet industrial needs without compromising quality. Thus, the usage of a continuous flow process for large scale synthesis reported in 1989 Horn *et al.* demonstrated continuous precipitation of β-carotene in tube reactor to obtain monodisperse nanoparticles (100 nm) in powder form.[6] In 2002, deMello and co-workers showed usage of micro-reactor for continuous synthesis of CdS nanoparticles from $Cd(NO_3)_2$ and Na_2S as cadmium and sulfur precursor respectively.[33] The key advantages of maintaining uniform heating and mixing attract many scientists to pursue continuous flow process for size-controlled synthesis of nanoparticle. Various nanomaterials were prepared using continuous flow process such as Au,[34] Pd,[25] CdS,[33] and $BaSO_4$[35] and had better stability and less aggregation than corresponding batch synthesis.

One of the important features for translation of a batch process into continuous flow synthesis is the development of rapid synthesis. For last few decade, microwave-assisted synthesis is becoming popular for rapid synthesis of nanomaterials due to fast and homogeneous heating.[36] Coupling of microwave and the continuous process would drastically increase the production rate. Many laboratories and industries have been using this coupled technology for synthesis of organic compounds.[37] Recently, this coupled technology has been realized for the synthesis of inorganic nanoparticles and has potential to meet production rate with expected industrial requirements.

1.5 Microwave-assisted synthesis of nanoparticles

Conventionally, the reaction solution is heated on a hot plate or oil bath which transfer heat to reaction flask by convection. Due to the convective heat transfer and intermediary glass barrier between heating source and reaction solution,[38] generates a thermal gradient in the reaction solution. Thermal gradient can alter the local nucleation and growth kinetics of nanomaterial which may result in poor quality of the product. This situation is undesirable for formation nanoparticles. Microwave heating and inductive heating have emerged as alternatives to conventional heating.

Rapid heating has been realized using microwave radiation. Microwave enhances reaction rates, so the reaction occurs in short time. This approach has appealed to chemists to carry out chemical reactions in a few minutes which takes several hours up on using the conventional heating method. House hold and industrial microwave oven operate at 2.45 GHz frequency. The energy of microwave photon is 1×10^{-5} eV, 1.2×10^{-6} eV and 1×10^{-3} eV at 2.45 GHz, 0.3 GHz and 30 GHz frequency, respectively, which are not sufficient to induce Brownian motion.[39] Hence, microwave energy cannot break a chemical bond. Microwave energy results heating of a solution containing dipolar molecules is known as dielectric heating. When the electric function of microwave interacts with the electric function of the dipolar molecule, molecules starts rotating. The rotational motion of a molecule causes friction with neighboring molecule as this friction energy is dissipated in the form of heat.[36] Microwave radiation can be absorbed by the solvents having high dielectric constant. The ability of given material or solvent to convert microwave energy into heat is given by the following equation.

$$tan\delta = \frac{\delta''}{\delta'}$$

, where Tan δ is the loss tangent, δ'' is the conversion efficiency of the electromagnetic light into heat energy and δ' is the dielectric constant, which shows polarizability of given material or molecules.

Mostly ethylene glycol, ethanol, propanol, benzyl alcohol, water, and N,N-dimethylformamide have been used for synthesis of nanomaterials due to the polar nature and high $tan\delta$ value. First publication on microwave synthesis appeared in 1985 from Komarneni and Roy et *al.* where they reported liquid phase synthesis of TiO_2 microsphere by the sol-gel process in kerosene.[40] During this period, Gedye et *al.* explored microwave heating to carry out some organic reactions.[41] Earlier, the synthesis of nanomaterials was carried out in a domestic microwave oven and it has no control over temperature and pressure which leads uncertainty in the product quality. However in last few years, microwave oven or reactors are well equipped with in situ measurement of temperature and pressure with IR sensor.[36] Online monitoring of reaction parameters such as temperature and pressure allow us to improve quality of nanoparticles by manipulating reaction parameters. Various metallic, bimetallic and metal oxides nanoparticles have been synthesized using microwave assisted technique. Some of these include, Au^{42}, Ag, Pd, Ni, Pt, Pd, PtRh, PtNi,[43] ZnO, $\alpha\text{-}Fe_2O_3$, $\beta\text{-}Fe_2O_3$, Fe_3O_4, CuO, Mn_3O_4, MnO_2, TiO_2, and Co_3O_4, etc.[44]

Microwave technology can be integrated with the flow synthesis of nanoparticles to produce the intended materials at large scale Very few reports are available on

continuous microwave assisted flow synthesis of nanoparticles (viz. metal, metal oxide and bimetallic nanoparticles). The relevant literature is summarized in Table 1.2

Table 1.2: Summary of the literature reports on the continuous flow synthesis of nanomaterials under microwave irradiation.

Author & Year	System	Reactor specification	Observation
Snatoshi *et al.*, 2010[45]	Ag	Pyrex pipe, I.D. = 8 mm, L = 135mm	Rapid synthesis of the silver nanoparticles originated from the microscopic heating by microwaves produce uniform shaped nanoparticles
Masateru *et al.*, 2011[46]	Ag	PTFE tubing, I.D. = 1mm, L = 10 cm	Continuous synthesis for 5 h. Yield > 93%
Masateru *et al.*, 2013[47]	Cu	Quartz tube, I.D. = 1.5 mm, L = 100 mm	Fluid temperature was controlled by temperature feedback module and auto tracking frequency function
Ki-Joong *et al.*, 2014[48]	CuInSe2	Segmented flow PTFE tubing, I.D. = 3.18, 1.59 and 0.79 mm Nucleation zone in microwave oven and growth zone in oil bath	The separation between nucleation and growth stages produce high-quality nanocrystals. Segmented flow which minimized deposition of the nanocrystal on the wall surface of the tubing
Eric *et al.*, 2014[49]	PbSe	Segmented flow PTFE tubing, Microwave zone = 4 cm Nucleation zone in microwave oven and growth zone in oil bath, (L=3.5 m)	Size varied from 11.2 to13.9 nm by adjusting the microwave nucleation temperature between 124 and 159˚C
Musafumi *et al.*, 2016[50]	Pd, Rh, Pt, Ru	Glass reactor volume = 10 mL Back pressure regulator 250 psi,	Well-dispersed Rh, Ru, and Pt nanoparticles were obtained
Mustafa *et al.*, 2016[51]	Au	Teflon tubing O.D. = 1/8 in., (~0.32 cm), Reactor volume = 6 mL,	The major experimental parameters including microwave power, citrate-to-gold molar ratio ([Cit]/[Au]), and reaction residence time have been investigated

		Back pressure regulator 20 psi,	systematically.
Pranaw et al., 2017[52]	Rh, RhAg	Segmented flow PTFE/PEEK tubing I.D.= 0.79 m., and L = 30.5 m., 3D droplet generator	Near-monodisperse cuboctahedral Rh nanoparticles are obtained under single-phase flow conditions. Two-phase microfluidic droplet flow method leads to the highly selective formation of Rh multipods.
Gustavo et al., 2017[3]	Ag nanocubes	Segmented flow Nucleation zone in a microwave oven. Teflon tubing O.D. = 1/16 in., L = 4.7 cm. Growth zone in oil bath, Teflon tubing O.D. = 1/16 in.,L = 23, 15 and 8 m.,	The seed-mediated growth of Ag nanocube. Separation of nucleation from growth events leads to uniform single crystalline Ag nanocubes.

These reports on microwave-assisted flow synthesis clearly show its potential as a reliable technology for producing more complex nanomaterial such as alloy, heterostructure, and inorganic-organic hybrid nanomaterials.

1.6 Preparation of organic particles

Another emerging class of material is organic small size particles/nanoparticles. Organic particles have recently attracted tremendous attention due to its applications in the nano-medicine[53], pigments, and foodstuff.[6, 17] The formation of small organic crystals needs to be studied to produce size controlled particles that would reflects a change in the properties such as dissolution rate, compressibility, flow-ability, and bioavailability. Various strategies have been developed for the wet chemical preparation of organic particles including reprecipitation, reverse micelle based synthesis and use of

microemulsions. Among these methods, reprecipitation is a widely employed technique and provides good control over reaction parameters that can give almost desired size of small organic particles (micro and nano range) and it is suitable for scale-up. Also, reprecipitation is relatively easy to explore and it doesn't require harsh reaction condition and complex instrumentation.
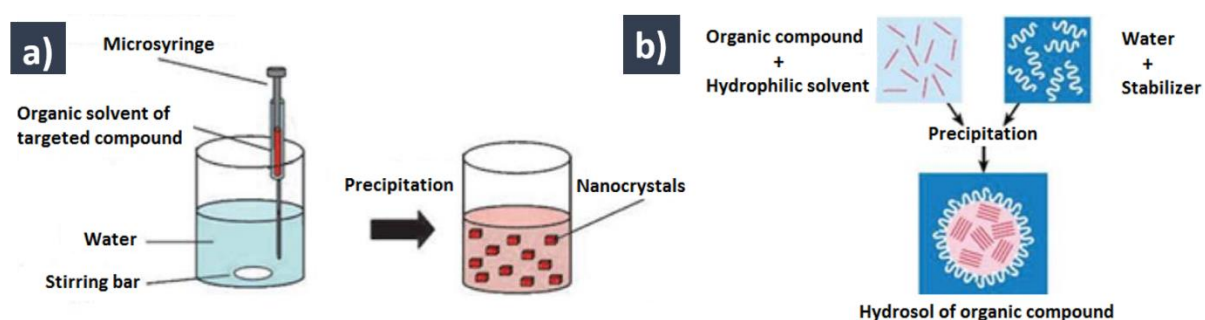
Figure 1.5: Schematics showing organic nanoparticles formed by using reprecipitation process, a) without stabilizer (Image is taken from reference 12). b) with stabilizer (Image is taken from reference 54).

Reprecipitation is a solvent exchange method in which organic molecules dissolved in a friendly solvent is precipitated by adding an anti-solvent. It is prerequisite that the anti-solvent must be miscible with the solvent. Here the formation of nanoparticles includes three steps dissolution, precipitation followed by rapid mixing and crystallization. The targeted organic compound is dissolved in a good solvent and rapidly injected into stirring antisolvent (poor solvent) (see figure 1.5). It has been observed that good solvent is eluted away from the target molecule and molecules get exposed to antisolvent resulting reprecipitation. Rapid mixing of solvents induces nucleation and growth within a short time,[54] In classical nucleation theory, it is assumed that small monodisperse particle is obtained from nucleation and growth continues in the

supersaturated solution. To attain uniform supersaturation, mixing plays a vital role and it should be faster than precipitation. Scaling-up this precipitation in a batch reactor is not viable because of inhomogeneous mixing and heat transfer. Addition of solvent to antisolvent decides how fast mixing and uniform mixing occurs? Ujiiye-Ishii and co-workers demonstrated controlled the addition of solvent using the pump as injection device, which produced quinacridone nanocrystal with controlled size and morphology in a semi-batch reactor.[17] Small size uniform nanoparticles were produced, compared to milling and manual injection method. These semi-batch processes did not ensure reproducibility and remain relevant only to synthesis of smaller quantities. As an alternative it is possible to use continuous flow process for the reprecipitation of organic particle in large quantity.

Continuous preparation of organic nanoparticles has been practiced in the microfluidic device due to rapid and homogeneous mixing. Taking advantage of micromixing, various nanoparticles have been produced such as silybin,[55] danazol,[53] spironolactone,[56], etc. Horn and co-workers developed continuous flow method for preparation of aqueous suspension of carotenoid (β-carotene) by reprecipitation method with continuous mixing chamber process[6]. Elevated temperature and pressure were used to keep fluid running, which prevents clogging. In reprecipitation reaction, tube or channel clogging is a serious issue which hampers practical use of microfluidic devices for scale-up. Clogging in channel or tube occurs due to formation of a viscous precipitate or dense suspension. On the other hand, low molecular weight organic compounds are not stable at elevated temperature and pressure condition. Hence, continuous flow reprecipitation needs to operate in normal condition. To tackle these issues, mixing of

fluid should be done in wall free environment and external force should be applied to enhance mixing and avoid clogging at normal a condition.

1.7 Objective and outline of thesis

The rapid expansion of nanotechnology is increasing demand for scalable synthesis of nanomaterials. In this thesis, we aimed at rapid continuous flow processes of nanomaterials. Systematic approaches to scale-up start with i) the development of novel synthesis in a batch and optimization of reaction parameters and ii) adopting batch parameter for continuous flow process.

In chapter 2, we investigate a reliable microwave-assisted method for rapid synthesis to obtain phase pure copper oxides. We optimize reaction parameter in a batch and understand the role of each parameter. Best reaction condition which produced phase pure small size copper oxide nanoparticles with maximum conversion is considered for microwave assisted continuous flow process. The semiconducting nature of copper oxide is further tested for its possible application as a gas sensing material and thermal conducting fluid (nanofluids).

In chapter 3, we present synthesis of multicomponent palladium supported nickel nanoparticles in microwave assisted continuous flow process. Reducing nature of benzyl alcohol, which also acts as a solvent is used for sequential reduction of nickel and palladium precursor. Sparking in the microwave is alleviated with addition of surfactant. We evaluate catalytic performance of a material for hydrogenation of nitro-aromatic compounds.

In chapter 4, instead of simple single component system, we aimed to develop flow process for bimetallic NiPt alloy nanoparticle. Simultaneous reduction of both the metal precursors is carried out to obtain variable alloy compositions by adjusting initial molar concentration in a batch. Optimized batch parameter translated to microwave assisted flow process and identical product quality was obtained. We have further evaluated electrochemical performance of NiPt alloy for hydrogen evolution reaction.

In chapter 5, we chose to develop flow process to obtain small sized organic particles of metformin hydrochloride as a model system. Reprecipitation method is studied to understand role of antisolvent to solvent ratio, concentration, temperature and additive in an ultrasound to obtain ultrafine particles. Clogging issue was resolved using an inverted impinging jet reactor in wall free environment in presence of ultrasound.

In chapter 6, summarizes the thesis work and important results.

1.7 References

1.   Roduner, E. *Chem. Soc. Rev.* **2006,** 35, 583-592.

2.   Burda, C.; Chen, X.; Narayanan, R.; El-Sayed, M. A. *Chem. Rev.* **2005,** 105, 1025-1102.

3.   Albuquerque, G. H.; Squire, K.; Wang, A. X.; Herman, G. S. *Cryst. Growth Des.* **2017**.

4.   Cui, C.; Gan, L.; Li, H.-H.; Yu, S.-H.; Heggen, M.; Strasser, P. *Nano letters* **2012,** 12, 5885-5889.

5.   Tartaj, P.; Morales, M. P.; Gonzalez-Carreño, T.; Veintemillas-Verdaguer, S.; Serna, C. J. *Adv. Mater.* **2011,** 23, 5243-5249.

6.   Horn, D. *Macromol. Mater. Eng.* **1989,** 166, 139-153.

7.   Zhang, J.; Liu, J.; Peng, Q.; Wang, X.; Li, Y. *Chem. Mater.* **2006,** 18, 867-871.

8.   Choi, S.-I.; Shao, M.; Lu, N.; Ruditskiy, A.; Peng, H.-C.; Park, J.; Guerrero, S.; Wang, J.; Kim, M. J.; Xia, Y. *ACS nano* **2014,** 8, 10363-10371.

9.   Stark, W.; Stoessel, P.; Wohlleben, W.; Hafner, A. *Chem. Soc. Rev.* **2015,** 44, 5793-5805.

10.   Pulit-Prociak, J.; Banach, M. *Open Chem.* **2016,** 14, 76-91.

11.   Ferrando, R.; Jellinek, J.; Johnston, R. L. *Chem. Rev.* **2008,** 108, 845-910.

12.   Patra, A.; Chandaluri, C. G.; Radhakrishnan, T. *Nanoscale* **2012,** 4, 343-359.

13.   He, G.; Pan, Q. *Macromal. Rapid Commun.* **2004,** 25, 1545-1548.

14.   Zhang, X.; Manohar, S. K. *J. Am. Chem. Soc.* **2004,** 126, 12714-12715.

15.   Li, F.; Qin, X. In *Synthesis of Polyaniline Nanoparticles*, Adv. Mate. Res., 2010; Trans Tech Publ: pp 237-240.

16.   Khan, S.; Matas, M. d.; Zhang, J.; Anwar, J. *Cryst. Growth Des.* **2013,** 13, 2766-2777.

17.   Ujiiye-Ishii, K.; Baba, K.; Wei, Z.; Kasai, H.; Nakanishi, H.; Okada, S.; Oikawa, H. *Mol. Cryst. Liq. Cryst.* **2006,** 445, 177/[467]-183/[473].

18.   Zhang, J.; Liu, H.; Wang, Z.; Ming, N. *Adv. Funct. Mater.* **2007,** 17, 3295-3303.

19.   Xiong, Y.; Xia, Y. *Adv. Mater.* **2007,** 19, 3385-3391.

20.   Cushing, B. L.; Kolesnichenko, V. L.; O'Connor, C. J. *Chem. Rev.* **2004,** 104, 3893-3946.

21.   Skrabalak, S. E.; Brutchey, R. L., Going with the Flow: Continuous Flow Routes to Colloidal Nanoparticles. ACS Publications: 2016.

22.   Jin, M.; Liu, H.; Zhang, H.; Xie, Z.; Liu, J.; Xia, Y. *Nano Res.* **2011,** 4, 83-91.

23.   Park, J.; An, K.; Hwang, Y.; Park, J.-G.; Noh, H.-J.; Kim, J.-Y.; Park, J.-H.; Hwang, N.-M.; Hyeon, T. *Nat. Mater.* **2004,** 3, 891-895.

24.   Klinkova, A.; Larin, E. M.; Prince, E.; Sargent, E. H.; Kumacheva, E. *Chem. Mater.* **2016,** 28, 3196-3202.

25. Wong, W. K.; Yap, S. K.; Lim, Y. C.; Khan, S. A.; Pelletier, F.; Corbos, E. C. *React. Chem. Eng.* **2017,** 2, 636-641.

26. Zhang, L.; Xia, Y. *Adv. Mater.* **2014,** 26, 2600-2606.

27. Hartman, R. L.; McMullen, J. P.; Jensen, K. F. *Angew. Chem. Int. Ed.* **2011,** 50, 7502-7519.

28. Pan, J.; El-Ballouli, A. a. O.; Rollny, L.; Voznyy, O.; Burlakov, V. M.; Goriely, A.; Sargent, E. H.; Bakr, O. M. *ACS nano* **2013,** 7, 10158-10166.

29. Ehrfeld, W.; Hessel, V.; Löwe, H. *Microreactors: New Technology for Modern Chemistry* **2000**, 1-14.

30. Ottino, J. M.; Wiggins, S. *Philos. Trans. R. Soc. London Ser. A* **2004**, 923-935.

31. Hartman, R. L.; Jensen, K. F. *Lab Chip* **2009,** 9, 2495-2507.

32. Makgwane, P. R.; Ray, S. S. *J. Nanosci. Nanotechnol.* **2014,** 14, 1338-1363.

33. Edel, J. B.; Fortt, R. *Chem. Comm.* **2002**, 1136-1137.

34. Sebastian Cabeza, V.; Kuhn, S.; Kulkarni, A. A.; Jensen, K. F. *Langmuir* **2012,** 28, 7007-7013.

35. Marchisio, D. L.; Rivautella, L.; Barresi, A. A. *AIChE Journal* **2006,** 52, 1877-1887.

36. Zhu, Y.-J.; Chen, F. *Chem. Rev.* **2014,** 114, 6462-6555.

37. Morschhäuser, R.; Krull, M.; Kayser, C.; Boberski, C.; Bierbaum, R.; Püschner, P. A.; Glasnov, T. N.; Kappe, C. O. **2012**.

38. Sauks, J. A Continuous Flow Microwave Reactor for Organic Synthesis. 2013.

39. Nüchter, M.; Ondruschka, B.; Bonrath, W.; Gum, A. *Green Chem.* **2004,** 6, 128-141.

40. Komarneni, S.; Roy, R. *Mater. Lett.* **1985,** 3, 165-167.

41. Giguere, R. J.; Bray, T. L.; Duncan, S. M.; Majetich, G. *Tetra. Lett.* **1986,** 27, 4945-4948.

42. Arshi, N.; Ahmed, F.; Kumar, S.; Anwar, M.; Lu, J.; Koo, B. H.; Lee, C. G. *Curr. Appl. Phys.* **2011,** 11, S360-S363.

43. Abdelsayed, V.; Aljarash, A.; El-Shall, M. S.; Al Othman, Z. A.; Alghamdi, A. H. *Chem. Mater.* **2009,** 21, 2825-2834.

44. Pinna, N.; Niederberger, M. *Angew. Chem. Int. Ed.* **2008,** 47, 5292-5304.

45. Horikoshi, S.; Abe, H.; Torigoe, K.; Abe, M.; Serpone, N. *Nanoscale* **2010,** 2, 1441-1447.

46. Nishioka, M.; Miyakawa, M.; Kataoka, H.; Koda, H.; Sato, K.; Suzuki, T. M. *Nanoscale* **2011,** 3, 2621-2626.

47. Nishioka, M.; Miyakawa, M.; Daino, Y.; Kataoka, H.; Koda, H.; Sato, K.; Suzuki, T. M. *Ind. Eng. Chem. Res.* **2013,** 52, 4683-4687.

48. Kim, K.-J.; Oleksak, R. P.; Hostetler, E. B.; Peterson, D. A.; Chandran, P.; Schut, D. M.; Paul, B. K.; Herman, G. S.; Chang, C.-H. *Cryst. Growth Des.* **2014,** 14, 5349-5355.

49. Hostetler, E. B.; Kim, K.-J.; Oleksak, R. P.; Fitzmorris, R. C.; Peterson, D. A.; Chandran, P.; Chang, C.-H.; Paul, B. K.; Schut, D. M.; Herman, G. S. *Mater. Lett.* **2014,** 128, 54-59.

50. Harada, M.; Cong, C. *Ind. Eng. Chem. Res.* **2016,** 55, 5634-5643.

51. Bayazit, M. K.; Yue, J.; Cao, E.; Gavriilidis, A.; Tang, J. *ACS Sustain. Chem. Eng.* **2016,** 4, 6435-6442.

52. Kunal, P.; Roberts, E. J.; Riche, C. T.; Jarvis, K.; Malmstadt, N.; Brutchey, R. L.; Humphrey, S. M. *Chem. Mater.* **2017,** 29, 4341-4350.

53. Zhao, H.; Wang, J.-X.; Wang, Q.-A.; Chen, J.-F.; Yun, J. *Ind. Eng. Chem. Res.* **2007,** 46, 8229-8235.

54. Horn, D.; Rieger, J. *Angew. Chem. Int. Ed.* **2001,** 40, 4330-4361.

55. Cui, G.-J.; Xu, L.-M.; Zhou, Y.; Zhang, J.-J.; Wang, J.-X.; Chen, J.-F. *Chem. Eng. J.* **2013,** 222, 512-519.

56. Dong, Y.; Ng, W. K.; Shen, S.; Kim, S.; Tan, R. B. *Int. J. Pharma.* **2011,** 410, 175-179.

Chapter 2

Microwave-Assisted Batch and Flow

Synthesis of CuO and Cu₂O Nanoparticles
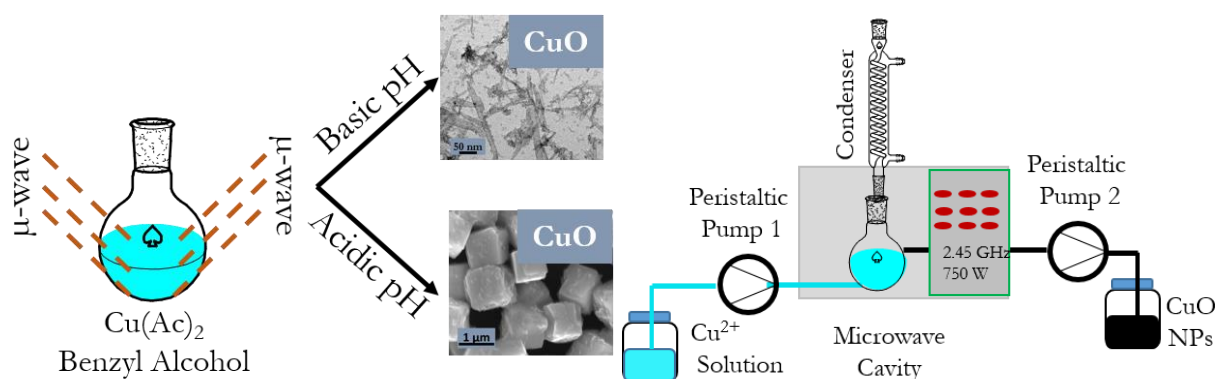
2. 1 Introduction

Demand for nanomaterial is increasing due to the advent of several interesting and useful application of nanomaterials. Among various nanomaterials, metal oxide nanomaterial has become an integral part of cutting-edge technology. This chapter focuses on developing new synthesis protocol to obtain pure phase copper oxide nanomaterials. Oxides of copper find an application in these semiconductor as well as automobile industry due to their charge transport and heat transport properties.[1, 2] Considering the advantage of nanosized particles, properties of nanoparticles of these oxides change drastically in comparison to their bulk counterpart. Also, the surfaces activity of nanoparticles also increases due to the high surface area resulting from the smaller size of nanoparticles.[3] CuO has been used as a sensor for reducing gases as well as an electrode material in Li-ion battery.[4, 5] Other hand, Cu_2O used as a catalyst in photo catalytic hydrogen evolution from the water.[6] Copper exists in multiple oxidation states (Cu^0, Cu^{1+} and Cu^{2+}) and hence can form oxides with different stoichiometry. The properties of these oxides vary, sometimes drastically, depending on the oxidation state and the metal-to-oxygen stoichiometric ratio. Copper forms three main types of oxides, *viz.* Cu_4O_3, Cu_2O and CuO.[7] In the recent time there has been an upsurge in the preparation of nanoscale particles of copper oxides. However, synthetically it is challenging to prepare copper oxides in pure phases and make these copper oxides available at affordable price in the market by synthesizing these nanomaterial in large quantity. Recently, continuous flow synthesis has shown potential as a promising technology to manufacture nanomaterials in large quantity without compromising the quality of nanomaterial.[8-10]

Before translating batch synthesis of CuO and Cu_2O to continuous flow synthesis,the following essential features while translating to continuous flow synthesis need to be satisfied: i) The reaction should involve minimum number of reagents ii) Reaction should complete in short time iii) Yield phase pure product and high quantities of nanoparticles and iv) Synthesis should not involve post-synthetic treatment. Here, we are looking for a simple method which involves fewer reagents and yields phase pure copper oxides in large quantities in short time. At the initial stage of development of continuous flow synthesis, we need to study batch process to understand the effect of each reaction parameter on the quality and quantity of product which would reduce the effort while adopting batch process to continuous flow synthesis.

Specially, the synthesis of Cu_2O without any impurities is regarded as a hard task due to the better stability of copper in +2 states as compared to +1. There are a few reported procedures on the synthesis of pure Cu_2O nanoparticles and mostly based on the hydrothermal synthesis, which is more energy intensive and time-consuming.[11, 12] Murphy *et al.* synthesized Cu_2O nanocubes by reducing Cu^{2+} with sodium ascorbate and using CTAB as a protecting agent.[13] Yang *et al.* prepared Cu_2O nanoparticles and transformed them into CuO nanoparticles by gas-phase oxidation at 200°C over a period of 2 hrs.[5] On the other hand, nanocrystalline CuO with a different morphology was prepared by adjusting hydrolysis rate with different concentration of precipitating agent under hydrothermal conditions for 20 hrs.[11] CuO nanocrystalline particles were prepared in N,N-dimethylformamide and converted to Cu_2O by reductive transformation in 8-42 hrs at 180°C. Klabunde *et al*. synthesized CuO nanorods using the hydrothermal method and reduced the CuO into Cu_2O and Cu metal in 4% hydrogen.[12] To obtain single phase

Cu_2O from the bivalent precursor, many reducing agents such as hydrazine, titanium tetrachloride, sodium tartrate and hydroxylamine, and so on are added to the reaction mixture.[14-17] Wang *et al*. reported that the control over the shape of Cu, Cu_2O nanotubes/nanorods can be exercised by reducing $Cu(OH)_4^{2-}$ with hydrazine and glucose, respectively, using CTAB as a shape-directing agent at room temperature.[18] Hydrothermal treatment of $Cu(OH)_4^{2-}$ precursor at 120 °C resulted in nanotubes and nanorods of monoclinic CuO. Song *et al.* demonstrated the conversion of Cu_2O to CuO by an increase in the pH of the solution by adding aqueous ammonia solution.[4] Qian *et al.* reported the synthesis of uniform crystalline Cu_2O cubes by reducing the copper-citrate complex solution with glucose and observed that the evolution of Cu_2O cubes takes place through intermediate steps that give multipods and star-shaped particles.[19]

Eventually, synthesis of copper oxide: (i) involves many steps, (ii) needs several chemical reagents, (iii) requires high temperature and (iv) is very time consuming. Since last two decades, microwave-based synthesis is becoming an attractive method due to rapid formation nanoparticles with increasing yield. Hence, preparation of metal oxides such as ZnO, Co_3O_4, TiO_2, Fe_3O_4 etc.[20-23] using microwave-assisted synthesis has been recently reported in the literature. In past few years, Markus Niederberger and co-worker exploited benzyl alcohol route for the synthesis of phase pure metal oxide by varying few reaction parameters for examples CoO, ZnO, Fe_3O_4, MnO, Mn_3O_4, HfO_2, In_2O_3, SnO_2, Ta_2O_5, TiO_2, ZrO_2 and $BaTiO_3$.[24-29] We reckon that a benzyl alcohol route is a viable option for rapid synthesis of phase pure copper oxides in microwave by varying reaction parameters and which could be easily extended to a continuous flow process. In addition

to that benzyl alcohol acts as solvent, reducing agent as well as a stabilizer to avoid aggregation,[30] which obliterates the need of multiple reagents.

In this chapter, we report the controlled synthesis of Cu_2O and CuO using a microwave-assisted synthetic strategy. It has been shown that both Cu_2O and CuO could be obtained from copper (II) acetate as the metal precursor and benzyl alcohol as the solvent which also acts as a reducing agent under the microwave condition. Phase pure nanoparticles of Cu_2O were formed when copper (II) acetate ($Cu(ac)_2$) was irradiated by microwave for 10 min in benzyl alcohol. On the other hand, CuO nanoparticles formed when small amount of the base was added to reaction mixture. Here we report that the effect of change in metal precursor and pH onto the formation of different products (CuO/Cu_2O). We have systematically studied the effect of substrate concentration on size of nanoparticle and batch volume on the conversion of $Cu(ac)_2$ into CuO. After optimizing the batch process, bath the parameters were considered for continuous flow synthesis of CuO NPs at a high production rate. The optical properties and hole mobilities of these nanostructures were determined and tested for the performance of copper oxides NPs for gas sensing application and nanofluids for heat exchange.

2.2 Experimental Section

2.2.1 Chemicals and Materials

Chemicals and materials were used as received or without further purification. Cu (II) acetate was purchased from *LobaChemie*. Cu (II) acetylacetonate purchased from *Sigma-Aldrich*, and benzyl alcohol, hydrazine hydrate 80%, NaOH, and 15% HCl were received from *Thomas Baker*.

2.2.2 Synthesis of copper oxides nanoparticles

2.2.2. A) Synthesis of copper oxide nanomaterials using precipitation technique in tertiary butyl toluene by reflux

0.5 g of $Cu(ac)_2$ was dissolved in the 25 mL of water. 0.2 g of CTAB was mixed with aqueous solution of $Cu(ac)_2$. Cu^{2+} ions are extracted into 25 mL of tertiary butyl toluene using CTAB as a phase transfer reagent with use of separating funnel. Cu^{2+} ions extracted into tertiary butyl toluene was used for the synthesis of copper oxides. After phase transfer of Cu^{2+} ions, 100 uL of 1 M NaOH was added to the Cu^{2+} solution of tertiary butyl toluene and refluxed with continuous stirring. The reaction product was observed in solution after 6h. After the product formation, reaction flask was allowed to cool at room temperature and washed three times using absolute ethanol and water. Separation and washing were done by centrifuge (at 9000 rpm for 20 min) and ultrasound. The resulting powder was dried at 60˚C for overnight and analyzed by XRD which revealed product contains a mixture of copper oxides and impurity.

2.2.2. B) Synthesis of copper oxide nanomaterials using benzyl alcohol under microwave irradiation
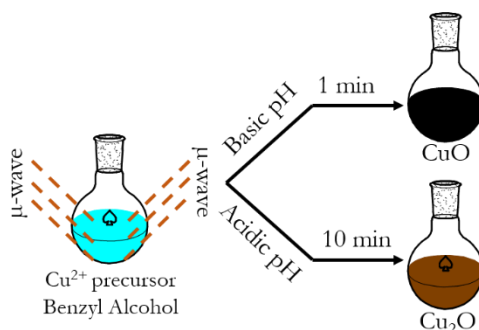
Figure 2.1: Schematic of microwave-assisted synthesis of CuO and Cu₂O nanoparticles.

0.199 g of Cu(ac)$_2$ mixed with 5 mL of benzyl alcohol in round bottom flask and small amount of 0.1 M NaOH was added. The reaction flask involving reaction mixture was placed in a microwave oven operating at 700 W with a 2.45 GHz frequency for 1 min with constant stirring. On other hand, without NaOH, Cu(ac)$_2$ solution was irradiate under microwave oven for 6 min with continuous stirring. The products with and without addition of NaOH were washed three times using absolute ethanol and water, and then isolated by centrifugation (at 9000 rpm, for 20 min) and re-dispersed by ultrasound. Both the products were dried at 60˚C for 12 hrs and analyzed by powder X-ray diffraction instrument (Panalytical Xpert Pro PXRD operated at 40 kV and 30 mA using Cu Kα radiation).

2.2.3 Synthesis of Cu₂O nanoparticles

Cu (II) acetate (0.199 g, mmol) was mixed with 5 mL of benzyl alcohol in a 50 mL round-bottom flask at room temperature. This flask containing the reaction mixture

was placed in a microwave oven operating at 700 W with a 2.45 GHz frequency for 10 min with continuous magnetic stirring. After microwave irradiation, the reaction flask was removed from the microwave oven and allowed to cool at room temperature. A reddish-brown colored product was observed. It was washed three times using absolute ethanol and water. This powder was re-dispersed in water by sonication and centrifuged at 9000 rpm for 20 min. The reddish-brown colored product was dried at 60˚C in an oven for 12 hrs. This product was identified to be Cu_2O nanoparticles. The same procedure was followed with the addition of a different amount of 15% of HCl to study the pH dependence.

2.2.4 Synthesis of CuO nanoparticles

The same procedure described above was followed except that 100 μL of NaOH (0.1 M) was added to the precursor's mixture (copper acetate + benzyl alcohol). In this case, the reaction mixture was kept in the microwave oven operating at 2.45 GHz frequency with 700 W power for 1 min. This small variation in reaction procedure led to the formation of a black product in short time. It was analyzed and identified as CuO nanoparticles. The amount of NaOH was slightly varied to change the pH of the solution. We also studied the synthesis of CuO and Cu_2O nanoparticles by replacing the metal precursor. All the other conditions remained the same as described above except the time for the reaction. The details of the precursor dependence on the type of product obtained are discussed in detail in Results and Discussion Section.

2.2.5 Continuous flow synthesis of Cu_2O nanoparticles

Flow synthesis of Cu_2O nanoparticles was carried out in a single continuous stirred tank reactor having 25 mL volume placed in microwave cavity as shown in

schematics (see Figure 1.14 a). 250 mL solution of $Cu(ac)_2$ in benzyl alcohol was prepared by maintaining optimized batch concentration (0.05M). The solution of $Cu(ac)_2$ was injected into CSTR at 25 mL/min flow rate using peristaltic pump so reactant experienced 1 min residence time in the reactor under irradiation of microwave. Magnetic stirring bead was placed in CSTR for continuous stirring. At the outlet, product was collected at 25 mL/min flow rate and washed three times with absolute ethanol and water using centrifuge and ultrasound. Dried sample was taken for the analysis.

2.3 Results and Discussion

To obtain phase pure copper oxides various methods were tried and then final set of conditions that give maximum yield with uniform particle properties was obtained. Effect of each parameter on size, morphology and phase of the product is discussed as below.

2.3.1 Synthesis of copper oxide using different methods
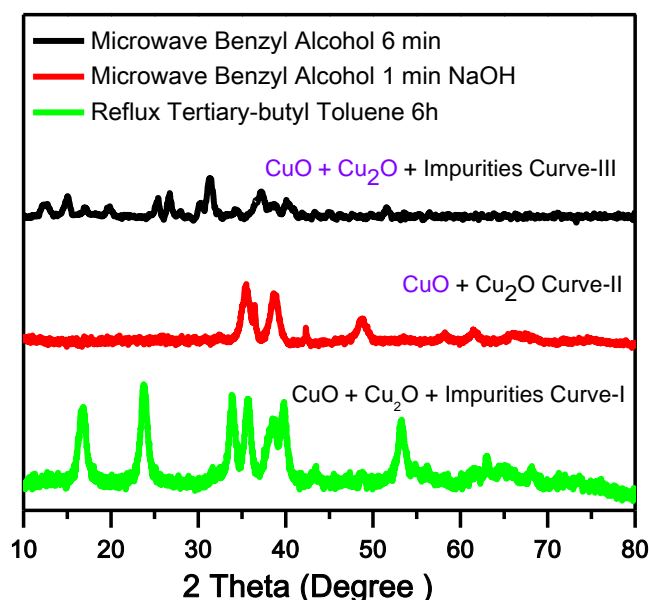
Figure 2.2: Powder X-ray diffraction (PXRD) patterns of copper oxides synthesis by different method.

Our aim is to produce phase pure copper oxide nanoparticles using minimum reagents in a short reaction time. We began to develop a new method of synthesis to obtain phase pure copper oxides and started with the precipitation method into an organic solvent (tertiary butyl toluene) by reflux technique as explained in section 2.2.2A. After six hours, the black colored precipitate was observed in the reaction flask. This black colored product was dried and analyzed under powder X-ray diffractometer. PXRD graph in figure 2.2 (Curve-I) shows that the product contains CuO, Cu$_2$O and other unknown

impurities. Here, we concluded that the conventional reflux technique is not a suitable method to produce phase pure copper oxide nanoparticles, it is very time consuming (6h) and it requires multiple steps and reagents (phase transfer reagents).

Our endeavor with the microwave-assisted synthesis of metal oxide nanoparticles was started. Microwave heating has proven to be very rapid[31]. After thorough literature survey, we devised our scheme as shown in figure 2.1. $Cu(ac)_2$ and benzyl alcohol were used to obtain copper oxide nanoparticles under microwave radiation as explained in Section 2.2.2 B. Benzyl alcohol acts as a solvent and it is good microwave absorber having 0.667 $\tan\delta$ value[32]. In the first attempt, we have synthesized copper oxide nanoparticles with NaOH. PXRD patterns of product has CuO and Cu_2O peaks, which indicates that CuO monoclinic phase is dominant in the product (see Figure 2.2 Curve-II). Same procedure was repeated without NaOH for 6 min. It was observed that the product contains CuO, Cu_2O and other impurity as identified by PXRD patterns as shown in figure 2.2 (Curve-III). In case of product obtained without NaOH, comprises large fraction of Cu_2O cubic phase. Results of microwave-assisted method were encouraging to study the effect of various reaction parameters such as precursor, reaction time, pH, and concentration to obtain phase pure copper oxides nanoparticles.

2.3.2 Effect of precursors

We studied effect of different copper precursors, copper(II)acetate ($Cu(ac)_2$) and copper acetylacetonate ($Cu(acac)_2$) at two different pH conditions, viz. pH = 4 and pH>12. At the acidic condition, a turbid brownish red product formed irrespective of the precursor used when irradiated for 10 min. The PXRD profile of product obtained (Figure 2.3a and b, curve II and VI) at acidic condition from both the precursors matched with Cu_2O phase (JCPDS card number 65-3288) and no trace of any impurity could be detected under the PXRD condition used. The peaks at 2Θ values 29.7°, 36.6°, 42.4°, 61.4°, and 73.8° are assigned to (110), (111), (200), (220), and (311) planes of the Cu_2O phase. Interestingly, while the reaction with $Cu(ac)_2$ took 10 min for completion, the reaction with $Cu(acac)_2$ as a precursor needed 40 min for completion. PXRD analysis of the reaction products obtained at basic pH conditions (Figure 2.3a, curve-I) indicated that the product obtained from $Cu(ac)_2$ to be purely the CuO phase (JCPDS card number 41-0254), while $Cu(acac)_2$ led to the formation of a mixture of Cu_2O and CuO phases (Figure 2.3a, curve-II).
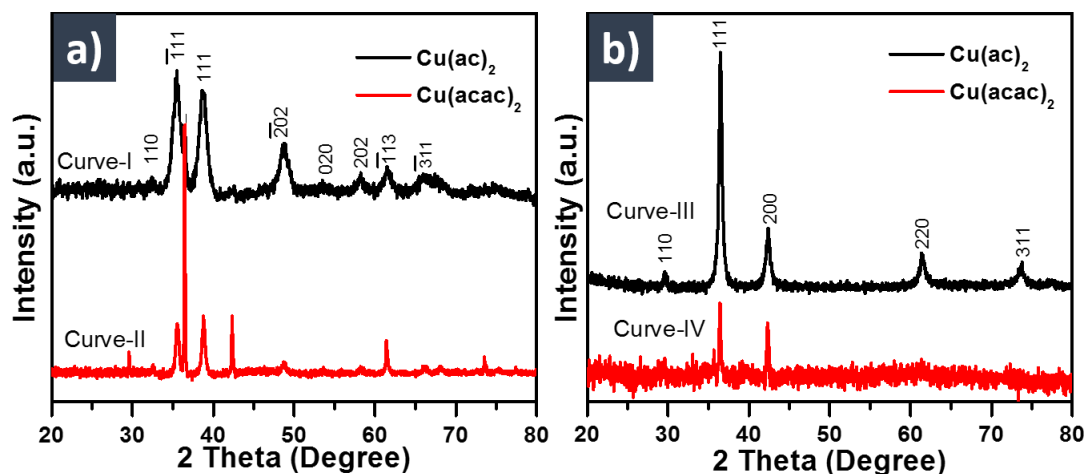
Figure 2.3: PXRD patterns of copper oxides nanoparticles synthesized in batch a) at pH 12 using Cu(ac)₂ and Cu(acac)₂ b) at pH 4 using Cu(ac)₂ and Cu(acac)₂.

Here, formation of copper oxides using $Cu(ac)_2$ without addition of base needed only 10 min, while continuing the reaction with $Cu(acac)_2$ beyond 40 min also did not change the composition of product mixture. Thus, from the above results it can be summarized that $Cu(ac)_2$ produces Cu_2O (at acidic condition) or CuO (at basiccondition). On the other hand, changing the precursor to $Cu(acac)_2$ led to the formation of Cu_2O (at acidic condition) or a mixture of CuO and Cu_2O (under basicconditions). Here, the formation of Cu_2O where Cu is in +1 oxidation state was a little surprising because in both the precursors used here, Cu is present in the +2 oxidation state. It has been proven that the benzyl alcohol which is used as a solvent, can act as a reducing agent,[33] when it is heated above 150°C. We reckon that under microwave conditions, benzyl alcohol must be acting as a mild reducing agent. Benzyl alcohol reduces the Cu^{2+} ions to Cu^{1+} ions, ensuring the product formed would be Cu_2O. At a basic pH, higher oxygen content may hamper the reducibility of benzyl alcohol. Therefore, addition of the base to $Cu(ac)_2$ leads to the formation of CuO nanoparticles. The longer reaction time of 40 min for $Cu(acac)_2$ to get converted to Cu_2O compared to 10 min when $Cu(ac)_2$was used as a precursor could be due to the stronger binding between the acetylacetonate ligand with Cu^{2+} ions as compared to the simple acetate ligand. The stronger binding of the acetylacetonate ligand to Cu (II) could also explain the reason for the formation of mixture of products with $Cu(acac)_2$ at basic pH conditions. Since, the reactions with $Cu(acac)_2$ were taking a significantly longer time and the product formed at basic pH conditions was in mixedphase we did not pursue reactions with this precursor further.

2.3.3 Effect of pH

2.3.3 A) Acidic pH
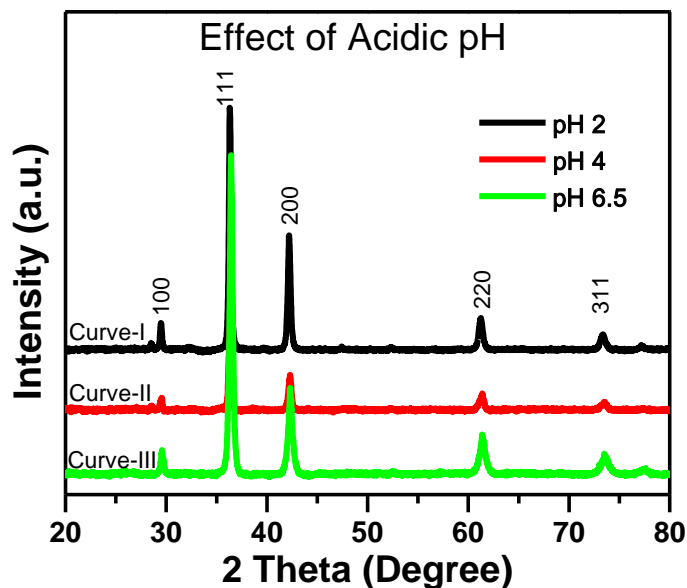
Figure 2.4: PXRD patterns of Cu$_2$O nanoparticles synthesized by microwave-assisted synthesis in batch at acidic pH.

Further, we have carried out a systematic study of products formed with Cu(ac)$_2$at different pH conditions (pH=2, 4 and 6.5). The pH of Cu(ac)$_2$dissolved in benzyl alcohol was 6.5 and therefore, a pH of 6.5 did not need any addition of acid or base. We achieved acidic condition such as pHs 2 and 4 by addition of 20 and 10μL solutions of 15% HCl, respectively. The microwave heating of these Cu(ac)$_2$solutions at different pH condition led to a change in the color of the solutions to reddish-brown within 10 min of the reaction. Samples obtained at pHs 2, 4, and 6.5 are referred to as samples IA, IIA and IIIA in this chapter, respectively. The PXRD patterns of samples IA, IIA and IIIA (see Figure 2.4) matched again with the Cu$_2$O phase without any trace of impurity.
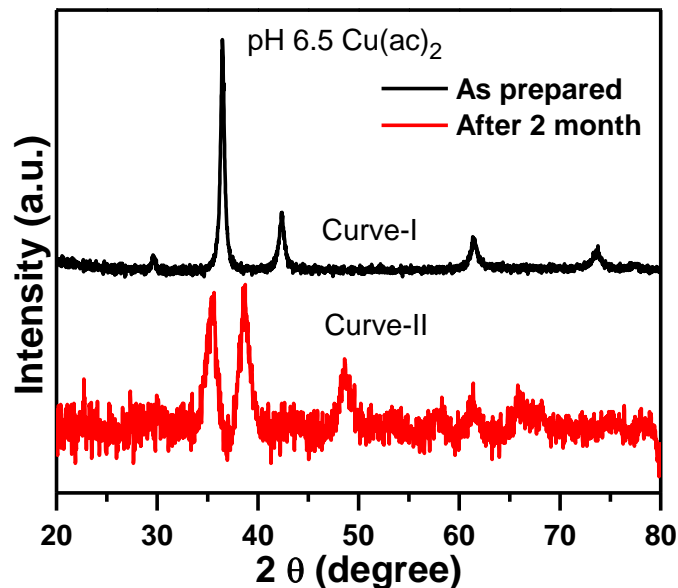
Figure 2.5: PXRD Patterns of batch synthesized Cu₂O nanoparticles by microwave at pH 6.5 (Curve-I As prepared and Curve-II after two month).

As we know Cu^{1+} oxidation state is prone to oxidize into Cu^{2+} oxidation state at ambient condition.The stability test was done for as prepared Cu_2O nanoparticles and after two months of storage at ambient condition. To prove the stability of Cu_2O NPs, PXRD of sample IA were recorded immediately after preparation and after twomonths of storage. As prepared Cu_2O nanoparticles discerns Cu_2O cubic phase (Figure 2.5, Curve-I). Cu_2O stored for two month at ambient condition was subjected to analysis. The corresponding PXRD patterns clearly indicate the Cu_2O (Figure 2.5, Curve-I) converted into CuO nanoparticles(Figure 2.5, Curve-II). Stability test revealed that Cu_2O nanoparticles oxidize into CuO when they come in contact with atmospheric oxygen.
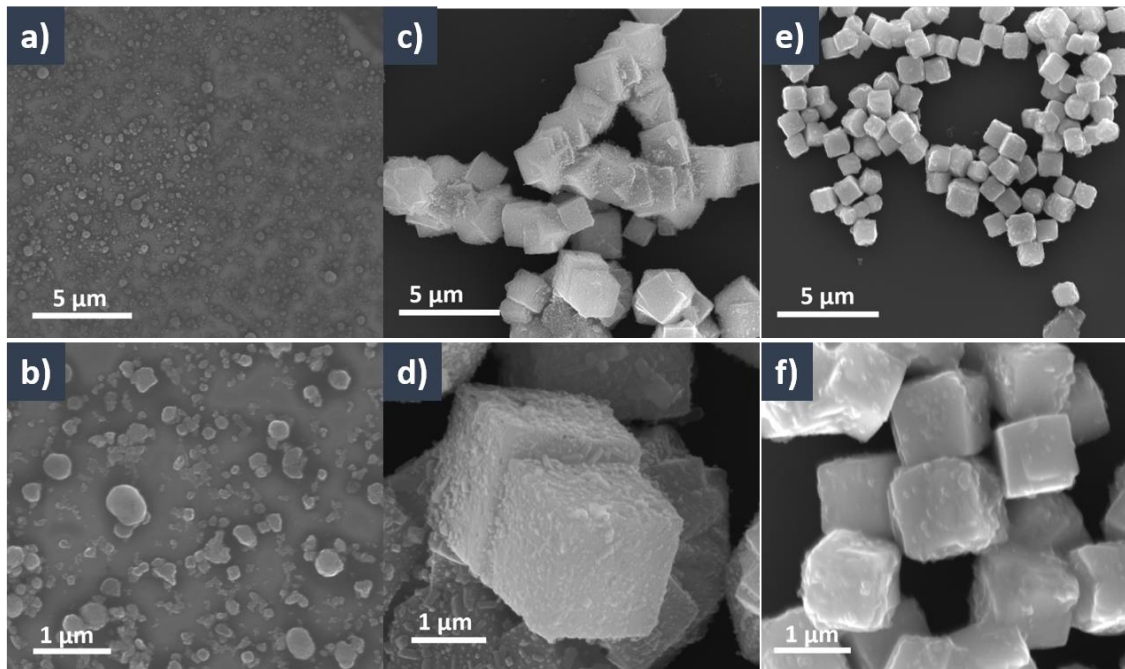
Figure 2.6: SEM image of Cu₂O nanoparticles synthesized by microwave in batch at pH 2 a) and b), pH 4 c) and d), and pH 6.5 e) and f).

The TEM images showed that at highly acidic (sample IA) conditions poly-disperse quasi spherical particles ranging from 100-200 nm (Figure 2.6 a, and b) are formed. Interestingly, the morphology of the particles obtained in case samples IIA and IIIA turned out to be cubic (Figure 2.6, c, d, e, and f). Cubes formed at pH 4 (sample IIA) are around a 2.9 μm size, which is bigger in size than those formed at pH 6.5 (sample IIIA). The average size of particles formed at pH 6.5 is 1.25 μm. The formation of cube-shaped Cu₂O particles has been well-reported in the literature.[13] The formation of cube morphology is ascribed to the cubic crystalline phase of Cu₂O and the formation kinetics. It has been established that when the reaction is carried out under slow conditions, the formation of the cubic morphology of Cu₂O is facilitated. To know influence of reaction

time upon morphology and formation of Cu_2O cubes at acidic condition pH 6.5, we have carried out synthesis at different reaction time (10, 15, and 20 min).
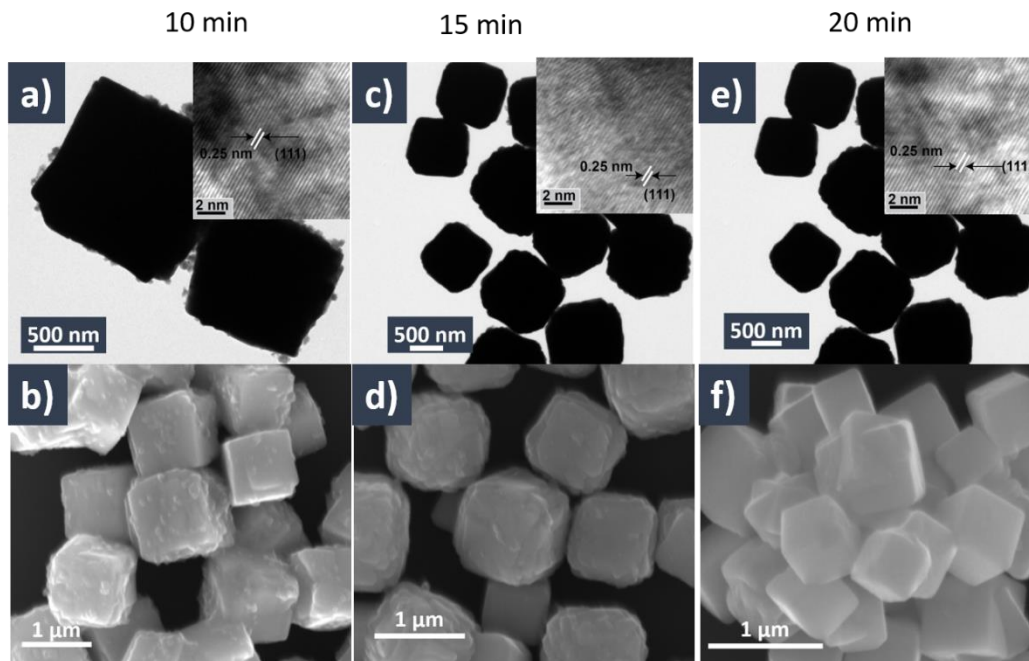
Figure 2.7: TEM images of Cu_2O particles synthesized at a) 10 min c) 15 min e) 20 min reaction time and SEM images b) 10 min, d) 15 min and f) 20 min.

TEM and SEM images show a change in morphology of Cu_2O cubes with increasing reaction time (see Figure 2.7). The surface of samples IA, synthesized at 10 min reaction is rough in comparison to samples synthesized at 15, and 20 min reaction time (see Figure 2.7). Formation of Cu_2O cubes can be ascribed to the intrinsic crystal structure of Cu_2O, which is cubic.

2.3.3 B) Basic pH
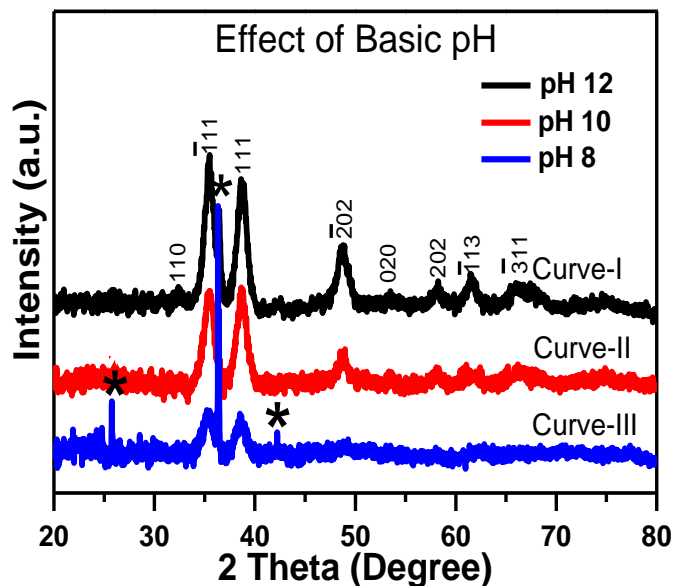
Figure 2.8: PXRD patterns of copper oxides nanoparticles synthesized at basic pH (Curve-I, pH 12), (Curve-II, pH 10)and (Curve-III, pH 8).

Subsequently, the same $Cu(ac)_2$ solution was subjected to microwave heating under basic pH conditions, namely, pH = 8, 10, and > 12. These pHs were attained by addition of 30, 70, and 100 μL of 0.1 M of NaOH solution to $Cu(ac)_2$ solution. The color of the reaction product obtained under the basic condition was black. We refer to the products of the reaction obtained at these basic pH conditions as sample IB (pH = 8), sample IIB (pH = 10) and sample IIIB (pH > 12). The PXRD analysis suggested that a pattern of sample IB comprised both phases of CuO and Cu_2O (Figure 2.8, curve III). On another hand, the XRD traces of sample IIB (Figure 2.8, curve-II) and sample IIIB (Figure 2.8, curve-I) correspond to a pure CuO phase (JCPDS card number 41-0254), and

no peak corresponding to the Cu_2O phase could be detected in these samples, and these samples were analyzed under TEM microscope
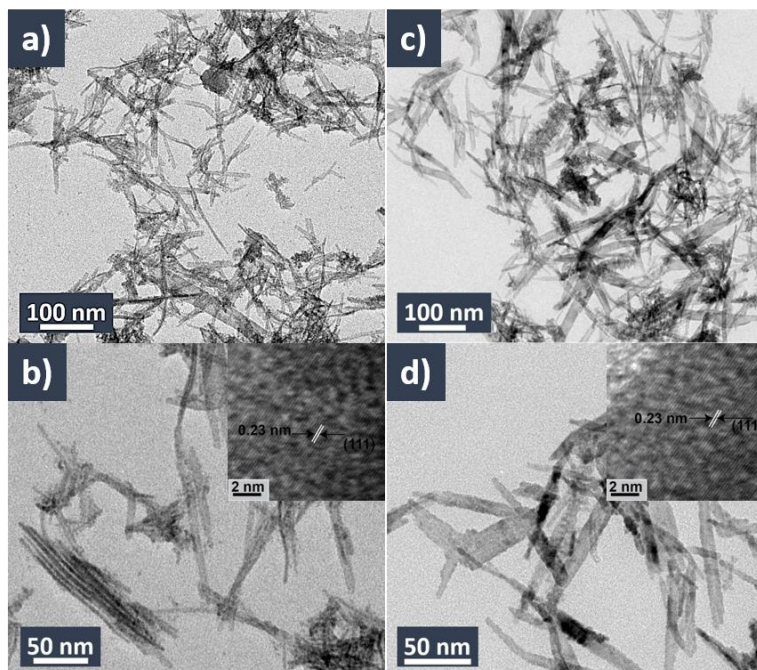
Figure 2.9: TEM images of CuO nanoparticles synthesized in batch by microwave at basic condition a) and b) pH 10 and c) and d) pH 12.

TEM images of samples IIB and IIIB exhibit nanobelts like morphology (Figure 2.9, a, and c), which seems to be resulting from the aggregates of small nanoparticles. The distance between lattice planes displayed in the inset of images in figure 2.9 (b and d) correspond to 0.23 nm, which is attributed to 111 planes of the monoclinic CuO phase. Here again, the formation of needle-shaped CuO nanoparticles is a well-observed phenomenon in literature, which is a reflection of the monoclinic crystalline nature of CuO. Further, we have studied the effect of reaction time at pH 12. There is no significant change in shape, size and morphology of CuO nanoparticles (see the figure 2.10).
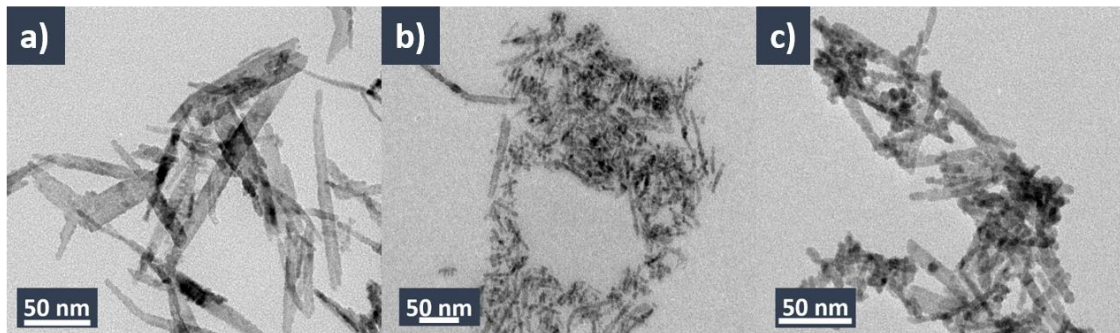
Figure 2.10: TEM images of CuO nanoparticles synthesized by microwave-assisted synthesis in batch at pH 12 by varying reaction time a) 1 min b) 2 min c) 3 min.

2.3.4 Effect of concentration

Table 2.1. Effect of concentration on the size and gravimetric % yield of CuO nanoparticles.

Concentration (M)	Crystallite size (nm)	% Yield (Gravimetric)
0.19	5.10	66
0.05	3.36	71

In order to adapt the batch process in a continuous flow synthesis, one of the critical features was the synthesis of nanoparticles should be less time-consuming. Here, we are ignoring synthesis of Cu_2O which consumes more time which is not amenable to adopt for microwave-assisted flow synthesis due to considering long terms technological problems, like the sustainability of microwave for continuous irradiation. Effect of $Cu(ac)_2$ concentration has been investigated.0.19M and 0.05 M concentrations of $Cu(ac)_2$ in 16 mL benzyl alcohol were selected to study the effect of concentration while keeping same reaction time see the Table No. 1.
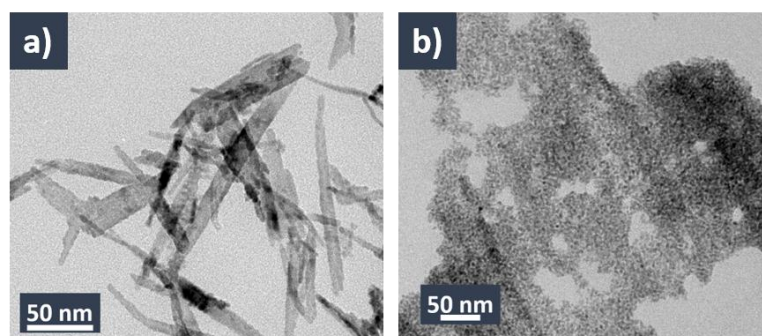
Figure 2.11: TEM images of CuO nanoparticles synthesized at a) 0.19M and b) 0.05M concentration of Cu(ac)$_2$ respectively.

At high concentration, CuO shows nanobelts structure along with some small size CuO nanoparticles (see Figure 2.11 a). The structure of nanobelts is attributed to monoclinic structure or topotactic character of Cu(ac)$_2$ translated to CuO due to some undissolved Cu(ac)$_2$ into benzyl alcohol. On other hand, CuO obtained at lower concentration (0.05M) are smaller in size (3-4 nm) and spherical in nature see Figure 2.11b). Change in concentration has impact on gravimetric yield of CuO nanoparticles. Percentage yield of CuO is increased when concentration decreased see Table No. 1. This increased yield attributed to solubility of Cu(ac)$_2$ into benzyl alcohol at 0.05 M and amount of added NaOH completely reacts with Cu(ac)$_2$ compare to 0.19 M concentration and increase the percentage gravimetric yield of CuO nanoparticles.

2.3.5 Effect of batch volume
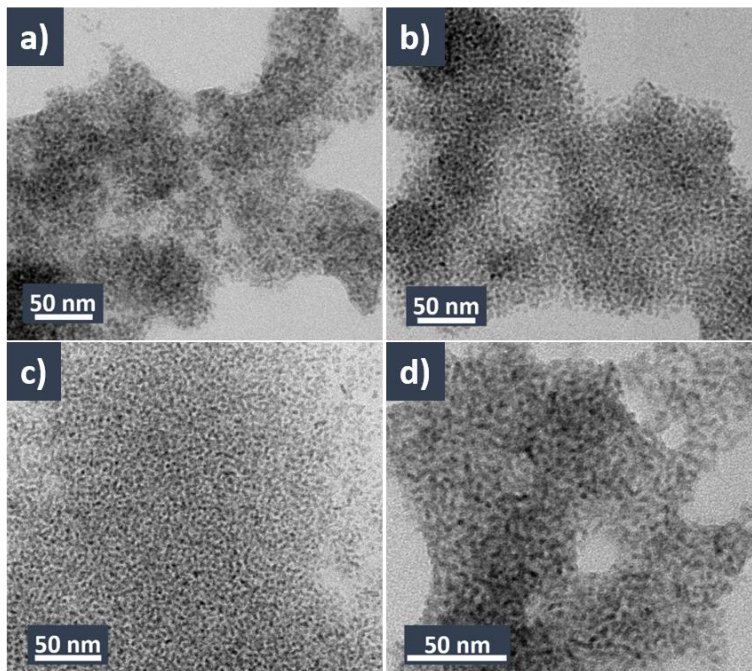
Figure 2.12: TEM images of CuO nanoparticles synthesized at different batch volume under microwave for 1 min a) 16 mL, b)25 mL, c) 50 mL and d) 100 mL.

After optimizing concentration, we wanted to investigate effect of batch volume on morophology of nanoparticles and percentage yield. Keeping all reaction condition same, synthesis of CuO nanoparticles was carried out at 16, 25, 50, and 100 mL batch volumes under microwave irradiation. The resulting product washed, dried, and analyzed under TEM. There is no significant effect on size and shape of CuO nanoparticless by varying batch volume(see Figure 2.12). The yield of CuO nanoparticles was varied with the batch volume. Percentage yield of CuO at 16 and 25 mL reaction volume is nearly equal 71% and 68% respectively. As increase in batch volume from 50 mL and 100 mL the percentge yields are decreased. For 50 mL and 100 mL yields are 50% and 45% respectively (see Table No. 2.2). This decrease in yield is ascribed to increase in

temperature as batch volume increases (see the Figure 2.13). Microwave spot size (area of microwave flux) is limitted for heating small volumes hence entire solution is not heated up uniformly. During microwave irraditon, small volume gets heated and transfers the heat to remaining volume when microwave spot size is small, hence, increase in the temperature at larger volume is very slow. This slow rise in temperature at 50 ml and 100 mL batch lead to low percentage yields.

Table 2.2. Gravimetric estimation of percentage yield of CuO nanoparticles under microwave radiation for 1 min having batch volume 16 mL, 25 mL, 50 mL, and 100 mL.

Volume (mL)	Crystallite size (nm)	% Yield (Gravimetric)
16	3.36	71
25	3.94	68
50	3.38	50
100	3.74	45
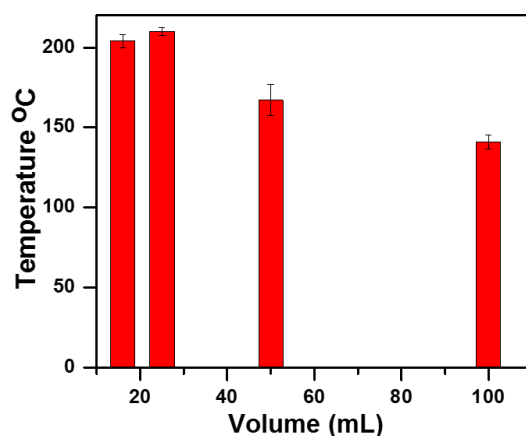
Figure 2.13: Temperature profile at different batch volumes (16 mL, 25 mL, 50 mL, and 100 mL).

2.3.6 Flow synthesis of CuO nanoparticles
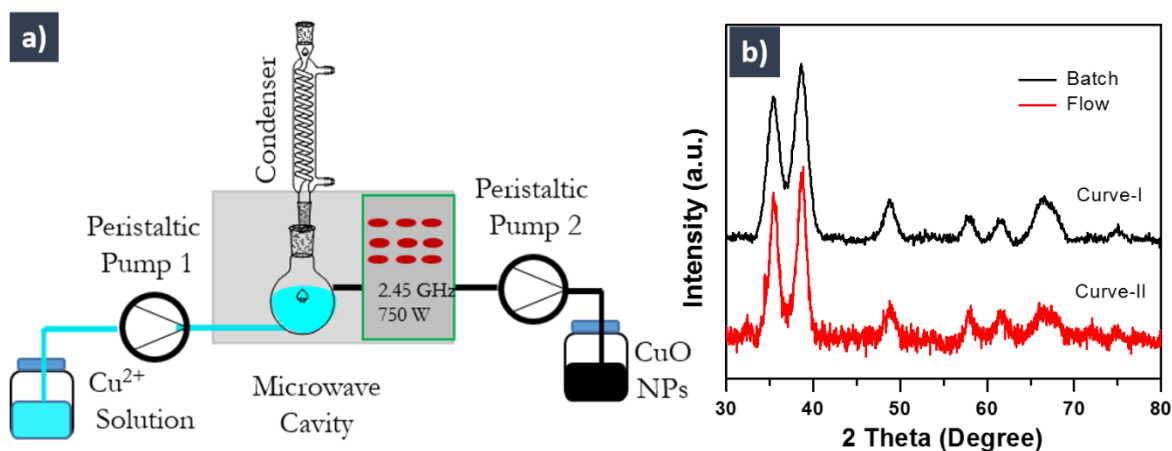
Figure 2.14: a) Schematics of setup for microwave assisted flow synthesis of CuO nanoparticles. b) PXRD patterns of CuO NPs synthesized by microwave assisted batch (Curve-I) and flow (Curve-II).

The parameters optimized in batch process were considered to carry out flow synthesis of CuO nanoparticles. 25 mL CSTR was fabricated to conduct continuous flow synthesis experiments by using experimental setup shown in the figure 2.14 a. All reaction parameters (pH, concentration and volume) maintained as described in batch process, flow rate for $Cu(ac)_2$ solution was 25 mL/min. The product collected was washed, dried and analyzed under PXRD and TEM instrument. Product obtained by flow has CuO monoclinic phase which is in agreement with batch samples prepared at pH12 (see Figure 2.14 b). TEM image of product displays that CuO nanoparticles are spherical in nature (see the Figure 2.15). The size of CuO nanoparticle is 4.6 nm which in good agreement with batch samples (3.94 nm). Thus, we have successfully translated batch process parameter to a continuous flow process that can help us synthesize these particles at a higher production rate (61 g / day).
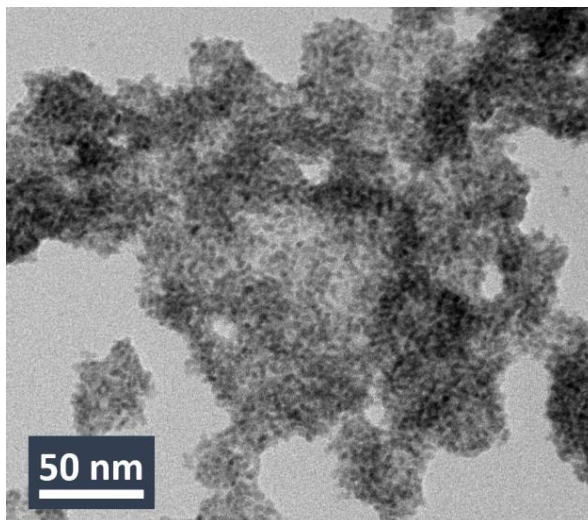
Figure 2.15: TEM image of CuO nanoparticles synthesized by microwave-assisted flow synthesis.

2.4 Applications

2.4.1 Gas sensing

Once phase pure synthesis of CuO and Cu_2O nanoparticles was achieved. We sought the use of these materials as sensor for reducing gaseous because of p-type of semiconducting nature. CuO nanoparticles prepared in batch at pH12 and Cu_2O nanomaterial in batch at acidic pH were selected for gas sensing. Before testing as gas sensor, we estimated the band gap of selected material by UV-visible instrument and cyclic voltammetry. The band gap of the copper oxides play crucial role in semiconducting devices (gas sensing devices).

2.4.1. A) Optical and electronic properties

The optical spectra of the obtained powders were recorded to determine the optical band gap and transmittance. Figure 2.16 (a, and b) displays the representative spectra obtained from samples IIIA and IIIB, respectively. We would like to mention here that optical spectra characteristics of samples IA and IIA resembled that of sample IIIA. Thus, we could conclude that the optical spectra depend more on the crystalline phase of the sample with little or no dependence on the size of the particles. The band gaps of these materials were extracted from Tauc's plot. For sample IIIA (Cu_2O), the band gap corresponds to 2.07 eV (Figure 2.16, a). The band gap for sample IIIB (CuO) was 1.42 eV. The transmittances of sample IIIB (CuO) was measured by drop-casting a thin film of these on quartz plate (Figure 2.16,b). We notice that films formed with sample IIIB (CuO) display good transmittance values in the 200 – 650 nm region, making it a good candidate for different light harvesting and sensor type applications.

Unfortunately, sample IIIA (Cu$_2$O) did not form good films and yielded in poor transmittance spectra despite repeated attempts.
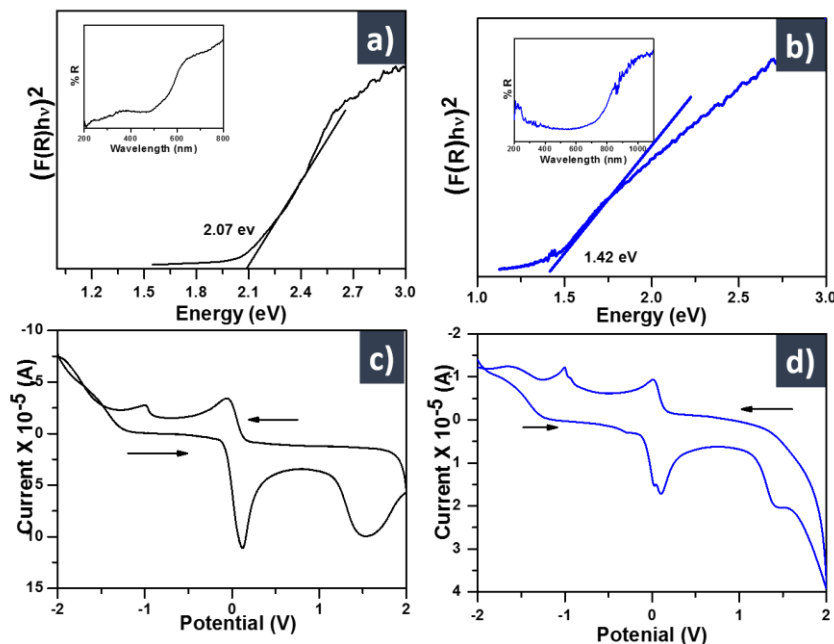
Figure 2.16. Tauc's plots obtained from the diffuse reflectance spectrometer (DRS) spectra of (a) sample IIIA and (b) sample IIIB. The insets in (a) and (b) display the actual DRS spectra. Cyclic voltammograms of (c) sample IIIA and (d) sample IIIB.

We also investigated the energy band structure of samples IIIA and IIIB using cyclic voltammetry in an inert atmosphere. A glassy carbon electrode was used as a working electrode. Dry acetonitrile was used as a solvent and 0.1 M of tert-butyl ammonium perchlorate was used as an electrolyte. 0.01 M of ferrocene was used as an internal standard. The oxidation and reduction peaks centered on 0 V are due to ferrocene, which was used as an internal standard. The onset of first oxidation with respect to the internal standard was used for the determination of the HOMO level. From the cyclic voltammetry valence band and conduction band, edges have been determined using equation 4 and 5.[34]

$$E_{HOMO} = -(E_{ox}^{onset} + 4.8eV)$$ (4)

$$E_{LUMO} = -(E_{red}^{onset} + 4.8eV)$$ (5)

The onset reduction and oxidation potential for sample IIIA were –0.88 V and 1.17 V, respectively (Figure 2.16, c). This corresponds to an energy band gap of 2.0 eV. The onset reduction potential and oxidation potential of sample IIIB were found to be – 0.64 V and 1.11 V, respectively (Figure 2.16, d). From these, energy band gap of CuO was determined to be 1.7 eV. Thus, the band gaps estimated from cyclic voltammetry are in reasonably good agreement with those determined from optical spectra. This again confirms our assertion that the band gap mainly dependent on the phase of the material and not on the particle size.

2.4.1. B) Device fabrication:
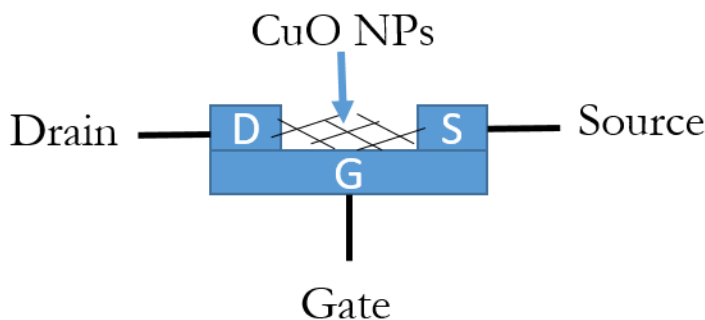
Figure 2.17: Schematics of field effect transistor device.

The FET devices were manufactured by drop casting the ethanol solution of Sample IIIA (Cu_2O) or sample IIIB (CuO) on prefabricated transistor electrodes shown in figure 2.17. The FET device contains n-doped silicon as a gate and SiO_2 as an insulating

layer (capacitance - 14nF/cm2). Gold source and drain electrode was used. This was purchased from Fraunhofer microelectronics institute. These electrodes were washed thoroughly using acetone and iso-propanol and dried with hot air. The sample IIIA (Cu_2O) or sample IIIB (CuO)was drop casted on FET device and heated at 100 °C to evaporate the solvents. After that in Ar atmosphere this was exposed to hydrazine vapor and again heated at 100 °C before I-V measurements of same device.

2.4.1. C) FET Characteristic for hydrazine gas sensing
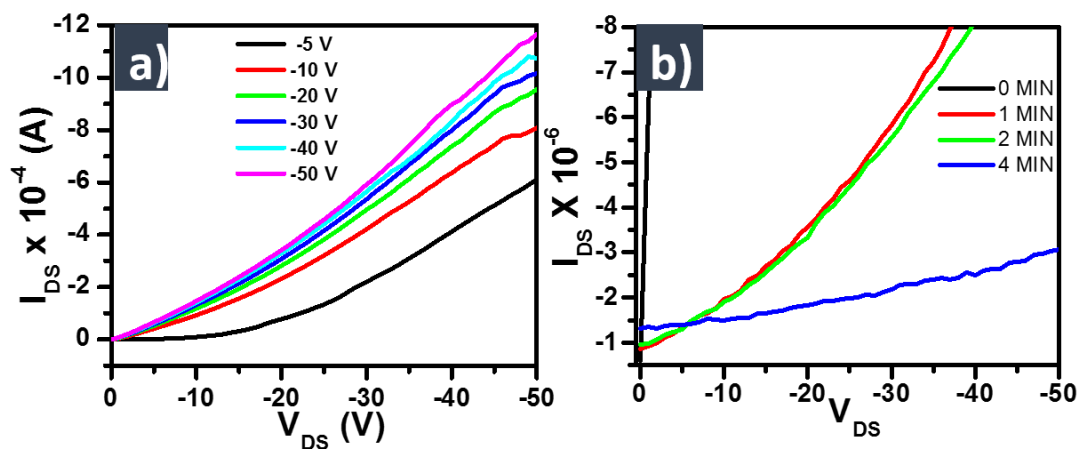
Figure 2.18: I–V curves of Sample IIIA (a) before hydrazine vapor exposure under different gate voltage. (b) After hydrazine vapor exposure for different time (the gate voltage used was -20 V).

We further probed the FET characteristic of representative samples IIIA and IIIB. For this, a thin film of the sample was cast over the FET substrates. The measurement was carried out under ambient condition. The V_D to I_D curve at different gate voltages for the sample IIIB (CuO nanobelt) is displayed in figure 2.18 a).Field effect transistors were

fabricated to determine the charge carrier mobility of the transparent material. CuO nanoparticles can be used as a hole transport layer in organic and hybrid solar cells. An increase in source-drain current with respect to source-drain voltage under negative gate voltage was observed for this sample. The output characteristic curves showed linear regime with small gate modulation. This is likely due to the bulk conductivity of CuO. Hole carrier mobility was calculated from the linear regime, which was found to be 3.57×10^{-2} cm^2 V^{-1} s^{-1}. A similar, experiment with nanoparticles of sample IIIA (Cu$_2$O spheres and cubes) did not yield discernible change in the drain current as a function of applied gate voltage. We attributed this to the lower stability and poor film forming ability of Cu$_2$O. It was reported that Cu$_2$O absorbs the oxygen, which leads to surface to be charged with oxygen. These surface adsorbed O$^-$ and O^{2-} species decrease carrier hole density in the surface charge layer and increase of resistance.[35] Finally, we wanted to examine FET response of CuO nanomaterial (sample IIIB) after exposing it to hydrazine vapor. The device fabrication is discussed in section 2.4.2. Accordingly, we measured dependence of drain-source current (I$_{DS}$) on the drain-source voltage (V$_{DS}$) at an operated gate voltage (V$_G$) of 20 V of the CuO FET device by exposing it to hydrazine vapor. As shown in Figure 2.18 b, the exposure of CuO to hydrazine vapor showed a decrease in I$_{DS}$. This decrease in current was attributed to conversion of CuO into Cu$_2$O on the surface of the material.
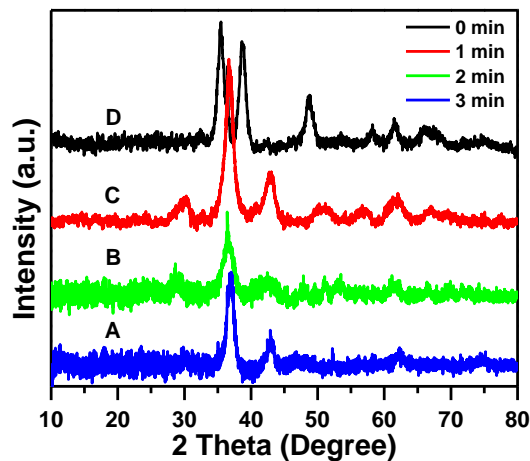
Figure 2.19: X-ray diffraction spectrum of CuO nanoparticles (Sample IIIB) after exposing to hydrazine at different time scale (0 min, 1 min, 2 min, and 4 min) prepared using microwave treatment.

Indeed, the PXRD pattern of sample IIIB exposed to hydrazine indicates a partial conversion of CuO into Cu_2O due to the reducing action of hydrazine vapor (see Figure 2.19). On the other hand, the value of I_{DS} decreases with exposure time due to an increase in the Cu_2O phase.
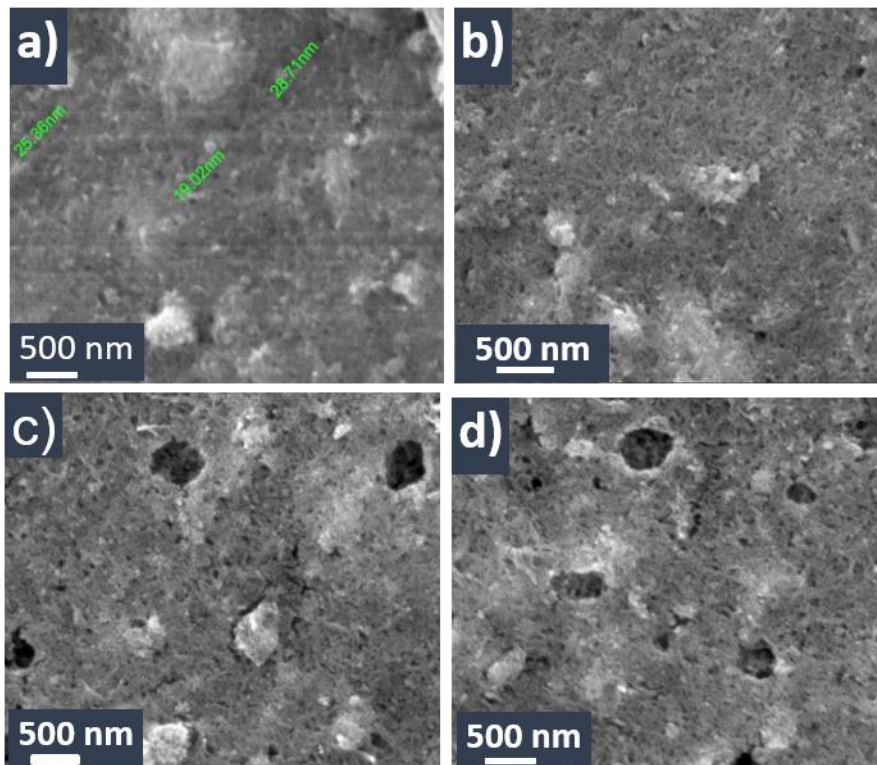
Figure 2.20: SEM images of CuO nanoparticles (Sample IIIA) after exposing to hydrazine at different time scale (0 min,1 min, 2 min, 4 min) prepared using Cu-AC under microwave treatment.

The SEM image of CuO exposed to hydrazine vapors at a different time interval reveals a morphological change wherein, some discontinuities in the film were seen to develop (see Figure 2.20). This discontinuous nature ultimately decreases hole mobility of the CuO thin film. In addition to that, since the HOMO energy level of CuO is commensurate with the work function of gold source - drain electrodes, injection of charge from gold metal electrodes to the HOMO of CuO nanomaterial is allowed. This kind of charge injection might be unfavorable in the case of the Cu_2O system.

2.4.2 Nanofluids

Dispersing metal and metal oxide nanoparticles in fluids can be called as nanofluids and they usually exhibit good thermal conducting properties compared with traditional fluids (water, mineral oil and ethylene glycol) used for heat transfer and fluids containing micro-particles.[36, 37] In technology evolution, microelectronics are included in many devices, during functioning of devices it generates heat which needs to be taken care. Nanofluids are the viable option due to high thermal conductivity, and it avoids clogging in the micro channel. Recently, dispersion of nanoparticles has been examined for fundamental properties and potential applications. Various metal oxide nanoparticles were tested for thermal conducting application such as Al_2O_3, CeO_2, TiO_2, and CuO nanoparticles.[38, 39] The thermal conductivity of CuO is33 W/m K which could be used for making nanofluids for the heat exchanger.[40] The thermal conductivity of ethylene glycol is 0.25 W/m K, which has been used as heat transfer fluid in various engines as coolants. Here, we want to investigate heat transfer capabilities of CuO nanofluids, in which CuO used was synthesized in batch and flow method.
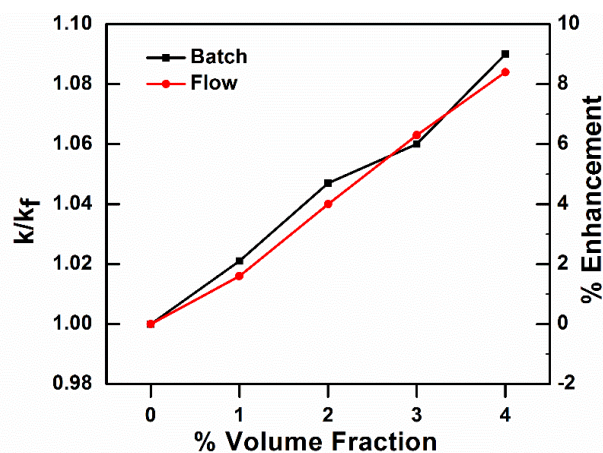
Figure 2.21: Measurement of thermal conductivity of CuO nanofluid in ethylene glycol.

To study thermal conductivity, CuO suspension was prepared by adding CuO nanoparticles into the ethylene and kept for sonication for 1h. After sonication, resulting suspension was stable and allow to cool at room temperature and further taken for thermal conductivity measurement.Transient hot-wire apparatus was used to measure the thermal conductivity of CuO nanofluids. The apparatus has platinum wire coated with teflon. To measure thermal conductivity, CuO nanofluids was added into the glass test tube. It was observed that the thermal conductivity enhancement for CuO nanofluids increases almost linearly with the volume fraction (see Figure 2.21). Nanofluids made by CuO nanoparticles synthesized in batch and flow method exhibit an almost similar improvement in thermal conductivity of ethylene glycol. 9% and 8.8% enhancement were observed for CuO nanoparticle prepared in batch and flow, respectively. Though dispersion of CuO nanoparticles shows enhancement, we produce CuO in large quantity by continuous flow synthesis. Hence, it could be used in the heat exchanger for cooling application in the engine or microelectronics.

2.5 Conclusions

In this chapter, phase pure copper oxides was synthesized in short time, involving minimum reagents, and energy efficiently using microwave-assisted synthesis from single precursor. Change in pH plays an important role to produce phase pure Cu_2O (acidic pH) and CuO (basic pH) nanoparticles. At acidic condition, benzyl alcohol acted as mild reducing agent that reduce Cu^{2+} into Cu^+ to get Cu_2O NPs. Optimized batch parameters such precursors, pH, concentration, and batch volume produced smaller size (~ 3.5 nm) CuO nanoparticles. Batch process parameters were successfully extended to continuous flow process for synthesis of smaller size(~ 4.6 nm) CuO nanoparticles. The production rate of CuO nanoparticles by continuous flow process is 61 g/day. CuO nanoparticles show good activity for gas sensing application as well as CuO nanofluids shows enhancement in thermal conductivity of ethylene glycol. Microwave-assisted flow synthesis strategy could be used to synthesize functional nanomaterial such as binary metal oxide, bimetallic and hybrid nanoparticles.

2.6 References

1.   Liu, M. S.; Lin, M. C.; Huang, I. T.; Wang, C. C. *Chem. Eng. Technol.* **2006,** 29, 72-77.

2.   Zhang, L.; Yuan, F.; Zhang, X.; Yang, L. *Chem. Cen. J.* **2011,** 5, 75.

3.   Roduner, E. *Chem. Soc. Rev.* **2006,** 35, 583-592.

4.   Park, J. C.; Kim, J.; Kwon, H.; Song, H. *Adv. Mater.* **2009,** 21, 803-807.

5.   Zhang, J.; Liu, J.; Peng, Q.; Wang, X.; Li, Y. *Chem. Mater.* **2006,** 18, 867-871.

6.   Morales-Guio, C. G.; Liardet, L.; Mayer, M. T.; Tilley, S. D.; Grätzel, M.; Hu, X. *Angew. Chem. Int. Ed* **2015,** 54, 664-667.

7. Meyer, B.; Polity, A.; Reppin, D.; Becker, M.; Hering, P.; Klar, P.; Sander, T.; Reindl, C.; Benz, J.; Eickhoff, M. *Phys. Stat. Sol. (b)* **2012,** 249, 1487-1509.

8. Hassan, A. A.; Sandre, O.; Cabuil, V.; Tabeling, P. *Chem. Commun.* **2008**, 1783-1785.

9. Salazar-Alvarez, G.; Muhammed, M.; Zagorodni, A. A. *Chem. Eng. Sci.* **2006,** 61, 4625-4633.

10. Zhang, D.; Wu, F.; Peng, M.; Wang, X.; Xia, D.; Guo, G. *J. Am. Chem. Soc.* **2015,** 137, 6263-6269.

11. Zhong, Z.; Ng, V.; Luo, J.; Teh, S.-P.; Teo, J.; Gedanken, A. *Langmuir* **2007,** 23, 5971-5977.

12. Chang, Y.; Teo, J. J.; Zeng, H. C. *Langmuir* **2005,** 21, 1074-1079.

13. Gou, L.; Murphy, C. J. *Nano Lett.* **2003,** 3, 231-234.

14. Bai, Y.; Yang, T.; Gu, Q.; Cheng, G.; Zheng, R. *Powder Technol.* **2012,** 227, 35-42.

15. Yu, Y.; Du, F.-P.; Jimmy, C. Y.; Zhuang, Y.-Y.; Wong, P.-K. *J. Solid State Chem.* **2004,** 177, 4640-4647.

16. Luo, Y.; Tu, Y.; Ren, Q.; Dai, X.; Xing, L.; Li, J. *J. Solid State Chem.* **2009,** 182, 182-186.

17. Ho, J.-Y.; Huang, M. H. *J. Phys. Chem. C* **2009,** 113, 14159-14164.

18. Cao, M.; Hu, C.; Wang, Y.; Guo, Y.; Guo, C.; Wang, E. *Chem. Comm.* **2003**, 1884-1885.

19. Wang, D.; Mo, M.; Yu, D.; Xu, L.; Li, F.; Qian, Y. *Crys. Growth Des.* **2003,** 3, 717-720.

20. Liang, Z.-H.; Zhu, Y.-J.; Cheng, G.-F.; Huang, Y.-H. *J. Mater. Sci.* **2007,** 42, 477-482.

21. Li, L.; Ren, J. *Mater. Res. Bull.* **2006,** 41, 2286-2290.

22. Dar, M. I.; Chandiran, A. K.; Gratzel, M.; Nazeeruddin, M. K.; Shivashankar, S. A. *J. Mater. Chem. A* **2014,** 2, 1662-1667.

23. Ai, Z.; Deng, K.; Wan, Q.; Zhang, L.; Lee, S. *J. Phys. Chem. C* **2010,** 114, 6237-6242.

24. Bilecka, I.; Djerdj, I.; Niederberger, M. *Chem. Comm.* **2008**, 886-888.

25.   Pinna, N.; Neri, G.; Antonietti, M.; Niederberger, M. *Angew. Chem. Int. Ed.* **2004,** 43, 4345-4349.

26.   Niederberger, M.; Antonietti, M. *Nanomaterials Chemistry: Recent Developments and New Directions* **2007**, 119-137.

27.   Pinna, N.; Garnweitner, G.; Antonietti, M.; Niederberger, M. *Adv. Mater.* **2004,** 16, 2196-2200.

28.   Niederberger, M.; Bartl, M. H.; Stucky, G. D. *Chem. Mater.* **2002,** 14, 4364-4370.

29.   Zhou, S.; Garnweitner, G.; Niederberger, M.; Antonietti, M. *Langmuir* **2007,** 23, 9178-9187.

30.   Pinna, N.; Niederberger, M. *Angew. Chem. Int. Ed.* **2008,** 47, 5292-5304.

31.   Zhu, Y.-J.; Chen, F. *Chem. Rev.* **2014,** 114, 6462-6555.

32.   Richel, A.; Nicks, F.; Laurent, P.; Wathelet, B.; Wathelet, J.-P.; Paquot, M. *Green Chem. Lett. Rev.* **2012,** 5, 179-186.

33.   Ganu, G. **1991**.

34.   Kumar, A.; Bokria, J. G.; Buyukmumcu, Z.; Dey, T.; Sotzing, G. A. *Macromolecules* **2008,** 41, (19), 7098-7108.

35.   Zhang, J.; Liu, J.; Peng, Q.; Wang, X.; Li, Y. *Chem. Mater.* **2006,** 18, 867-871.

36.   Choi, S. U.; Eastman, J. A. *Enhancing thermal conductivity of fluids with nanoparticles*; Argonne National Lab., IL (United States): 1995.

37.   Das, S. K.; Choi, S. U.; Yu, W.; Pradeep, T., *Nanofluids: science and technology*. John Wiley & Sons: 2007.

38.   Khaleduzzaman, S.; Saidur, R.; Mahbubul, I.; Ward, T.; Sohel, M.; Shahrul, I.; Selvaraj, J.; Rahman, M. *Ind. Eng. Chem. Res.* **2014,** 53, 10512-10518.

39.   Kim, J.; Park, Y.-S.; Veriansyah, B.; Kim, J.-D.; Lee, Y.-W. *Chem. Mater.* **2008,** 20, 6301-

6303.

40.   Liu, M. S.; Lin, M. C.; Huang, I. T.; Wang, C. C. *Chem. Eng.Technol.* **2006,** 29, 72-77.

Chapter 3

Batch and Flow Synthesis of Palladium

Supported Nickel Nanoparticles
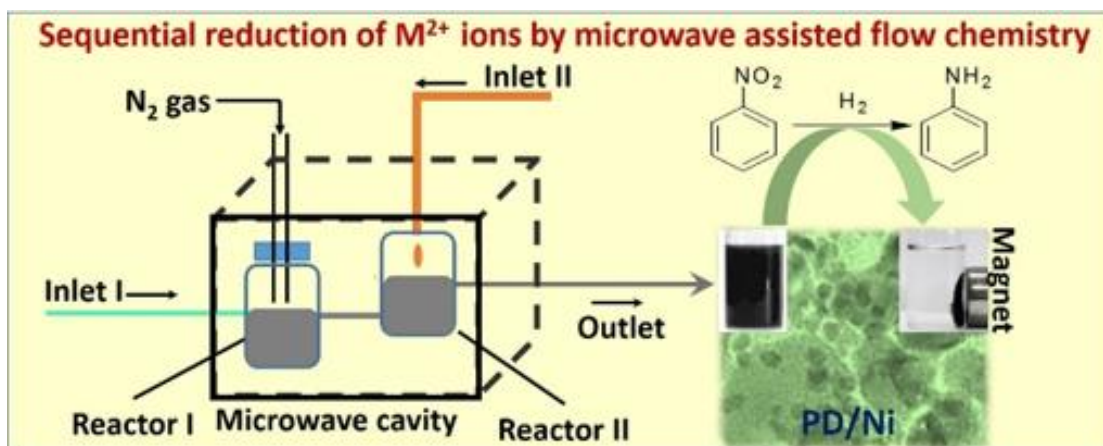
3.1 Introduction

In the previous chapter the microwave-assisted batch and flow synthesis of the semiconducting copper oxides nanoparticles is reported.[1] There are other types of nanomaterials such as metallic, bimetallic, inorganic-organic and organic nanoparticles which can also be synthesized in a more efficient manner. Among these nanomaterials, bimetallic nanoparticle have got tremendous attention due to their impressive magnetic and catalytic properties.[2, 3] More importantly the catalytic properties of bimetallic nanoparticle show more activity than their monometallic counterpart. This makes these material find use as a catalyst for various organic transformation.[4] Hence, the demand for bimetallic nanomaterial has increased abruptly.[5] The catalytic properties of such materials are highly sensitive to the size, shape, and composition of nanomaterials. A slight fluctuation in reaction parameter can lead to change in shape, size, and composition of nanomaterials. Thus the controlled synthesis of a bimetallic nanomaterials at large scale remains challenging. In order to overcome this challenge, it is necessary to understand the effect of each synthesis parameter and establish new synthetic protocol involving fewer reagents/precursors, rapid synthesis that is amenable to scale-up. In chapter 2, we have shown that a microwave-assisted flow synthesis is a viable option for controlled and scalable synthesis.

Over last few years, the continuous flow synthesis of nanoparticle by microwave-assisted method has become an important scale-up option. Tang *et al.* synthesized Au nanoparticle using a microwave-assisted flow reactor.[6] Herman *et al.* showed the use of segmented flow microwave for the synthesis of size-controlled PdSe nanoparticle.[7] Suzuki *et al.* exploited a polyol process for continuous flow synthesis of monodisperse

silver nanoparticle by using $AgNO_3$ and PVP as a stabilizer.[8] In a recent report, Kunal *et al.* disclosed the scalable synthesis of bimetallic RhAg alloy nanoparticle using microwave-assisted continuous flow synthesis method.[9] This literature report shows that microwave-assisted synthesis is utilized for the preparation of monometallic and semiconducting nanoparticle involving multiple reagents. Therefore, development of the same protocols to synthesize bimetallic system could be tedious as it would need complex downstream processing. To circumvent such issues in this chapter a simple procedure for the synthesis of palladium supported on nickel (Pd/Ni) in a batch and a continuous flow manner is presented, where the solvent can be recycled and reused.

Pd@Ni, and PdNi alloy exhibit excellent catalytic activity for the cross coupling and hydrogenation reaction than the monometallic nanoparticle.[10, 11] Initially, we started with the synthesis of Ni nanoparticle from $Ni(ac)_2$ in batch as well as flow synthesis is demonstrated. In the first phase of synthesis, Ni nanoparticle are produced in a batch mode, which is further extended to flow synthesis. Once the protocol for synthesis of Ni nanoparticle is optimized, we used these nanoparticle as a precursor for deposition of Pd in batch and flow synthesis modes. Here, we have exploited microwave-assisted protocol for the synthesis of deposition of Pd on Ni nanoparticle in the shortest period and reproducible manner using fewer reagents. As discussed in the previous chapter, the benzyl alcohol was used as a solvent and reducing agent under microwave conditions to obtain Ni nanoparticle from $Ni(ac)_2$. Further, this protocol was extended for subsequent reduction of Ni^{2+} and Pd^{2+} ions in flow synthesis by optimizing reaction parameters. These batch and flow synthesized Pd/Ni exhibit excellent catalytic activity for hydrogenation of nitro, alkene, and alkyne compounds.

3.2 Experimental section

3.2.1 Chemicals and Materials

Nickel (II) acetate tetrahydrate and palladium (II) acetate (abbreviated as $Ni(ac)_2$ and $Pd(ac)_2$, respectively, in rest of this work), anhydrous benzyl alcohol (99.9% purity), oleylamine (70%), and diphenyl ether (99%) were purchased from *Sigma-Aldrich* and used without any further purification. Palladium on active carbon support (Pd/C) in 5% and 10% palladium loading was received from *Sigma-Aldrich*. Methanol and acetone were used from *Thomas Baker Chemicals*.

3.2.2 Synthesis of Ni nanoparticle

3.2.2. A) Batch synthesis of Ni nanoparticle

62 mg of $Ni(ac)_2$ was mixed with 16 mL of benzyl alcohol in 25 mL round bottom flask and dissolved by sonication for 15 min. The solution of $Ni(ac)_2$ became a clear green solution. (NOTE: [i] $Ni(ac)_2$ is not very soluble in benzyl alcohol, and [ii] Magnetic bar could not be used for stirring due to ferromagnetic nature of Ni, which attracted to magnetic bar led to aggregation of Ni nanoparticle). This resulting solution was purged continuously by bulling with N_2 gas and placed into the microwave oven operated at 700 W and 2.45 GHz frequency for 8.5 min. Black colored precipitate appeared in reaction solution after 8.5 min and microwave irradiation was immediately stopped. Then the reaction flask was allowed to cool to room temperature and the product was separated by applying a magnet externally and the supernant was discarded. Product was washed three times by a mixture of acetone: methanol (1:1 v/v) and dried at 75°C for 12 hrs.

3.2.2. B) Continuous flow synthesis of Ni nanoparticle

For flow synthesis, a 20 mL volume continuous stirred tank reactor (CSTR) connected to the silicon tubing was used for flow synthesis of Ni nanoparticle. The set-up was almost similar as mentioned in figure 3.9, except a CTSR-II and syringe pump. The CSTR placed into microwave oven was attached to the condenser through which a dip tube was inserted and N_2 gas was continuously purged through the dip tube. 150 mL solution of $Ni(ac)_2$ in benzyl alcohol was prepared by maintaining aforementioned batch concentration section 3.2.2. A). Ni^{2+} solution was injected into CSTR by peristaltic pump at flow rate 2 mL/min. Before Ni^{2+} reaches to CSTR, the microwave irradiation was started. Black colored product started appearing in reactor. After a few minutes of formation of black colored precipitate, sparking was observed.

3.2.3 Synthesis of Ni nanoparticle with OAm

3.2.3. A) Batch synthesis of Ni nanoparticle with OAm

After observing the sparking in CSTR as mentioned in section 3.2.1B), the synthesis of Ni nanoparticle was revisited. Here, 0.62 mg of $Ni(ac)_2$ was disperse in 15 mL of benzyl alcohol in 25 mL of round bottom flask by sonication. In resulting dispersion, 1 mL of ollylamine (OAm) was mixed by sonication for 15 min and placed inside the microwave. After 4 minutes of microwave irradiation, black colored product started forming in the round bottom flask, after which microwave irradiation was stopped. Further treatment of the product was same as mentioned in section 3.2.2(A).

3.2.3. B) Continuous flow synthesis of Ni nanoparticle with OAm

The flow setup as mentioned in section 3.2.1B was used for further experiments. 150 mL of Ni^{2+} solution was prepared with benzyl alcohol and OAm by maintaining

above batch concentration. This solution containing OAm was passed into reactor at 4 mL/min to maintain 5 min residence time. Product was collected at a flow rate 4 mL/min from the outlet that is extended outside the microwave using another peristaltic pump operated in suction mode. The rest of the procedure is similar to that mentioned in section 3.2.2(A). Interestingly, no sparks were observed in this case even reaction was continued for a long time (~40 min), which indicated that the Ni does not get deposited.

3.2.4 Sequential reduction of Ni^{2+} and Pd^{2+}

3.2.4 A) Batch synthesis of Pd/Ni with OAm

The same procedure as mentioned in section 3.2.2(A) was followed to study the formation of Ni NP dispersion. 8 mL aliquot of Ni nanoparticle dispersion was taken in 25 mL round flask for Pd/Ni preparation. To this aliquot, 8 mL of 2×10^{-3} M $Pd(ac)_2$ solution of diphenyl ether was mixed by sonication for 2 min and this solution kept into microwave oven for microwave treatment and treated for 4 min. The product obtained was allowed to cool to room temperature and then separated by using a magnet externally. Individual Pd NP was observed in supernatant, which was discarded. Magnetically separated product was washed three times using 50% acetone and 50% methanol mixture and dried in oven at 75°C for 12 hrs.

3.2.4 B) Continuous flow synthesis of Pd supported on Ni support

For sequential reduction of metal ions, the flow steps as shown in figure 9 were used. Ni nanoparticle were obtained in CSTR-I following the procedure as described in section 3.2.1. B). These Ni nanoparticle entered into CSTR-II (24 mL volume) by overflow at a flow rate of 4 mL/min. In CSTR-II, $Pd(ac)_2$ solution of 4×10^{-3} M in

diphenyl ether was injected through syringe pump at 2 mL/min flow rate into Ni nanoparticle solution. The flow rates of Ni nanoparticle and $Pd(ac)_2$ solution were modified in such a way that they experienced a 4 min residence time in CSTR-II under microwave irradiation. As mentioned before, the product was collected through an outlet outside the microwave by continuously withdrawing it using a flexible tube connected to a peristaltic pump to ensure that there is no accumulation of reaction mixture in any CSTR. Separation and drying of this product was carried out as mentioned in section 3.2.4 A).

3.2.5 Procedure for Hydrogenation of Nitro Compound

Hydrogenation of the organic substrate was carried out in a SS316 high pressure autoclave reactor (Anton Parr, USA). In each case, 5 mmol of organic substrate was taken in 100 mL of methanol as a solvent and 20 mg of Pd/Ni catalyst was dispersed in the reaction mixture using sonication for 10 min. The reaction mixture was kept in a stainless steel reactor (SS316) and sealed. Hydrogen gas was filled in the reactor at 20 bar pressure and stirred at 1000 rpm. Aliquots of 2 mL each were removed after 5 min time intervals and analyzed by gas chromatography. After the reaction was completed, the catalyst was separated by applying an external magnet. The catalyst was washed using a mixture of 50% acetone and 50% methanol three times, dried in a vacuum oven at 75°C for 12 hrs, and reused for the next reaction cycle

3.3 Results and discussion

Here, we extended the use of benzyl alcohol to reduce Ni^{2+} and Pd^{2+} ions into corresponding metals. Schematics of the devised two-step scheme is displayed in figure 3.1.

Step – I: Synthesis of Ni NPs

Step – II: Deposition of Pd on Ni NPs
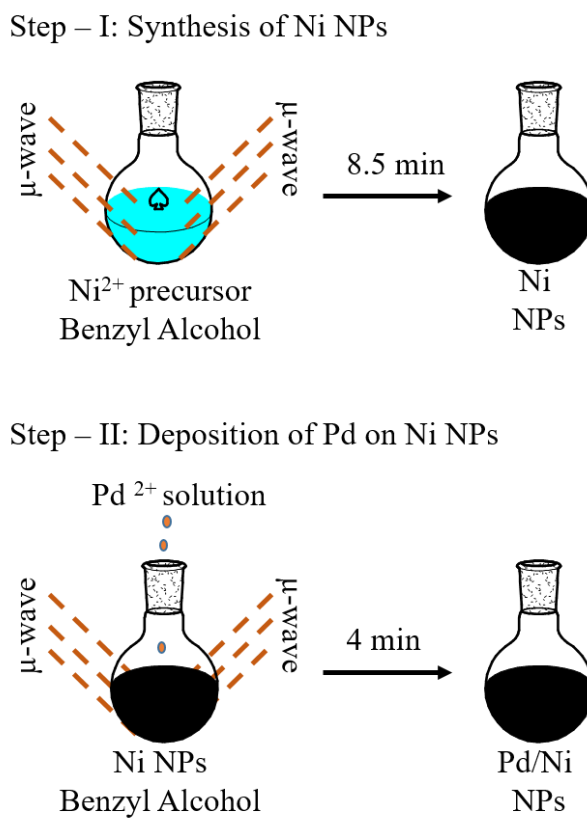
Figure 3.1: Schematics of sequential reduction of Ni^{2+} and Pd^{2+} in batch by microwave- assisted synthesis.

Before venturing to synthesis of Pd/Ni, we began with the microwave-assisted synthesis of Ni nanoparticle in a batch. Ni(ac)$_2$ was not very soluble in benzyl alcohol Ni(ac)$_2$ + benzyl alcohol solution was irradiated for 8.5 min. On the other hand, Conventional heating method required 6h reaction time to accomplish synthesis of Ni nanoparticle using Ni(ac)$_2$ + benzyl alcohol solution. The microwave heating enabled to

enhance reaction rate in comparison to conventional heating technique. The black colored product obtained in the batch was analyzed by PXRD instrument. PXRD patterns discern that product formed is pure FCC structure of Ni metal which in agreement with JCPDS card No. 04-0850 (see Figure 3.2, Curve-I). Formation of Ni nanoparticle proven that benzyl alcohol acted as reducing agent.
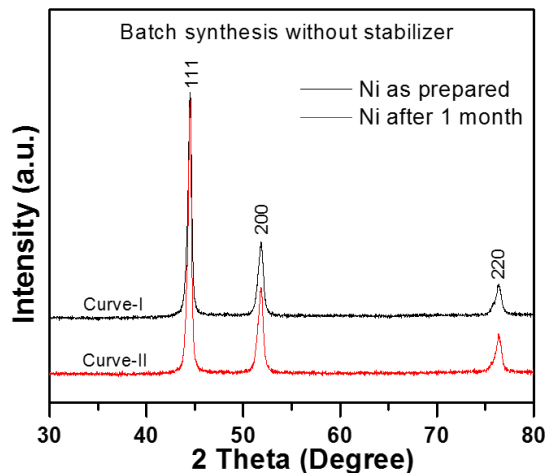
Figure 3.2: X-ray diffraction pattern of Ni nanoparticle prepared by microwave-assisted synthesis in a batch (curve-I) and of Ni nanoparticle stored for a month (curve-II).

If there is not enough passivation on the surface of Ni, the pure Ni nanoparticle are known to oxidize into Ni^{2+}, so we did stability study of the Ni nanoparticle. Ni nanoparticle were stored at ambient condition for a month and once again subjected to measurement of PXRD pattern. No impurities were observed and NiO peak was found to remain present in the recorded PXRD patterns from the original sample (see Figure 3.2 curve-II), which indicates that Ni nanoparticle are stable for a month. Size of Ni nanocrystal deduced from 111 plane using Scherrer equation turned out to be 28 nm. TEM image analysis of Ni nanoparticle clearly shows that Ni nanoparticle are different in size and shape and polydisperse in nature (see Figure 3.3, a and b). The average size

calculated from TEM image analysis is 33 ± 10 nm which is in agreement with crystal size deduced from PXRD. Rapid reduction of Ni(ac)$_2$ under microwave heating conditions led to non-uniformity in the shape of Ni nanoparticle due to very fast volumetric heating.
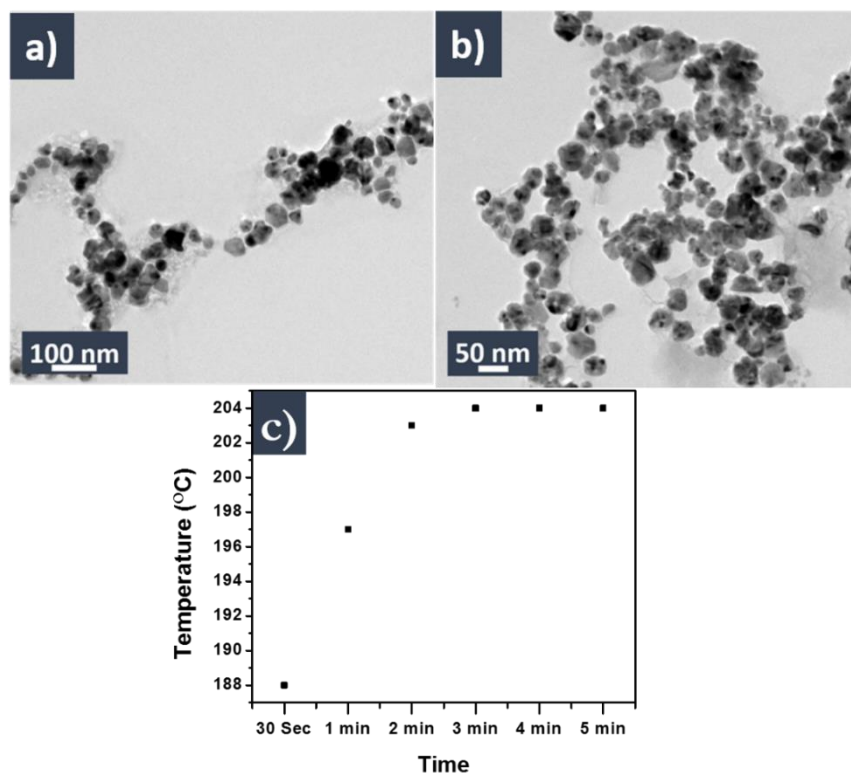
Figure 3.3: a) and b) TEM images of Ni nanoparticle prepared without OAm. c) Time-dependent temperature profile during microwave irradiation at 700 W with frequency 2.45 GHz.

To know the effect of fast heating, rise in the temperature was measured by using thermocouple dipped into pure benzyl alcohol under microwave irradiation. (NOTE: Temperature measurements were not possible during formation of Ni nanoparticle as the formed particles were seen to get stuck to the thermocouple and later generated spark into the reactor.) The results indicate that the temperature rises from room temperature to 204°C within 4 min (see Figure 3.3c) of microwave irradiation. The fast heating cause

rapid reduction of Ni^{2+} to Ni in short period and started nucleation of Ni. The reduction was not allowed to attain thermodynamically stable structure/shape due to OAm present in solution.

Once the batch protocol for synthesis Ni nanoparticle was established it was extended for continuous flow synthesis. For flow synthesis, single CSTR was used which was connected to silicon tubing at the inlet and outlet and the setup was almost similar as mentioned in figure 3.9, except a CTSR-II and syringe pump. $Ni(ac)_2$ + benzyl alcohol solution was injected into CSTR, and microwave heating was started before solution reaches to CSTR. After a few minutes of the appearance of the product, sparking was seen in the microwave oven. Immediately after sparking, we stopped the microwave due to safety reasons. The addition of inert phase and change in geometry of the reactor did not help to resolve the sparking issue. It was observed that the formed Ni nanoparticle were sticking on the glass wall of the reactor and after sufficient exposure to microwave they generated a spark. It has been observed that the particles were settled at the bottom and aggregated into a solution which clogged outlet capillary see the photographic image of the reactor in figure 3.4 a, and b). In the red encircled region and pointed arrow particles show aggregates and particles stuck on the glass wall of the reactor (see the Figure 3.4 a, and b). It is well-known that when a metal placed in a microwave for sufficient time, sparks get generated because of charge accumulation and mobilization of electrons[12]. These sparks can lead to an explosion and can deteriorate product quality. We also noted that during the flow synthesis of Ni nanoparticle in the absence of any stabilizer a few nanoparticle settled at the bottom of the reactor and stuck to the wall

which led to the spark generation. One reason for this destabilization of nanoparticle is the incomplete dissolution of Ni(ac)$_2$ in benzyl alcohol.
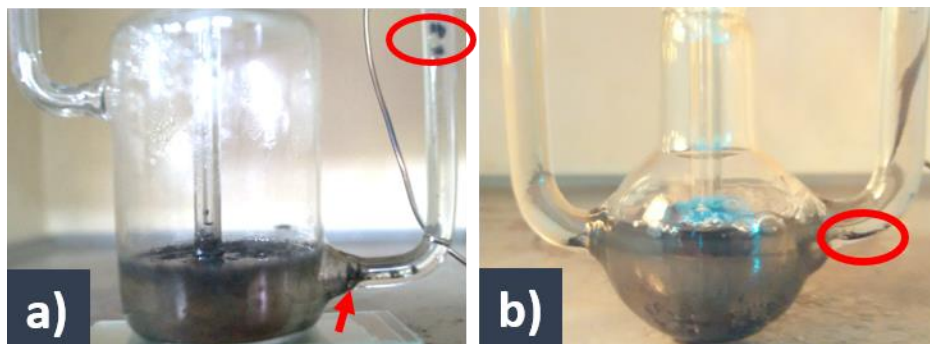
Figure 3.4: Photograph of CSTRs immediately after a spark in the reactor during Ni NP synthesis in the flow.

To resolve the potentially hazarduous issue of metal sparking, OAm was used to dissolve Ni(ac)$_2$ into benzyl alcohol. After addition of OAm, the color of solution changed into green to blue (see Figure 3.5, a and b).
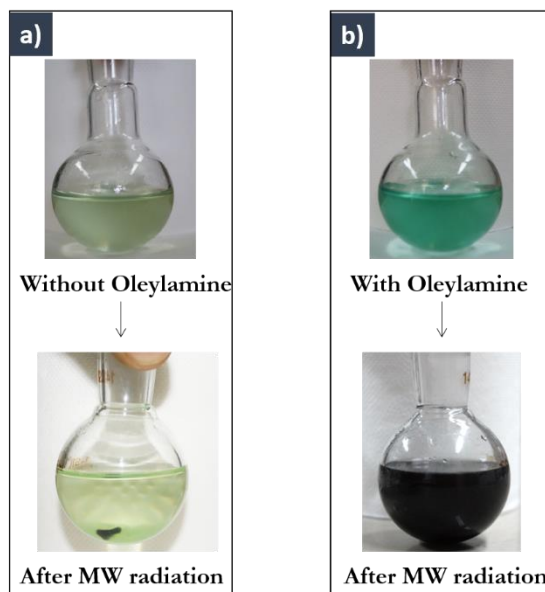
Figure 3.5: Color change in solutions where a shows Ni^{2+} in benzyl alcohol without OAm and heterogeneous nucleation observed in solution after microwave irradiation and b shows Ni^{2+} in benzyl alcohol with OAm and homogeneous nucleation in solution after microwave irradiation.

The resulting solution in OAm when heated by microwave, black colored precipitate appeared after 4 min which is half-time than a synthesis of Ni nanoparticles without OAm. The OAm is known to acts as a reducing agent to form metallic and bimetallic nanoparticles[13]. Hence, shortening of the reaction time caused by reducing ability of OAm, which adds up to the reduction of Ni^{2+} with benzyl alcohol is proven to be an excellent reducing agent. Above all, after irradiation of Ni^{2+} solution without OAm tends to form Ni nanoparticle by heterogeneously into the solution (see Figure 3.5, a). On the other hand, the same solution with OAm showed homogenous nucleation and stabilized the nanoparticle into solution (see Figure 3.5, b).
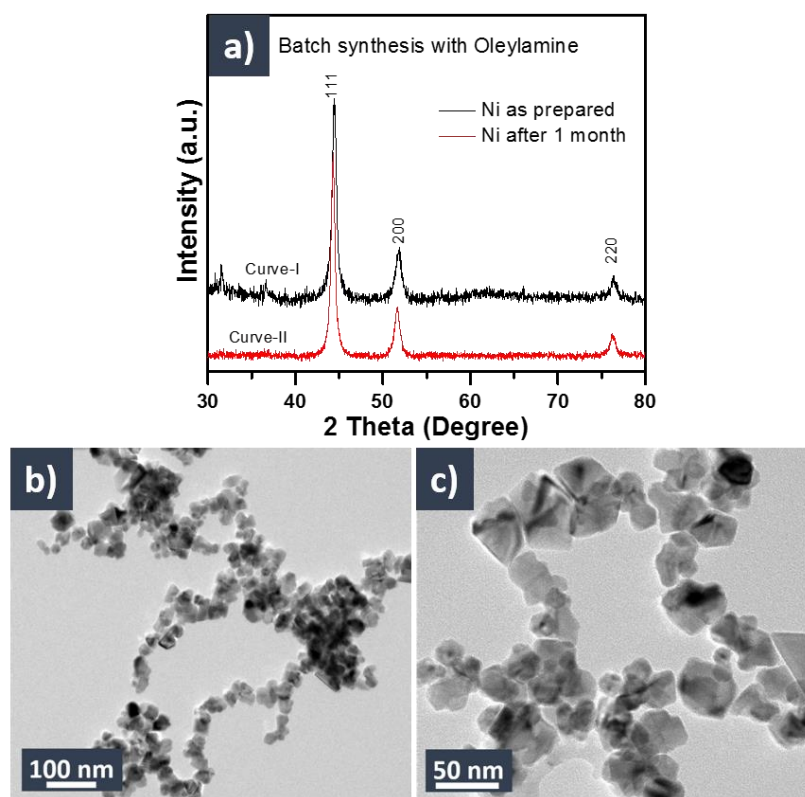
Figure 3.6: a) X-ray diffraction pattern of Ni nanoparticle prepared with OAm using flow synthesis (Curve-I) Ni nanoparticle, (Curve-II) Ni nanoparticle stored for a month. TEM images nanoparticle prepared using OAm b) and c) Ni nanoparticle.

The PXRD pattern corresponding to the pure Ni metal nanoparticle obtained using OAm was in agreement with JCPDS card No. 04-0850 (see Figure 3.6 curve-I). Also, PXRD recorded after a month long storage did not show NiO or any other impurity peak (see Figure 3.6 Curve-II). PXRD patterns reveals that the Ni nanoparticle prepared with OAm are stable for a month. TEM image depicts that nanoparticle are polydisperse in shape and size (see Figure 3.6, a and b). The average size deduced from TEM images is 19.3 ± 5.3 nm which is smaller than the particles obtained without OAm in a batch process. The small size of nanoparticle attributed to stabilization OAm at early stage of particle growth. Here, addition of OAm helped for complete dissolution of $Ni(ac)_2$ and stabilization of nanoparticle which could avoid the spark.

Further, the batch protocol for the synthesis of Ni nanoparticle with OAm was extended for continuous flow synthesis. The same procedure was followed as mentioned section 3.2.2(B), except the addition of OAm to the Ni^{2+} solution and carried out synthesis in single CSTR. This time we didn't observe any spark in the reactor and even the reaction was continued up to 40 min. Here, addition OAm helped to dissolve $Ni(ac)_2$ and acted as a stabilizer which keeps nanoparticle into dispersion for few minutes. Ni nanoparticle were drawn out by a peristaltic pump at flow rate of 4 mL/min and collected in collection flask. As result of the OAm present into the solution, particles didn't stick to the wall of the reactor due to the steric repulsion between particle and reactor surface[14]. The product obtained in continuous flow method was analysed by PXRD instrument which again reveals pure Ni metal formation (Figure 3.7, a, Curve-I). The PXRD patterns recorded after a month of storage of nanoparticle also showed that Ni nanoparticle are stable and do not undergo oxidation (Figure 3.7, a curve-II). The TEM image (Figure 3.7,

b and c) discerned that the particle shape is not well defined, but the average size is 11 nm, which is smaller than those obtained via the batch process. Eventually, addition of OAm to Ni(ac)$_2$ solution play essential role to avoid the spark in microwave oven.
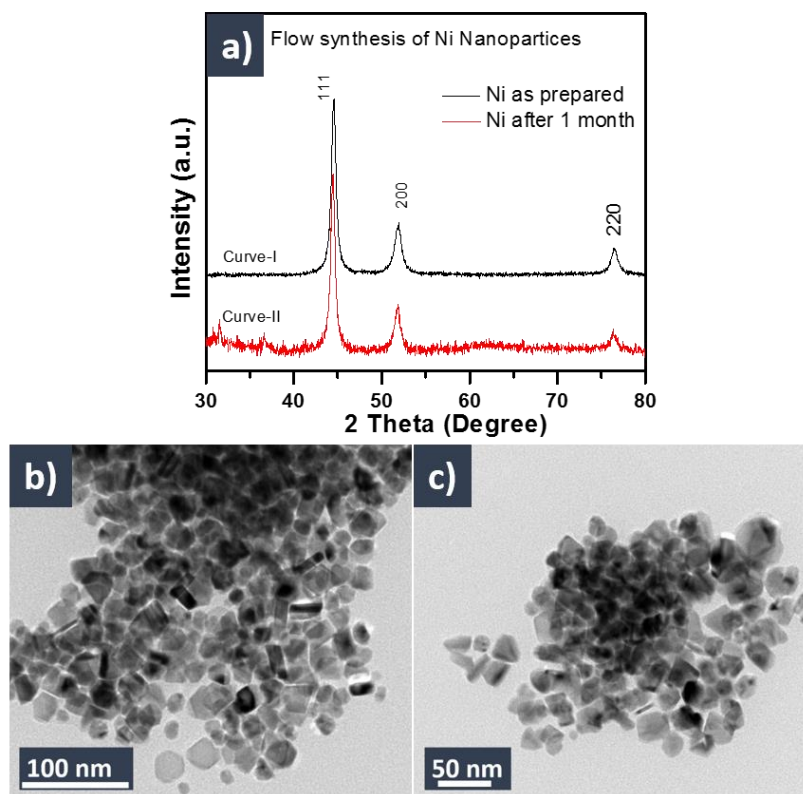
Figure 3.7: a) X-ray diffraction pattern of Ni nanoparticle prepared with OAm using flow synthesis (Curve-I) Ni nanoparticle, (Curve-II) Ni nanoparticle stored for a month. And TEM images nanoparticle prepared using OAm a) and b) Ni nanoparticle.

After establishing continuous flow process for synthesis Ni nanoparticle without a spark, we proceeded to the sequential reduction of Pd^{2+} onto Ni support. First, we studied the sequential reduction of Pd^{2+} on to Ni in a batch format. 2×10^{-3} M Pd(ac)$_2$ solution of diphenyl ether was added to already prepared benzyl alcohol containing Ni NP dispersion which acts as a support for Pd deposition. This solution was irradiated for 4 min and the

product was separated by applying an external magnet. After magnetic separation, in supernatant black colored Pd particles could be present which was discarded and the magnetically separated product was dried and taken for further analysis. PXRD patterns recorded for Pd/Ni prepared by batch synthesis reveals the presence of Pd on Ni (see Figure 3.8, a). Diffraction peak at 40.2˚ values assigned to 111 plane of Pd FCC crystal structure along with it, peak at 44.46˚, 51.83˚, and 76.43˚ values assigned to 111, 200, and 220 planes. TEM images of Pd/Ni shows smaller sized spherical Pd nanoparticle present on the surface of Ni nanoparticle (see Figure 3.8, a and b). The size measured from TEM images of Pd nanoparticle is nearly 5 nm. Depositon of Pd on Ni support was confirmed by EDX mapping of elemental distrubution of Ni and Pd see in the Figure 3.8, d, and e respectively. Amount of Pd laoding estimated with ASS analysis turned out to be 7.8%. Development of batch synthesis of Pd/Ni demonstrated Pd loading is possible using sequetial redution of Ni^{2+} and Pd^{2+} by microwave technique.
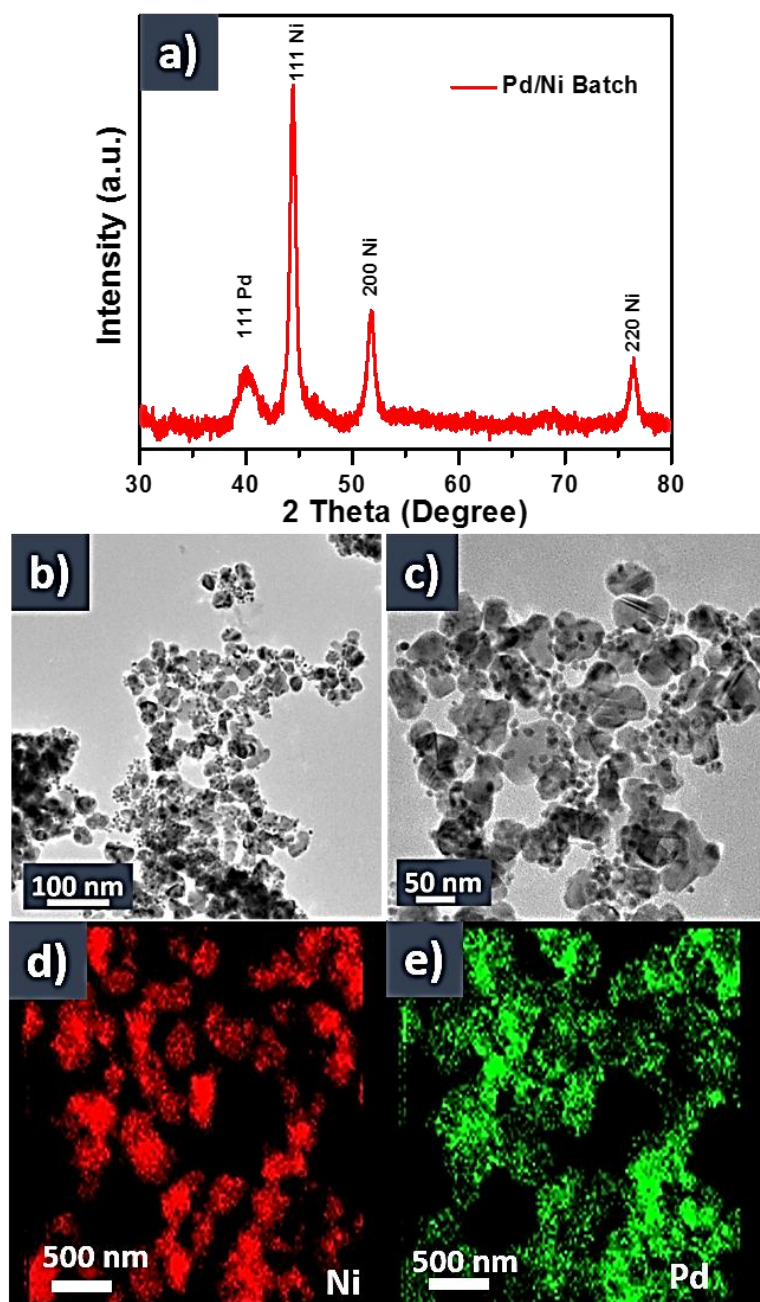
Figure 3.8: a) and b) TEM images of Pd/Ni nanoparticle synthesized in batch under microwave irradiation for 4 min. EDX mapping of elemental distribution for c) Ni and d) Pd for Pd on Ni prepared in batch in the presence of OAm.
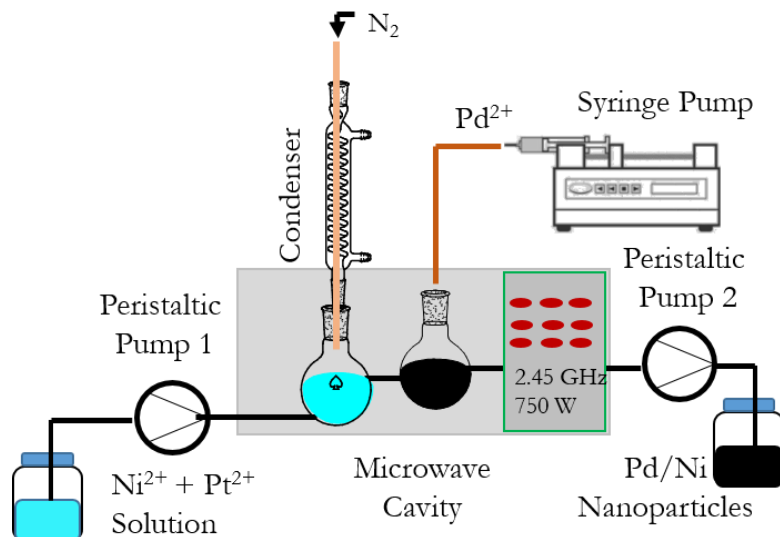
Figure 3.9: Schematic of flow synthesis setup for synthesis of Pd/Ni nanoparticle.

To realize sequential reduction in flow, two CSTRs in series were placed in mcirwave oven connected by silicon tubing as shown in schematic (see Figure 3.9). CSTR-I was attached to condeser and CSTR-II has two inlets, one for incoming Ni nanoparticle solution and other one from top is for incoming Pd(ac)$_2$ solution and has a vent to escape trapped vapour. A dip-tube was used to purge nitrogen gas in CSTR-I. Two peristaltic pump were used: Pump-I is for injection of Ni(ac)$_2$ solution through silicon tubing at flow rate of 4 mL/min. Pump-II is placed at outlet and works in suction mode to draw out nanoparticle into collector flask through silicon tubing. Syringe of Pd(ac)$_2$ solution hosted in syringe pump and flow rate was kept 2 mL/min. When synthesis of Pd/Ni was conducted under microwave irradiation, Ni nanoparticle appeared in CSTR-I were allowed to flow into CSTR-II where Pd(ac)$_2$ solution injected for Pd deposition on Ni nanoparticle which was drawn from CSTR-I and resulting product was collected at outlet.
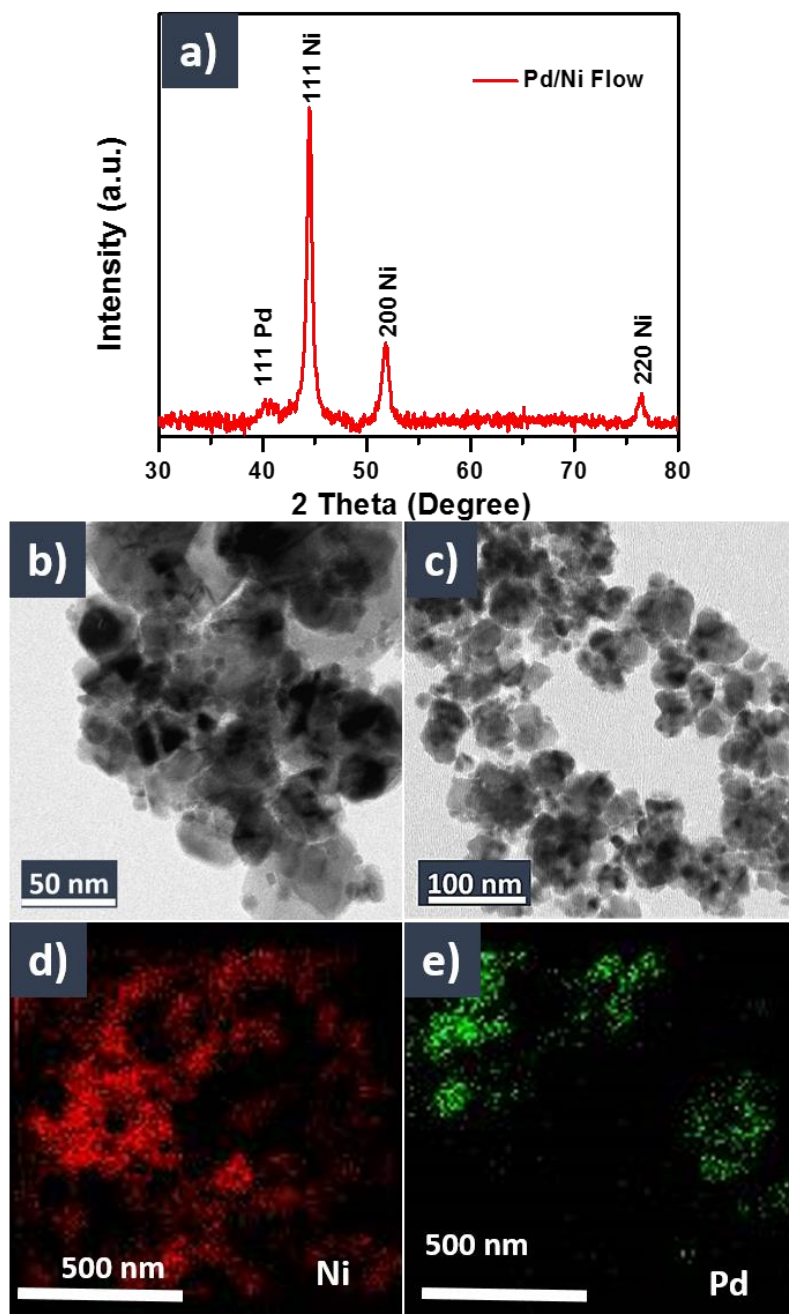
Figure 3.10: a) and b) TEM images of Pd/Ni nanoparticles synthesized by microwave-assisted flow synthesis. And EDX mapping of elemental distribution for c) Ni and d) Pd for Pd on Ni prepared in flow in the presence of OAm.

The product was separated by external magnet and washed, dried and taken for analysis. PXRD patterns of product obtained from sequential redcution in a flow

indicates Pd is present. Diffraction peak at 40.2^0 for 111 planes clearly depicts that Pd exsist with Ni nanoparticle (see Figure 3.10, a). In TEM images of same samples display smaller size Pd nanoparticle were present with Ni nanoparticle (see Figure 3.10, b and c). From EDX mapping of elemental distribution, it is evident that Pd nanoparticle are presnt on the surface of the Ni nanoparticle (see Figure 3.10, d, and e). From AAS analysis, amount of Pd laoding determined to be 6.8%. The heating of Pd(ac)$_2$ in the presence of Ni nanoparticle leads to the formation of Pd anchored on Ni nanoparticle. Pd nanoparticles anchored on Ni surface due to secondary(heterogeneous) nucleation on Ni support. Pd anchored on Ni support is attributed defects site and hot spot led to heterogeneous nucleation[15]. Although, Pd is deposited on Ni nanoparticle, individual Pd nanoparticles were formed in solution. These Pd individual nanoparticle were suspended in solution when Pd/Ni nanoparticle separated by magnet. It may be also pointed out that the nanoparticle that were obtained via continuous flow methods were significantly smaller in size. We credited this to better homogeneity maintained in the reaction mixture due to (i) the presence of OAm and (ii) the short residence time in the reactor.

3.4 Catalysis

After development of batch and continuous flow synthesis of Pd/Ni nanoparticle in the presence of OAm, we used Pd/Ni nanoparticle as a catalyst for hydrogenation of organic compound and tested their catalytic activity for standard hydrogenation of nitrobenzene. The catalysts synthesized in a batch and continuous flow methods were named as Pd/Ni-B and Pd/Ni-CNF respectively. The hydrogenation reactions were conducted with pure hydrogen gas at room temperature at 20 bar hydrogen pressure in methanol. Hydrogenation was carried out using the Pd/Ni nanoparticle prepared in the presence of OAm. We compared the activity of Pd/Ni-B and Pd/Ni-CNF catalysts with the commercial 5% Pd on carbon (Pd/C) and 10% Pd/C catalysts (see Figure 3.11, a).
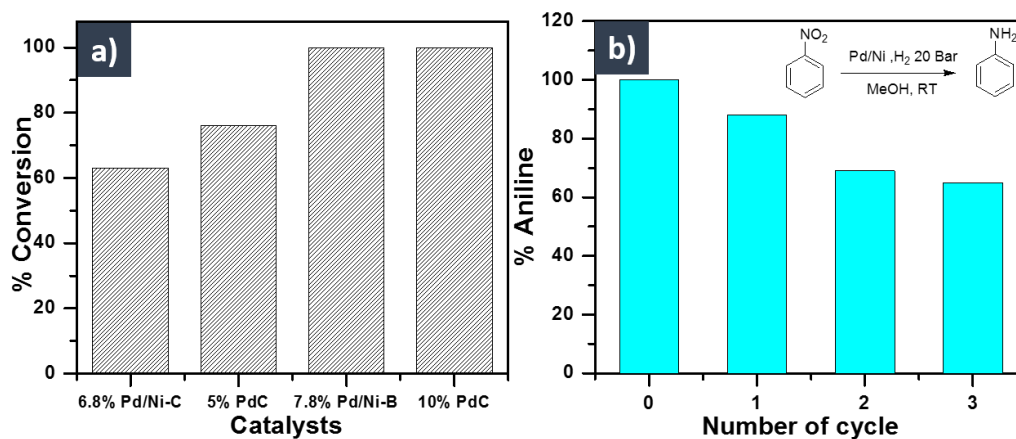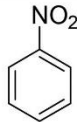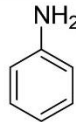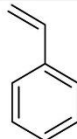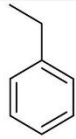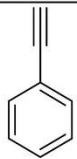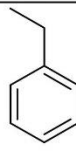
Figure 3.11.a) Comparison of conversion efficiency of nitrobenzene to aniline with 7.8% PD/Ni catalyst and commercial 5% Pd/C and 10% Pd/C catalysts. And b) Conversion efficiencies of the same reaction with recovered catalysts.

It was observed that complete transformation of nitrobenzene to aniline took place within 30 min with the Pd/ Ni-B catalyst. The time taken for completion of hydrogenation of nitrobenzene was the same as that observed for 10% Pd/C (70 −800 m^2/g). When the same reaction was repeated with Pd/Ni-CNF (surface area ~ 18 m^2/g)

and 5% Pd/C (surface area ~ 700−1000 m^2/g) catalysts at other identical conditions, the conversion was 63% and 76%, respectively. From these results, it can be summarized that Pd/Ni-B catalyst displays reasonably good catalytic activity. It may be worth mentioning here that though the Pd loading in our Pd/Ni−B catalyst is slightly lower than that of the commercial 10% Pd/C, these two catalysts display similar efficiencies. Since Pd/Ni-B catalyst shows better catalytic activity compared to Pd/Ni-CNF catalyst, we used the same for hydrogenation of several other organic substrates as mentioned in Table No. 3.1.

Table 3.1. Hydrogenation of aromatic nitro compounds, Alkene and Alkyne^a (Pd/Ni-B^b and Pd/Ni-CNF^c)

Entry	Substrate	Product	Yield	Time
1	NO$_2$ (benzene ring)	NH$_2$ (benzene ring)	100^b 100^c	30 min 60 min
2	NO$_2$ (benzene ring with CH$_3$)	NH$_2$ (benzene ring with CH$_3$)	100^b	180 min
3	(styrene)	(ethylbenzene)	100^b	5 min
4	(phenylacetylene)	(ethylbenzene)	100^b	5 min

^{a}Reaction conditions: 5 mmol of substrate, 20 mg of Pd/Ni-B catalyst, room temperature, 20 bar pressure, and methanol as solvent. ^{b}Pd/Ni-B and ^{c}Pd/Ni-CNF.

The observations from Table 3.1 indicate that all the substrates got converted to their hydrogenated products within a reasonable period of time. The NMR spectral analysis of the products recorded from the samples prepared from crude products obtained from these substrates without any purification (see Figure 3.12 and 3.13) did not show any impurities getting formed in this synthesis. As mentioned previously the presence of Ni imparts a ferromagnetic nature to the catalyst allowing its easy separation by applying an external magnetic field. Accordingly, we performed the recyclability study employing the magnetically separated catalysts again using the hydrogenation of nitrobenzene as the standard reaction. It is satisfying that 66% nitrobenzene got converted into aniline within 30 min even though the catalyst was used after a third cycle (see Figure 3.11, b).
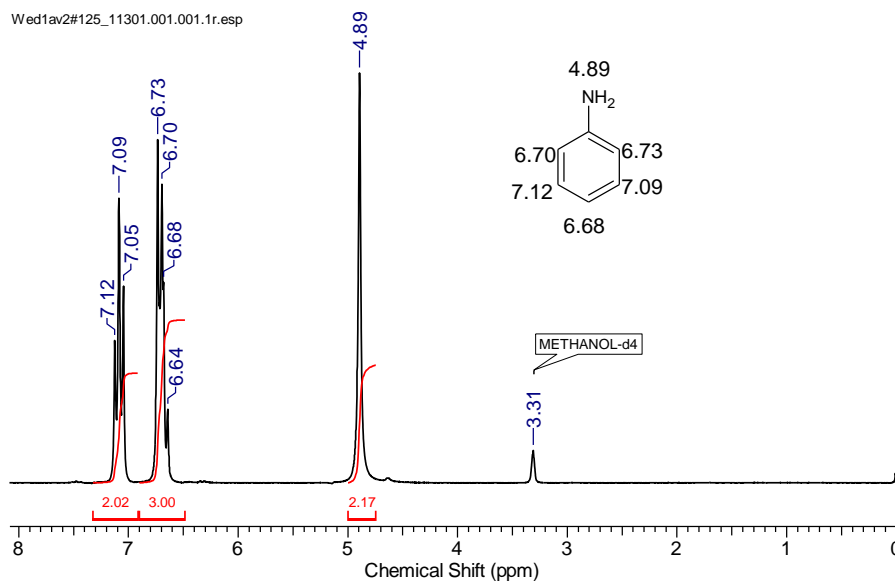
Figure 3.12: H₁-NMR for aniline after hydrogenation of nitrobenzene.
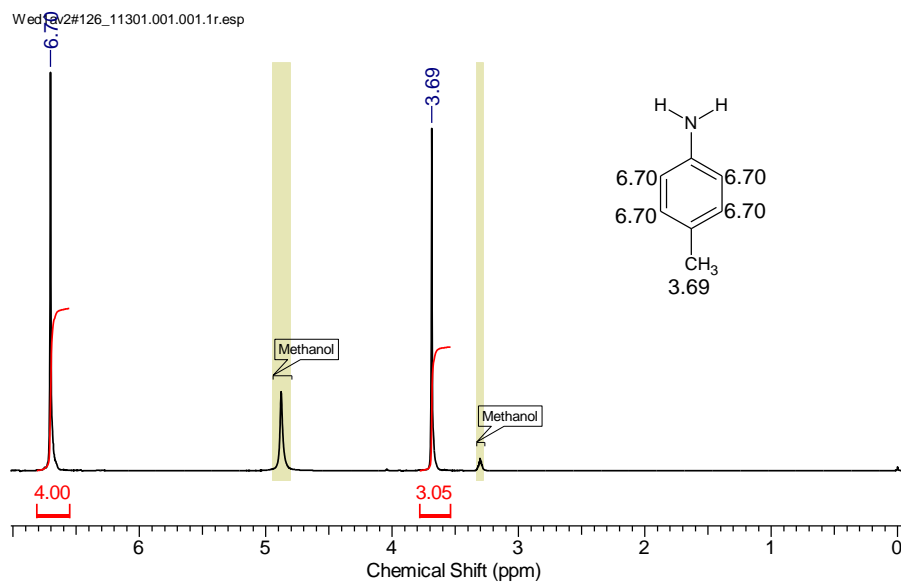
Figure 3.13: H₁-NMR for p-toluidine after hydrogenation of nitro-toluene.

3.5 Conclusions

We have successful synthesized Ni and Pd/Ni nanoparticles using microwave assisted synthesis using benzyl alcohol as the solvent and reducing agent. Addition of OAm to $Ni(ac)_2$ solution to benzyl alcohol reduces Ni^{2+} into Ni in a short time. Same strategy could be used to prepare nickel supported palladium nanocomposite in batch as well as in continuous flow manner. This synthesis protocol for these bimetallic nanoparticles was found to be highly reproducible. The Ni supported Pd nanomaterial was found to be an active catalyst for the hydrogenation of alkene, alkyne and aryl nitro compounds. The catalyst used could be easily retrieved by using an external magnet. The recyclability study shows that catalyst is active after three cycles. The flow synthesis approach reported here is can be subjected to numbering-up for producing the material in larger quantity. It can also be used for other supports such carbon, metal oxide, and polymer as well to prepare supported metal catalysts.

3.6 References:

1. Nikam, A. V.; Arulkashmir, A.; Krishnamoorthy, K.; Kulkarni, A. A.; Prasad, B. *Cryst. Growth Des.* **2014,** 14, 4329-4334.

2. Ahrenstorf, K.; Albrecht, O.; Heller, H.; Kornowski, A.; Görlitz, D.; Weller, H. *Small* **2007,** 3, 271-274.

3. Zhang, D.; Wu, F.; Peng, M.; Wang, X.; Xia, D.; Guo, G. *J. Am. Chem. Soc.* **2015,** 137, 6263-6269.

4. Yan, Y.; Du, J. S.; Gilroy, K. D.; Yang, D.; Xia, Y.; Zhang, H. *Adv. Mater.* **2017,** 29, 1605997-1605997.

5.   Mulvaney, P.; Weiss, P. S., Have Nanoscience and Nanotechnology Delivered? ACS nano: 2016; Vol. 10, pp 7225-7226.

6.   Bayazit, M. K.; Yue, J.; Cao, E.; Gavriilidis, A.; Tang, J. *ACS Sus. Chem. Eng.* **2016,** 4, 6435-6442.

7.   Hostetler, E. B.; Kim, K.-J.; Oleksak, R. P.; Fitzmorris, R. C.; Peterson, D. A.; Chandran, P.; Chang, C.-H.; Paul, B. K.; Schut, D. M.; Herman, G. S. *Mater. Lett.* **2014,** 128, 54-59.

8.   Nishioka, M.; Miyakawa, M.; Kataoka, H.; Koda, H.; Sato, K.; Suzuki, T. M. *Nanoscale* **2011,** 3, 2621-2626.

9.   Kunal, P.; Roberts, E. J.; Riche, C. T.; Jarvis, K.; Malmstadt, N.; Brutchey, R. L.; Humphrey, S. M. *Chemistry of Materials* **2017,** 29, (10), 4341-4350.

10.   Son, S. U.; Jang, Y.; Park, J.; Na, H. B.; Park, H. M.; Yun, H. J.; Lee, J.; Hyeon, T. *J. Am. Chem. Soc* **2004,** 126, (16), 5026-5027.

11.   Jian, S.; Li, Y. *Chin. J. Cata.* **2016,** 37, 91-97.

12.   Shanmugharaj, A.; Ryu, S. H. *Electro. Acta* **2012,** 74, 207-214.

13.   Mourdikoudis, S.; Liz-Marzán, L. M. *Chem. Mater.* **2013,** 25, 1465-1476.

14.   Mallikarjuna, N. N.; Varma, R. S. *Cryst. Growth Des.* **2007,** 7, 686-690.

15.   Anumol, E. A.; Kundu, P.; Deshpande, P. A.; Madras, G.; Ravishankar, N. *ACS nano* **2011,** 5, (10), 8049-8061.

Chapter 4

Batch and Flow Synthesis of NiPt Alloy Nanoparticles
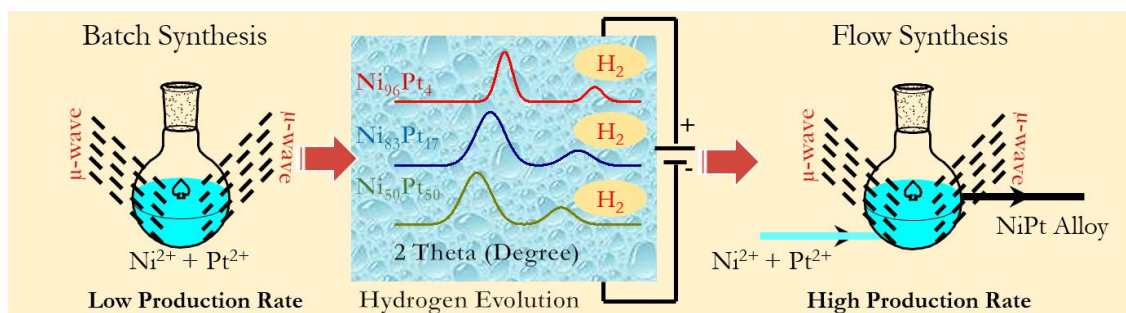
4.1 Introduction

Bimetallic nanoparticles exhibit unique properties than their mono-metallic nanoparticles. These unique properties are caused due to combination of two metals and vary with composition of both metals, size, shape and surface structure. These changes in the properties of alloy nanoparticles are attributed to the synergetic effects of both the metals.[1] Due to this unique change in properties alloy nanoparticles find applications in the field of catalysis,[2] biomedicine,[3] and energy generation.[4] Hence, synthesis of the alloy nanoparticles at industrial scale would be necessary to meet the growing demand for the alloy nanomaterial. Altogether, challenges will be mountainous while developing a new synthetic strategy and important features of synthesis stratedgy would be i) less-time consuming, ii) control over composition, size and shape and iii) scalability.

In chapter 2, we have established benzyl alcohol route for sequential reduction of Ni^{2+} and Pd^{2+} to synthesize Pd/Ni heterostructure. Reduction of Ni^{2+} and Pd^{2+} were carried out separately which is a relatively easier task than the simultaneous reduction of both metal ions. In this chapter, we want to focus on the synthesis of alloy nanoparticles in batch and continuous mode. In the literature, there are very few reports on the continuous flow synthesis of alloy nanoparticles. Kunal *et al.* demonstrated synthesis of RhAg alloy nanoparticles using droplet flow under microwave irradiation.[5] Zhang *et al.* reported one step, facile and ultrafast synthesis of phase and size-controlled Pt-Bi intermetallic nanocrystal through continuous flow microfluidic device.[6] The controlled phase of Pt_1Bi_1 and Pt_1Bi_2 was synthesized at 260˚C and 360˚C respectively, using polyethylene glycol as a solvent. Wu *et al.* reported microfluidic reactions in a capillary tube reactor for rapid synthesis of ultrafine, surfactant-free PtSn alloy nanocrystals which

are directly deposited on to various carbon supports with high-density and uniform loading.[7] Synthesis of PtSn alloy on carbon support is also reported in pressurized condition. Nu *et al.* synthesized NiPt-octahedra in continuous flow reactor for scalable synthesis by droplet flow.[8] In this report, $W(CO)_6$ was used to generate gas which caused segmented flow and also acted as the reducing gas. However, WO_3 was formed as an impurity during the synthesis. Generally, alloy synthesis requires high temperature and pressure, involving toxic reagents, long time and is energy intensive, which hinders applicability and scalability of alloy synthesis. We want to develop simple, ultrafast synthetic strategy involving non-toxic reagents and lower energy requirements which could be adopted for flow synthesis. Consistent with the previous chapter we want to synthesis Ni-based alloy that has higher industrial relevance. Typically, to form an alloy nanoparticles, crystal structure of both metals should be same and lattice constant difference of two metals should be minimum. In that context, Ni and Pt metal have FCC crystal structure, and lattice constant difference between Ni and Pt is 11%. Hence, NiPt alloy nanoparticles is a suitable candidate to explore microwave-assisted flow synthesis. Above all, NiPt alloy nanoparticles has tremendous industrial relevance in the field of energy generation.[9] NiPt alloy nanoparticles has been used as a catalyst in many electrochemical processes for energy generation such as fuel cell and water splitting for hydrogen energy. Practical implementation of the fuel cell and water splitting technology are hindered due to high cost of Pt/C catalyst. Yi *et al.* reported the NiPt based nanomaterial had higher mass activity than commercial Pt/C catalyst for hydrogen generation reaction.[10] In this chapter, we report a new synthetic strategy for the synthesis of NiPt alloy nanoparticles using benzyl alcohol route under microwave heating in batch.

Batch parameters will be considered to adopt for microwave-assisted flow synthesis of NiPt alloy at a high production rate.

4.2 Experimental Section

4.2.1 Chemicals and Materials, Nickel (II) acetate tetrahydrate and Platinum (II) acetylacetonate (abbreviated as $Ni(ac)_2$ and $Pt(acac)_2$ respectively in rest of the thesis), anhydrous benzyl alcohol (99.9% purity), and oleylamine (70%) were purchased from *Sigma-Aldrich* and used without any further purification. Methanol, ethanol, and acetone were used from *Thomas Baker Chemicals*.

4.2.2 Synthesis of NiPt nanoalloy in a batch reactor
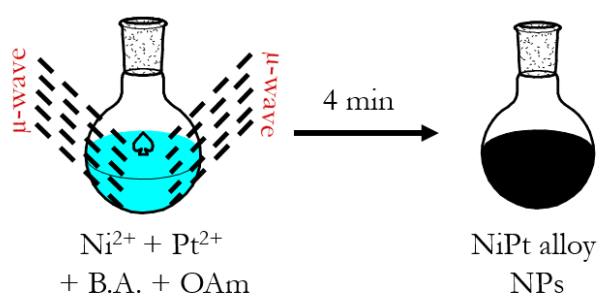
Figure 4.1: Schematics of microwave-assisted batch synthesis of NiPt alloy nanoparticles.

Synthesis of NiPt nanoparticles was carried out in a batch reactor under microwave irradiation (see Figure 4.1). 62 mg of $Ni(ac)_2$ (0.25 mmol), 4 mg $Pt(acac)_2$ (0.01 mmol), and 1 mL oleylamine was dissolved in 15 mL of (99.9%) anhydrous benzyl alcohol in a 25 mL round-bottom flask and sonicated for 15 min at room temperature. The flask containing the reaction mixture was placed in a microwave oven (Ragatech Pvt. Ltd, India, 700 W, 2.45 GHz) for 4 minutes without any stirring. After the microwave irradiation, the reaction flask was removed from the microwave oven and the reaction mixture was allowed to cool at room temperature. A black colored product was observed in the reaction flask. The product was washed three times using a mixture of acetone and ethanol using sonication and centrifuged at 10000 rpm for 10 min. The supernatant of the

solution was discarded after separating the product by centrifugation. The product was dried at room temperature. NiPt nanoalloy with different composition were prepared by varying initial molar concentration is shown in table 4.1 and other parameter were kept the same.

Table 4.1. Experimental details for the synthesis of NiPt alloy nanoparticles.

Ni/Pt Ratio (mmol)	Pt(acac)$_2$ (mmol)	Ni(ac)$_2$ (mmol)
25:1	0.010	0.25
5:1	0.050	0.25
1:1	0.048	0.044

4.2.3 Acetic acid treatment

To remove oleylamine coverage, NiPt nanoparticles can be treated with acetic acid (see Figure 2). NiPt nanoparticles covered with oleylamine were dispersed in 7 mL of methanol by ultra-sonication for 5 min. 7 mL of Glacial acetic acid was added to the NiPt dispersion and was homogenized by ultra-sonication for 5 min. The resulting dispersion was stirred for overnight at room temperature. The product was washed and dried as mentioned in Section 4.2.2. The product obtained after acetic acid treatment named as NiPt − AAT.

RT, 12 h
Methanol

NiPt-Oam
+ Acetic acid

NiPt NPs
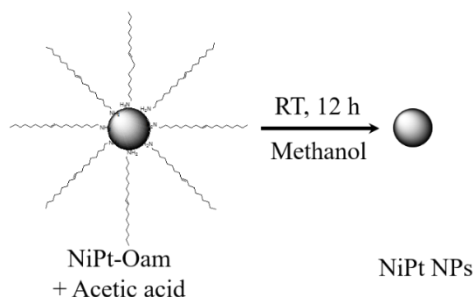
Figure 4.2: Schematics of acetic acid treatment of the NiPt alloy nanoparticles.

4.2.4 Loading of NiPt−AAT alloy on carbon

20 mg of NiPt−AAT sample and 80 mg of X-72 Vulcan carbon was dispersed into 10 mL ethanol separately for 0.5 h. The resulting two dispersions were mixed and homogenized by ultra-sonication for 5 min. This dispersion was kept for stirring for 12 h for NiPt alloy loading on carbon. The product was dried at room temperature for a day. The resulting product was taken for structural and electrochemical analysis.

4.2.5 Flow synthesis of NiPt nanoalloy

Continuous experiments for the synthesis of NiPt nanoalloy were carried out in a 16 mL continuous stirred tank reactor (CSTR). The concentrations of the reactants were kept the same for continuous experiments as that of batch experiments. CSTR was placed in a microwave oven operating at 2.45 GHz and 700 W (see Figure 4.12 schematics of setup for flow synthesis). Pt^{2+} and Ni^{2+} reaction solution was injected using peristaltic pump through silicon tubing into the CSTR placed in a microwave oven at the flow rate of 4 mL/min. Black colored product was observed after 5 min of microwave irradiation and was collected at the outlet. Black colored product was separated by centrifugation at 10000 rpm and washed three times using 50% v/v methanol and acetone mixture. After purification of product, it was kept for drying in at ambient condition for 12 h.

4.3 Results and discussions

4.3.1 Batch synthesis of NiPt alloy nanoparticles

It is well-known fact that alloy formation is very sensitive to reduction rates of both the metal precursors. The homogeneous alloy is obtained when the reduction rate of both the metal precursors are equal. Before synthesizing NiPt alloy nanoparticles, we studied relative rates of reduction of $Ni(ac)_2$ and $Pt(acac)_2$ in presence of benzyl alcohol and oleylamine. To know the reduction rate of $Pt(acac)_2$ and $Ni(ac)_2$, reduction reactions were carried out in separate reaction flask for both metal precursors. In case of reduction of $Pt(acac)_2$, we have observed black colored precipitate into the reaction flask after 3.5 minutes of microwave irradiation. On the other hand, in chapter 2, we have shown Ni nanoparticles can be obtained within 4 min. It is noted that $Pt(acac)_2$ reduces faster compare to $Ni(ac)_2$ and difference between reaction time is 30s. Simultaneous reduction for both metal precursors would lead to formation of Pt rich NiPt alloy.

In pursuit of synthesis of NiPt alloy nanoparticles, $Ni(ac)_2$ and $Pt(acac)_2$ were dissolved in benzyl alcohol and oleylamine mixture and irradiated with microwave radiation. We have obtained different alloy composition by varying the initial molar concentration of $Ni(ac)_2$, and $Pt(acac)_2$. Formation of the NiPt alloy was confirmed by PXRD analysis. The recorded PXRD patterns of alloy show different diffraction patterns than individual Ni and Pt metal which indicates alloy formation with varying composition of Ni and Pt. It is observed that all the diffraction peaks for alloy show shift towards the Ni FCC diffraction peaks as an increase in initial molar concentration $Ni(ac)_2$ (see Figure 4.3, pink to red color from bottom to top). Black colored diffraction pattern belongs to Nickel FCC crystal structure, and peaks are assigned to planes 44.13 (111), 55.36 (200), 76.43 (220).

Ni$_{96}$Pt$_{04}$, Ni$_{83}$Pt$_{17}$, and Ni$_{50}$Pt$_{50}$ are the alloy composition assumed on the basis of the initial molar concentration of Ni(ac)$_2$ and Pt(acac)$_2$. With the increase in Ni composition in nanoparticles, the (111) peak shifted to higher angle indicating a reduction of inter-planar spacing. Alloy composition variation is estimated by the lattice constant of the NiPt alloy. The relationship of the lattice constant derived from PXRD patterns and Ni composition in nanoparticles is shown in figure 4.3 a). The lattice constant deduced from PXRD and calculated using Vegard's law are in correlation with each other (see Figure 4.3 b). There is a linear relationship between the lattice constant and the Ni composition, confirming as synthesized alloy have a solid solution structure.
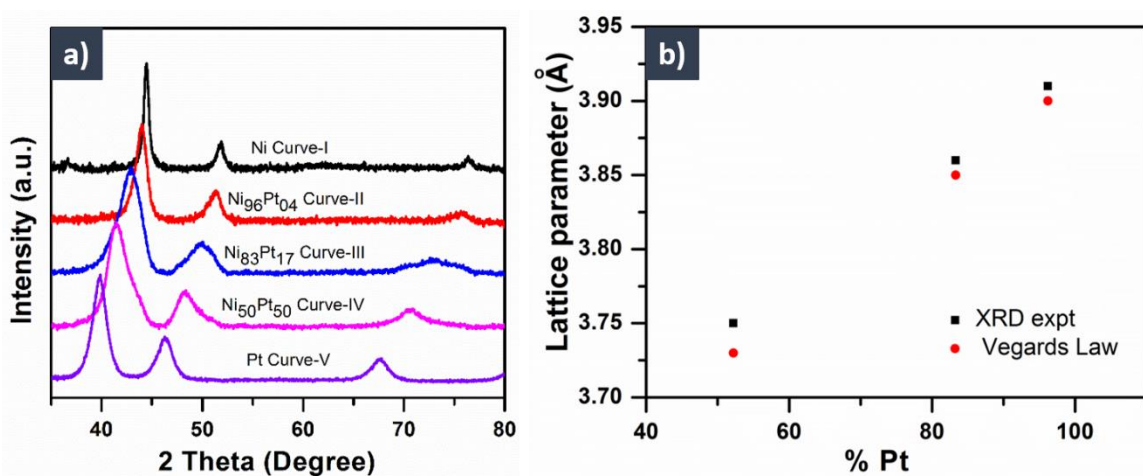
Figure 4.3: a) PXRD patterns of NiPt alloy synthesized using microwave heating by varying the initial molar concentration of Ni(ac)$_2$ and Pt(acac)$_2$ precursors b) Comparison of lattice constant estimated from PXRD and Vegard's law.

The composition of alloy nanoparticles was estimated using atomic absorption spectroscopy (AAS) shows disagreement with the initial molar concentration. In Table, 4.1 we can see a concentration of Pt is high in the all the alloy composition which attributed higher reduction rate of Pt(acac)$_2$ than the Ni(ac)$_2$ precursor into respective

metal. We found that initial molar concentration is not matching with AAS analysis because there could be unconverted Pt and Ni precursor left into the solution.

Table 4.2. Alloy composition estimated by atomic absorption spectroscopy.

Sample Name	Molar % of Ni	Molar % of Pt
$Ni_{96}Pt_{04}$	80	20
$Ni_{83}Pt_{17}$	50	50
$Ni_{50}Pt_{50}$	11	89

Morphology of NiPt nanoparticles was observed under transmission electron microscope. TEM images indicate that NiPt alloy nanoparticles are poly-disperse in nature (see Figure 4.4). Broad size and non-uniform morphology of nanoparticles can be ascribed to fast microwave heating as well as the small difference in the reduction rates. For the high heating rate, the growth of NiPt alloy nanoparticles occurs under a kinetically favorable condition which results in formation branched or anisotropic nanoparticles[11]. Moreover, kinetically controlled growth is mainly induced due to the presence of oleylamine which causes hindrance for new incoming atom to deposit on already existing particles. The average size of $Ni_{50}Pt_{50}$ is 31 nm and 15 nm for $Ni_{96}Pt_{04}$ alloy nanoparticles. Increasing the Pt composition increases the size of nanoparticles due to enhanced growth rate.
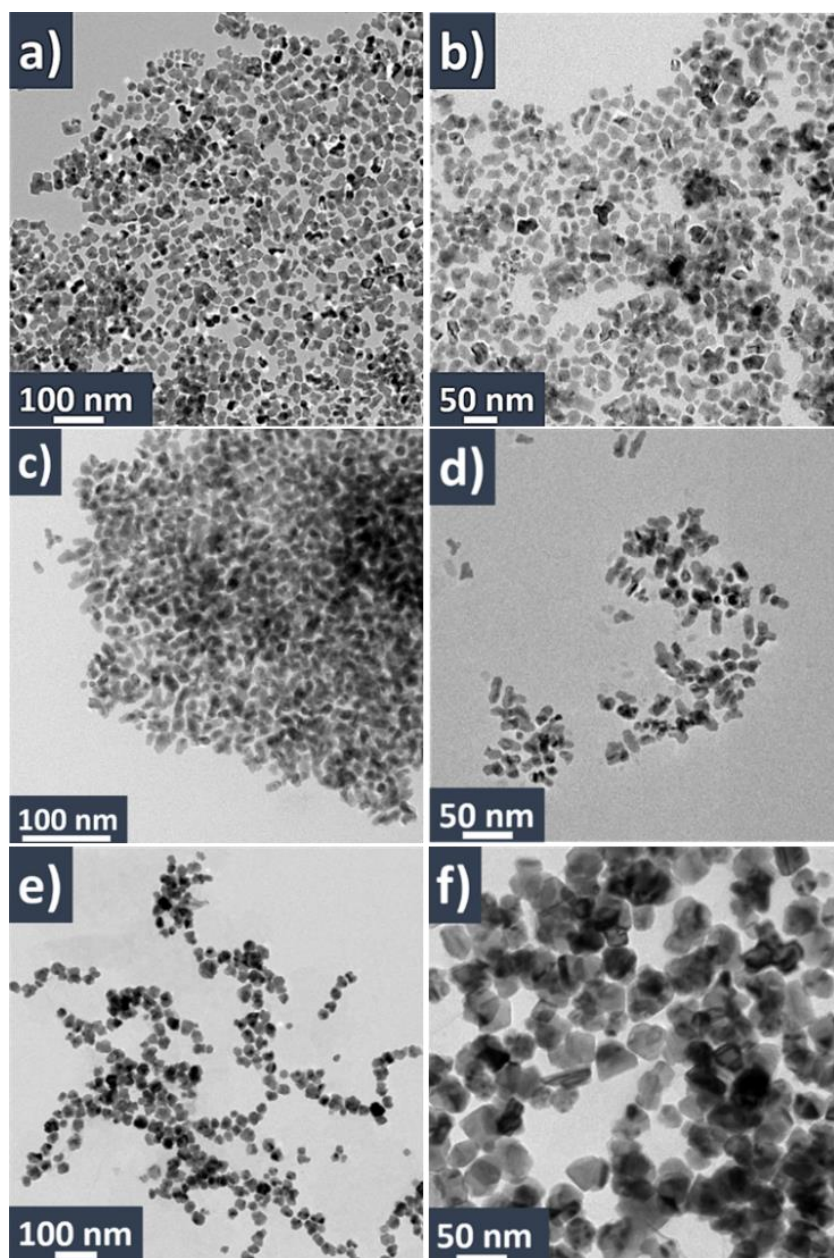
Figure 4.4: TEM images of NiPt alloy with variable initial molar concentration a) and b) Ni$_{96}$Pt$_{04}$, c) and d) Ni$_{83}$Pt$_{17}$, e) and f) Ni$_{50}$Pt$_{50}$.

Due to surface capping on NiPt by oleylamine, the surface of alloy becomes less available for catalysis and surface stabilizer act as an insulator for electron transfer. Hence, NiPt alloy nanoparticles covered with oleylamine was treated with acetic acid.

After acetic acid treatment, PXRD patterns of NiPt acetic acid treated (abbreviated as NiPt−AAT in this chapter) samples was recorded (see Figure 4.5).
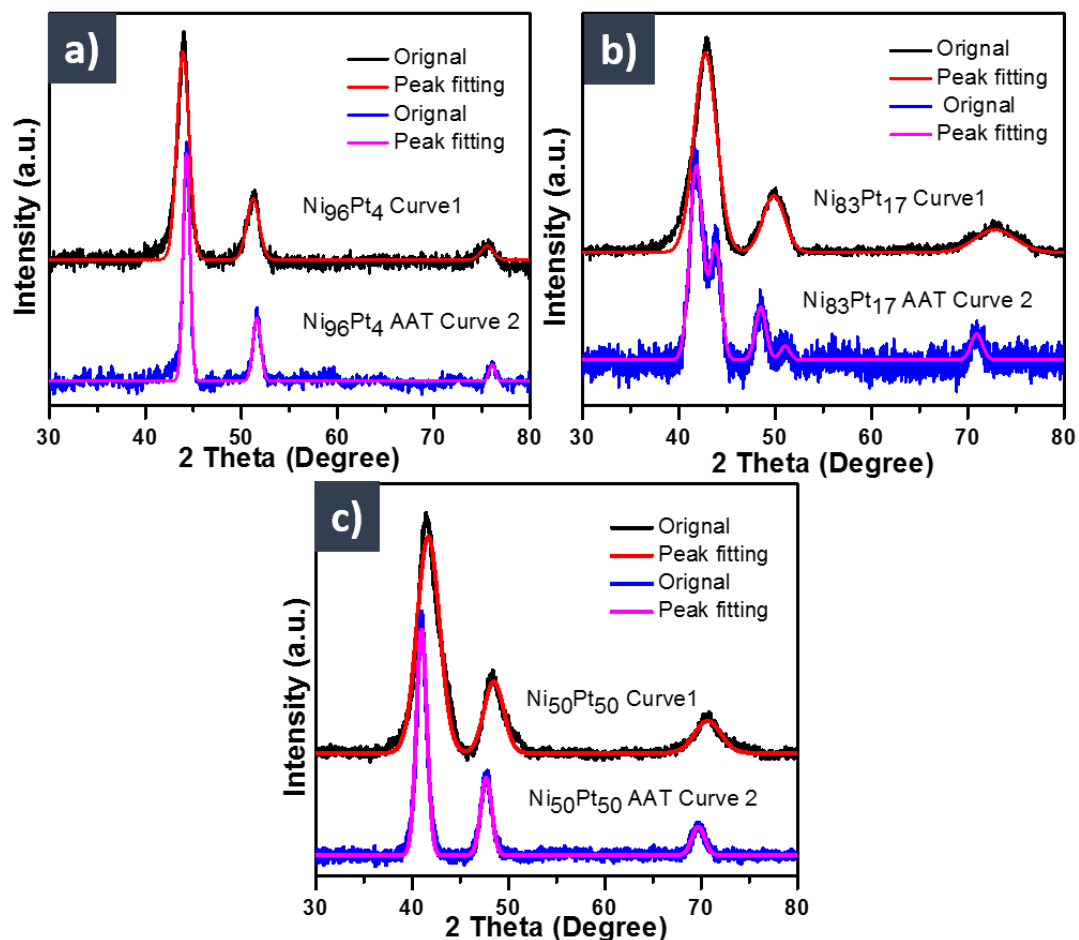
Figure 4.5: The PXRD patterns of NiPt alloy after the acetic acid treatment a) $Ni_{96}Pt_{04}$ (Curve-1) and $Ni_{96}Pt_{04}$−AAT (Curve-2), b) $Ni_{83}PT_{17}$ and $Ni_{83}Pt_{17}$ −AAT, and c) $Ni_{50}Pt_{50}$ and $Ni_{50}Pt_{50}$− AAT.

Change in diffraction pattern was observed in comparison to without treatment of acetic acid. The change in PXRD could be due to leaching of Ni metal into solution by acetic acid treatment. PXRD peak shifted towards low angle that indicates Ni metal is dissolved in acetic acid from alloy nanoparticles. As a result, oleylamine is detached from

the surface of NiPt nanoparticles. Interestingly, PXRD pattern of $Ni_{83}Pt_{17}$ shows peak from individual Ni and Pt crystal structure which indicates phase segregation of alloy after acetic acid treatment (see Figure 4.5b). After treatment with acetic acid, NiPt alloy was washed three times with methanol. NiPt alloy was tested as cathode material for hydrogen evolution reaction.

Table 4.3. Alloy composition estimated by atomic absorption spectroscopy after **acetic acid treatment.**

Sample Name	Molar % of Ni	Molar % of Pt
$Ni_{96}Pt_{04}$	32	68
$Ni_{83}Pt_{17}$	26	74
$Ni_{50}Pt_{50}$	2	98

The composition of the alloy nanoparticles was estimated using AAS which indicates that there is a decrease in Ni content after acetic acid treatment (see table no. 3). Due to etching of Ni, we observed phase change of NiPt nanoalloy which also caused structural changes. To know the structural changes, these samples were further analyzed under transmission electron microscope (TEM). TEM images of NiPt alloy clearly show there is change in the morphology of all alloy composition after acetic acid treatment (see the Figure 4.6). Once alloy nanoparticles are treated with acetic acid, it forms framework structure when Ni is etched away. TEM image of sample $Ni_{96}Pt_{04}$ − AAT shows aggregates after the acetic acid treatment nanoparticles of $Ni_{96}Pt_{04}$ (see Figure 4.6 a and b). This networked structure of aggregates caused due to removal of surface stabilizer which leads to aggregation. $Ni_{96}Pt_{04}$ alloy nanoparticles contains 4% of Pt content when Ni etched into solution, Pt content is not sufficient to retain their framework structure.

After Ni etching, $Ni_{96}Pt_{04}$ alloy did not retain its framework structure of alloy nanoparticles and tend to form aggregates of smaller NiPt alloy nanostructure. On the other hand, when $Ni_{83}Pt_{17}$ alloy nanoparticles treated with acetic acid, Ni content dissolve into a solution which results in a structural change in $Ni_{83}Pt_{17}$ sample (see Figure 4.6 c and d). Interestingly, NiPt alloy structure was retained due to 50% of Pt content present in the $Ni_{83}Pt_{17}$ samples. $Ni_{50}Pt_{50}$ sample undergo aggregation when placed on the grid due to the removal of surfactant after acetic acid treatment but the structure of nanomaterial remain intact. Here, 89% of platinum was present in $Ni_{50}Pt_{50}$ samples, when Ni etched into solution amount of platinum is sufficient to retain its structure (see Table No. 4.3). It is well-known fact that the introduction of Pt into Ni can reduce the chemical potential of pure metallic nickel and stabilizes it thermodynamically[12].
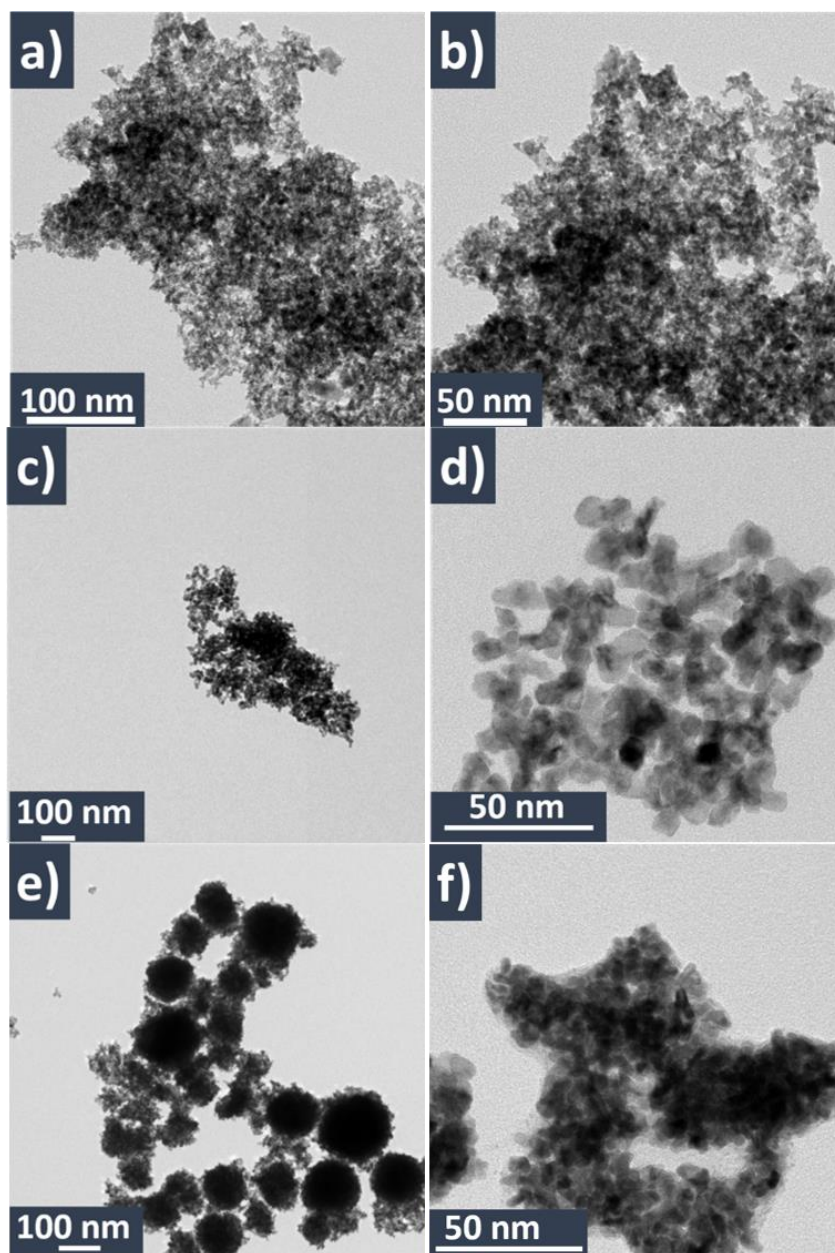
Figure 4.6: TEM images of NiPt alloy after acetic acid treatment (AAT) a) and b) Ni$_{96}$Pt$_{04}$−AAT, c) and d) Ni$_{83}$Pt$_{17}$ −AAT e) and f) Ni$_{50}$Pt$_{50}$− AAT.
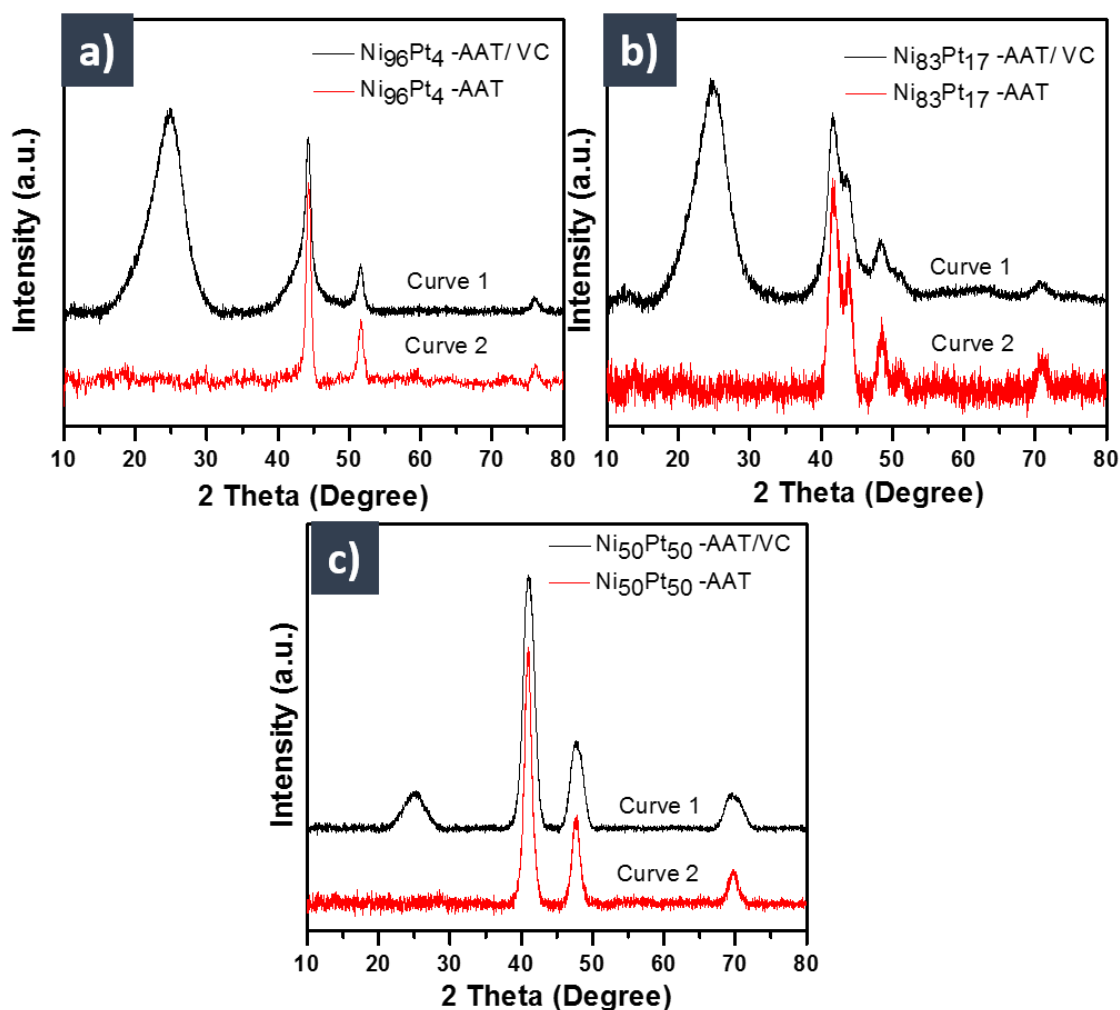
Figure 4.7: The PXRD patterns of NiPt−AAT alloy nanoparticles before and after 20% loading on X-72 Vulcan carbon.

To know the activity of NiPt−AAT alloy nanoparticles for hydrogen evolution reaction, 20% loading of NiPt−AAT alloy nanoparticles on X-72 Vulcan carbon sample were prepared in ethanol as mentioned in section 4.2.4. After drying of the samples, PXRDs were recorded for the all the samples which indicates NiPt−AAT nanoparticles were present on X-72 Vulcan carbon (see Figure 4.7). Diffraction peak at 26.4˚ corresponds to 002 peak of Vulcan carbon and rest of the diffraction peaks corresponds to NiPt−AAT alloy of respective samples. Here, X-72 Vulcan carbon is conducting support

which imparts stability and facilitates electron transfer reaction for hydrogen evolution[13]. To confirm loading of NiPt on vulcan carbon we characterized NiPt−AAT/C samples under transmission electron microscope. TEM images indicate NiPt−AAT nanoparticles were successfully loaded on Vulcan carbon (see Figure 4.8). Interestingly, we didn't observe individual NiPt−AAT nanoparticles without carbon support, which proves that the NiPt−AAT nanoparticles are present on a carbon support. In case of $Ni_{96}Pt_{04}$−AAT/C and $Ni_{83}Pt_{17}$−AAT/C samples, NiPt−AAT nanoparticles are present on the carbon support in aggregated form (see Figure 4.8 a, b, and c, and d respectively). On the other hand, $Ni_{50}Pt_{50}$−AAT nanoparticles are very well dispersed on carbon support. Individual $Ni_{50}Pt_{50}$−AAT nanoparticles, as well as very few aggregates, are present on the carbon support (see Figure 4.8 e, and f).
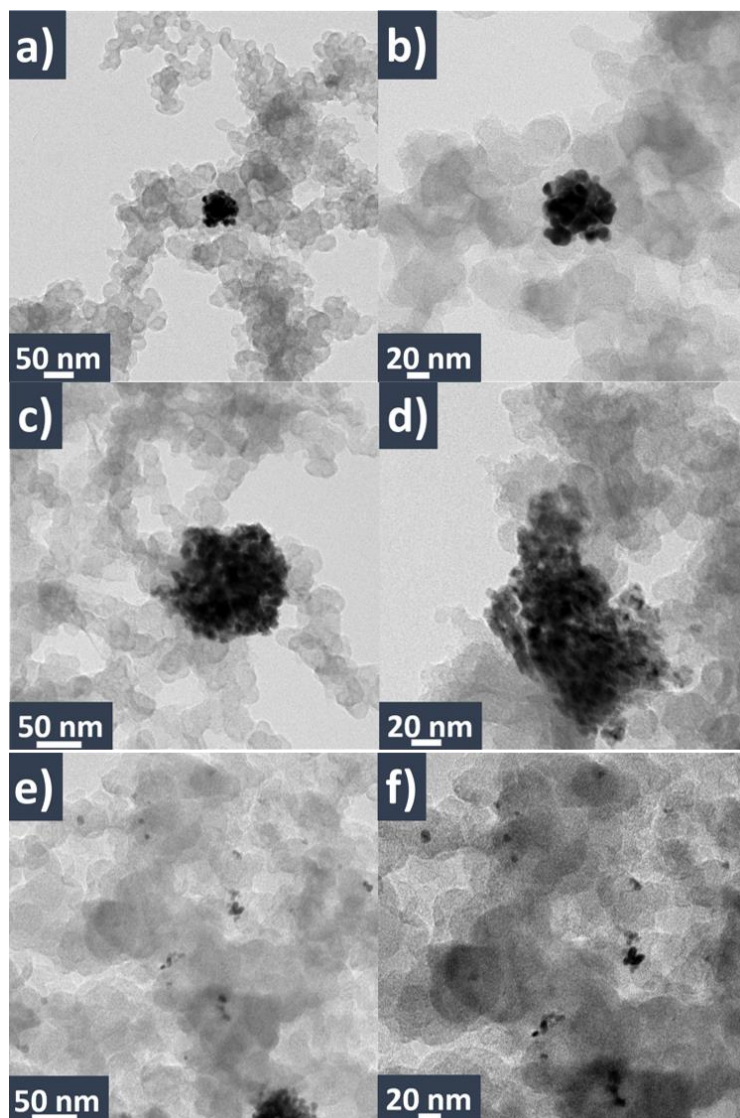
Figure 4.8: TEM images of NiPt−AAT alloy nanoparticles after 20% loading on X-72 Vulcan carbon a) and b) Ni$_{96}$Pt$_{04}$−AAT/C, c) and d) Ni$_{83}$Pt$_{17}$−AAT/C, and e) and f) Ni$_{50}$Pt$_{50}$−AAT/C.

4.3.2 Electrochemical study

The electrocatalytic efficiency of 20 weight % NiPt nanoalloy loaded on Vulcan carbon were investigated for electrochemical hydrogen evolution reaction (HER) in acidic media (0.5 M H_2SO_4) using CHI 660E (compliance voltage: ± 13 V) electrochemical workstation using standard three electrode system. Carbon supported electro-catalyst $Ni_{50}Pt_{50}$−AAT/C nanoalloy was dispersed in 0.5% Nafion (in 1:1 water: ethanol) maintaining 10 mg/mL concentration of $Ni_{50}Pt_{50}$−AAT/C. 2 uL dispersion of $Ni_{50}Pt_{50}$−AAT/C electrocatalyst was casted on glassy carbon electrode (2mm dia.) using micropipette. After casting the $Ni_{50}Pt_{50}$−AAT /C, the electrode was allowed dry at room temperature. Ag/AgCl and platinum flag were used as a reference and counter electrodes, respectively. All potentials are reported with respect to the RHE. Electrochemical measurements were conducted in an inert atmosphere, and all LSVs (Linear Sweep Voltammograms) were IR compensated. Durability test of the electrocatalystwas done by repetitive cycling at-least upto 10K scans. (Note; same procedure was followed to evaluate HER activity for $Ni_{83}Pt_{17}$−AAT/C, $Ni_{96}Pt_{04}$−AAT/C and commercial Pt/C).

First, we evaluate the electrocatalytic activity of NiPt AAT/C by recording linear sweep voltammograms. Figure 4.9 a) displays the linear sweep voltammograms (LSVs) for NiPt−AAT/C of different compositions and commercial Pt/C catalyst. Onset potential values for $Ni_{50}Pt_{50}$−AAT /C, $Ni_{83}Pt_{17}$−AAT /C, $Ni_{96}Pt_{04}$−AAT /C, are almost similar (i.e. 30 mV) and lower than Pt/C catalyst (40 mV). However, current density for $Ni_{50}Pt_{50}$− AAT /C is 1571 A/cm^{2}and turn to be highest compared to rest of the NiPt −AAT /C and Pt/C catalysts. Current density corresponds to number electron withdrawal for hydrogen evolution which suggests that among all catalyst, $Ni_{50}Pt_{50}$ −AAT /C is the most suitable

catalyst.
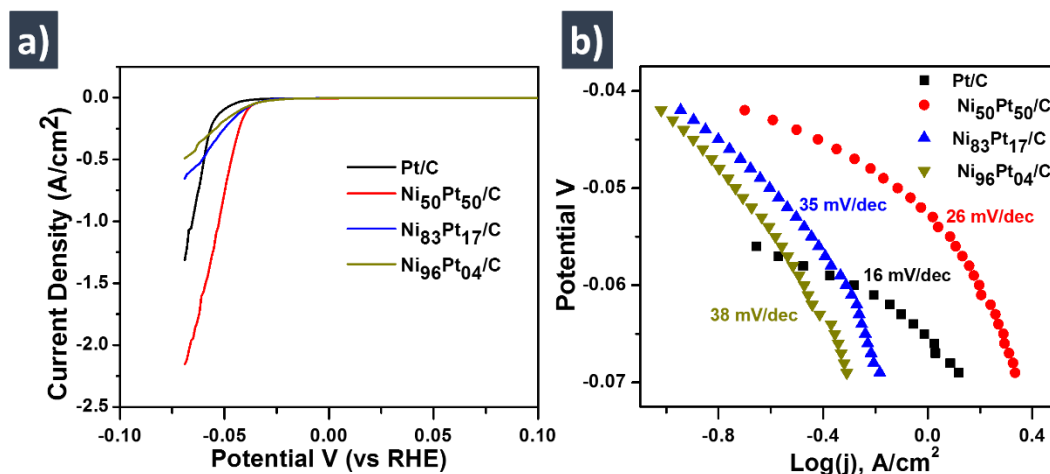
**Figure 4.9: a) Linear sweep voltammogram recorded in 0.5M H₂SO₄at Scan rate –
10 mV/s and 2500 RPM. And b) Tafel slope for Pt/C and NiPt/C nanoalloys having
different Ni:Pt compositions.**

The electro-catalytic activity of all the catalysts was further evaluated on the basis
of Tafel slopes. From figure 4.9 b) one can easily note that Tafel slope value for $Ni_{50}Pt_{50}-$
AAT/C is 26 mV/Dec which is slightly more than the commercial Pt/C (16
mV/Dec).Interestingly, we have observed the non-linear behavior of Tafel plot for
$Ni_{50}Pt_{50}-$AAT /C which indicates the over potential dependent modification in HER
mechanism. Tafel slope determined from the two linear regions and Tafel slope value
turned to be 15 mV/dec for $Ni_{50}Pt_{50}-$AAT/C. Results of Tafel slope can be summarized
that $Ni_{50}Pt_{50}-$AAT/C catalyst favors faster hydrogen evolution compare to commercial
Pt/C catalyst. The actual efficiency of the catalysts was estimated based on current
density at 60 mV potential and given in Table No. 4.4. Current density for $Ni_{50}Pt_{50}-$
AAT/C is almost three times higher than commercial Pt/C catalyst. Therefore, based on

onset potential, Tafel slope and current density $Ni_{50}Pt_{50}-AAT/C$ is found to be most efficient electrocatalyst for the HER.

Table 4.4. Details value of onset potential, Tafel slope and efficiency.

Electro-catalyst	Onset Potential (@ j = 25mA), mV	Tafel Slope, mV/dec	Efficiency (j@ = 60 mV), mA/cm^2
Pt/C	40	20	522
$Ni_{50}Pt_{50}/C$	30	26	1571
$Ni_{83}Pt_{17}/C$	30	35	486
$Ni_{96}Pt_{04}/C$	30	38	337
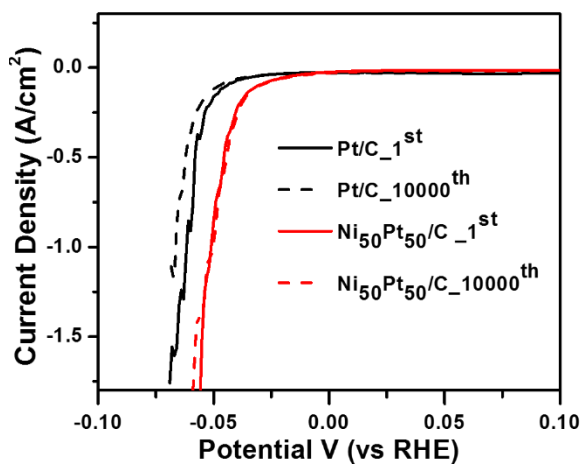
Figure 4.10: Durability test conducted for Pt/C and $Ni_{50}Pt_{50}/C$ through repetitive linear sweep voltammograms in 0.5M H₂SO₄. Scan rate – 2000 mV/s and 3500 RPM.

Importantly, the durability of electrocatalyst is a vital aspect for the technological applications hence we have checked their durability for 10000 repetitive LSVs (see Figure 4.10). Repetitive LSVs measurements of Pt/C catalyst indicated the slight decrease in HER activity, regarding onset potential and current density, whereas onset potential, and current density for $Ni_{50}Pt_{50}-AAT/C$ remained same up to 14000 scans which confirmed that $Ni_{50}Pt_{50}-AAT/C$ was the durable catalyst. We attempted to understand the durable nature of compared $Ni_{50}Pt_{50}-AAT/C$ to Pt/C using cyclic

voltammetry (CV). Cyclic voltammograms were recorded after few LSVs and after stipulated repetitive LSVs, (see the Figure 4.10). In case of Pt/C catalyst, initial cyclic voltammogram indicates the well defined crystallographic character of Pt which was modified after repetitive scans (see the figure 4.11 a). On the other hand, initial cyclic voltammograms of $Ni_{50}Pt_{50}$−AAT/C exact overlaps with cyclic voltammogramsrecorded after 10000 cycle(see the figure 4.11 b). This electrochemical study can be concluded as $Ni_{50}Pt_{50}$−AAT/C is highly stable and durable catalyst for HER.
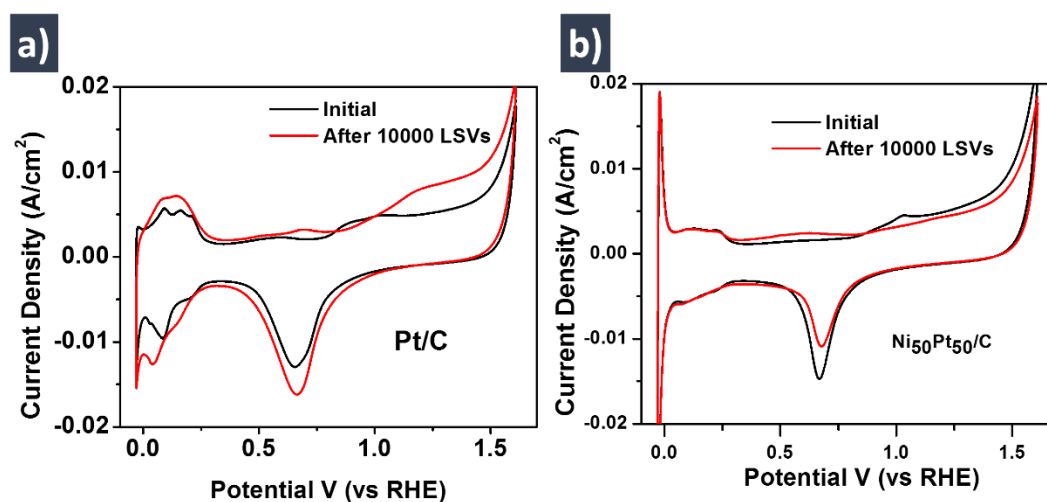
Figure 4.11: Cyclic voltammograms recorded in 0.5M $H_2SO_4$for A) Pt/C. And B) $Ni_{50}Pt_{50}$/C catalyst before and after 10000 LSVs. Scan rate – 50mV/s.

4.3.3 Flow synthesis of NiPt alloy nanoparticles
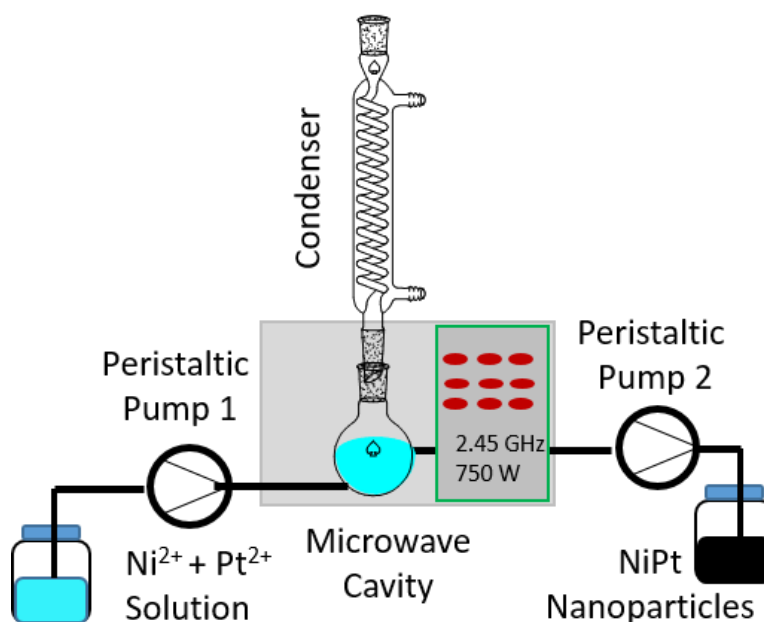
Figure 4.12: Schematics of flow synthesis setup for synthesis of NiPt alloy nanoparticles.

After batch synthesis and evaluation of NiPt nanoparticles for HER, our goal is to synthesize NiPt nanoparticles in flow to increase the production rate by maintaining product quality of alloy nanoparticles. NiPt nanoparticles were synthesized using flow setup as shown in figure 4.12. Batch concentration $Ni(ac)_2$ and $Pt(acac)_2$ was maintained when synthesis was carried out in flow synthesis. A solution of $Ni(ac)_2$ + $Pt(acac)_2$ was injected into CSTR in continuation of microwave irradiation. After few minutes, the black colored precipitate was appeared in the reactor and collected at the outlet. PXRD of NiPt samples synthesized by flow was recorded (see Figure 4.13). These diffraction patterns compared with batch synthesized NiPt alloy. The diffraction pattern of alloy $Ni_{96}Pt_{04}$ synthesized inflow exactly matches with batch synthesized $Ni_{96}Pt_{04}$ alloy nanoparticles which reveals product obtained flow retain its quality (see Figure 4.13 a).

On other hand, PXRD of $Ni_{83}Pt_{17}$ synthesized by flow show slight shift in diffraction which depicts phase segregation during flow synthesis (Figure 4.13b, Curve-II) is prominent compare to $Ni_{83}Pt_{17}$ synthesized in batch (Figure 4.13b, Curve-I).
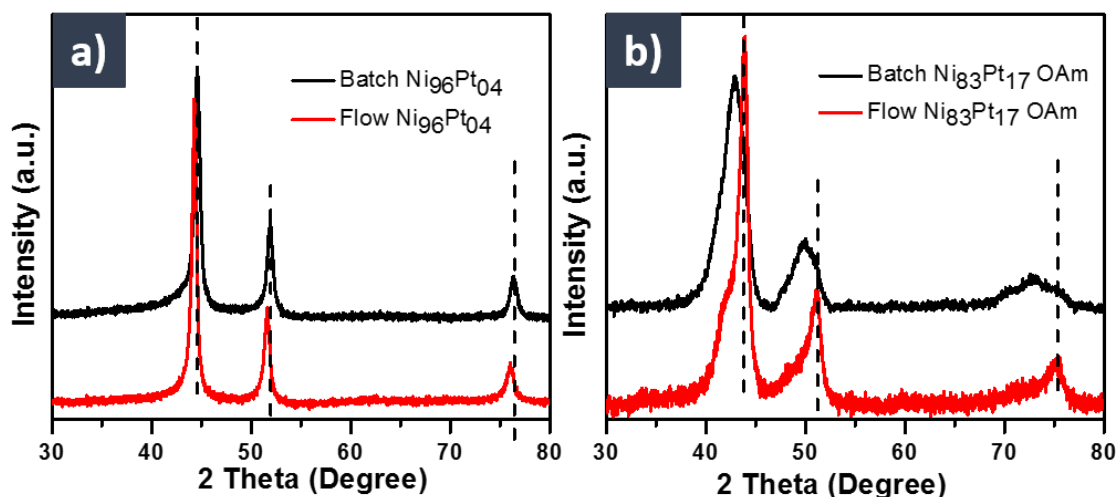
Figure 4.13: PXRD patterns of NiPt alloy synthesized in flow and batch a) $Ni_{96}Pt_{17}$ b) $Ni_{83}Pt_{17}$.
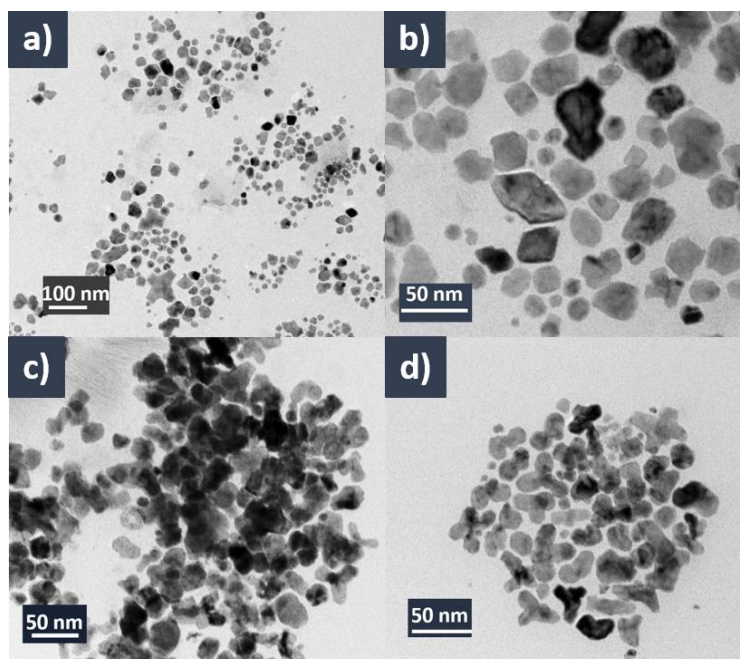
Figure 4.14: TEM images of NiPt alloy nanoparticles synthesized in flow a) and b) $Ni_{96}Pt_{04}$ (Average size, 16 nm) and c) and d) (Average size, 17 nm).

TEM images of flow synthesized $Ni_{96}Pt_{04}$ alloy shows particles are polyhedral in shape and contains cube shaped nanoparticles (see Figure 4.14 a, and b). The shape of $Ni_{96}Pt_{04}$ nanoparticle is similar to the $Ni_{96}Pt_{04}$ alloy obtained in batch with average size is16 nm. Furthermore, $Ni_{83}Pt_{17}$ alloy obtained by flow synthesis shows branched structure, which are in good agreement $Ni_{83}Pt_{17}$ alloy nanoparticles obtained in batch and average size of particles is 17 nm (see Figure 4.14 c, and d). In flow synthesis, the dead time is almost negligible compared to batch synthesis. Hence, production rate by flow synthesis is always higher than the batch synthesis. Here, we achieved 140 mg/h production rate for the synthesis of NiPt alloy nanoparticles by using continuous flow synthesis approach.

4.4 Conclusions

A simple, rapid and novel synthesis of NiPt alloy nanoparticles was developed using microwave-assisted synthesis method. Electrochemical performance for HER of the NiPt alloy was better than the commercial Pt/C. The durability of $Ni_{50}Pt_{50}$ catalyst was better than rest of the NiPt alloy composition. Batch process was successfully transformed to flow process using a CSTR. Microwave-assisted continuous flow process was developed for the synthesis of NiPt which is valuable electro catalyst for hydrogen generation and fuel cell. Adopting to continuous flow synthesis resulted in high production rate (140 mg/h) due to negligible dead time compare to batch process.

4.5 References

1. Gu, J.; Zhang, Y.-W.; Tao, F. F. *Chem. Soc. Rev.* **2012,** 41, 8050-8065.

2. Bu, L.; Zhang, N.; Guo, S.; Zhang, X.; Li, J.; Yao, J.; Wu, T.; Lu, G.; Ma, J.-Y.; Su, D. *Science* **2016,** 354, 1410-1414.

3. Pankhurst, Q. A.; Connolly, J.; Jones, S.; Dobson, J. *J. Phys. D: App. Phys.* **2003,** 36, R167.

4. Wang, P.; Zhang, X.; Zhang, J.; Wan, S.; Guo, S.; Lu, G.; Yao, J.; Huang, X. *Nat. Comm.* **2017,** 8.

5. Kunal, P.; Roberts, E. J.; Riche, C. T.; Jarvis, K.; Malmstadt, N.; Brutchey, R. L.; Humphrey, S. M. *Chem. Mater.* **2017,** 29, 4341-4350.

6. Zhang, D.; Wu, F.; Peng, M.; Wang, X.; Xia, D.; Guo, G. *J. Am. Chem. Soc.* **2015,** 137, 6263-6269.

7. Wu, F.; Zhang, D.; Peng, M.; Yu, Z.; Wang, X.; Guo, G.; Sun, Y. *Ang. Chem.In. Ed.* **2016,** 55, 4952-4956.

8.   Niu, G.; Zhou, M.; Yang, X.; Park, J.; Lu, N.; Wang, J.; Kim, M. J.; Wang, L.; Xia, Y. *Nano letters* **2016,** 16, 3850-3857.

9.   Ding, J.; Bu, L.; Guo, S.; Zhao, Z.; Zhu, E.; Huang, Y.; Huang, X. *Nano letters* **2016,** 16, 2762-2767.

10.   Shen, Y.; Lua, A. C.; Xi, J.; Qiu, X. *ACS App. Mater. Inter.* **2016,** 8, 3464-3472.

11.   Shen, T.; Chen, M.; Du, C.; Sun, Y.; Tan, Q.; Du, L.; Chen, G.; Yin, G. *J. Alloys Comp.* **2015,** 645, 309-316.

12.   Ding, T.; Wang, W.; Zhou, X.; Zhang, L.; Wang, C.; Jiang, J.; Yang, W.; Yang, Q. *APL Materials* **2016,** 4, 015702.

13.   Antolini, E. *Appl. Cata. B.* **2009,** 88, 1-24.

Chapter 5

Batch and Continuous Flow Precipitation of

Organic Particles

5.1 Introduction

For the last three decades, synthesis of inorganic or hybrid (organic-inorganic) nanoparticles has made a mark in nanotechnology because of its unique properties. Synthesis of inorganic nanomaterials has been established to get desired properties of specific materials in nanoform.[1] On the other hand, ultrafine organic particles are becoming popular in colloidal chemistry due to their applications in the electronics, nano-medicine[2], and food industry.[3] Synthesis of small size organic particles/nanoparticles is needed to establish for getting desired properties. Organic particles are formed by the assembly of organic molecules in solution where structural flexibility of organic molecules, size and shape of the particles can tune the properties[4] such as dissolution rate, compressibility, flowability, and bioavailability.[5] Hence, controlled and size-tunable synthesis of low molecular weight (LMW) organic particles are being explored, and it is in infancy. Traditionally, ball milling is used for micronization of the drugs which results in polydispersity in the particles as well as impurity arising from the milling materials.[6] Spray drying, high-pressure homogenization, and supercritical precipitation are different methods used for the preparation of small size drug particles.[7-9] These methods give low yield, poor shape selectivity, particle agglomeration, and also require extreme conditions (such as low temperature and high pressure), expensive instrumentations, and inhibiting large-scale production of small size drug particles. Liquid antisolvent precipitation (LASP)/reprecipitation is becoming popular for the production of small drug particles in the last decade. In this process, precipitation accomplished by diminishing the power of the solvent (S) regarding solute dissolved in a solution. A non-solvent for solute called as antisolvent (AS) is added to the solution. The method is applicable to a wide range of materials such as active pharmaceutical ingredients (APIs), inorganic and organic crystals, polymers and proteins. LASP method is able to produce drug

particles at the normal conditions without the involvement of sophisticated instrumentation.[10] Various small size low molecular weight (LMW) organic crystals have been produced using LASP methods such as ibuprofen, glyburide, artemisinin,[11] silibinin,[12] β-carotene,[13] griseofulvin,[14] and curcumin.[15] Mainly, LMW small size organic particles play an important role in making the stable formulation of active pharmaceutical ingredients (APIs). Though significant efforts have been taken into the direction towards the synthesis of small-sized organic particles in the recent years, it was not enough for realizing scaled up high throughput industry-relevant applications.

Stability of dispersion, dissolution, compressibility, compaction, the flowability of APIs is important properties which depend upon the size of particles. To get desired properties of the APIs, one needs to understand synthesis of ultrafine organic particles. Typically, LASP method has been used to prepare small size organic particles in a batch process. As already mentioned in earlier chapters and discussed that batch format has its own limitation for heat and mass transfer. As LASP is a solvent exchange method, mixing of solvents plays a vital role to produce smaller size particles.[16] The solvent exchange is a diffusion limited phenomenon,[17] where fast and efficient mixing can result in small size monodisperse particles.[10, 18] Slow and inefficient mixing results in locally non-uniform nucleation and growth rates leading to polydispersed particles. In case of LASP in the conventional batch method, processing large volume and controlled the addition of reagent to achieve homogeneous mixing becomes very difficult. Currently, large size continuous stirred tank reactor or homogenizers are used where controlled addition is achieved, the mixing time scales are not smaller than the precipitation time scales. Moreover achieving spatial homogeneity in large tanks is not an easy task.[19] To resolve these issues, we have suggested an alternative method for continuous flow synthesis of LMW small size API or

organic particles using inverted jet reactor. As a model system, we chose metformin hydrochloride (MHC) API for this purpose. MHC is LMW drug molecules cure type-2 diabetes[20]. Although MHC is a water-soluble API, the objective was to produce small size MHC particles and in future which can be encapsulated into organic stabiliser and achieve control drug release and targeted drug release in an aqueous environment.

5.2 Experimental Section

5.2.1 Chemicals and Materials

Metformin Hydrochloride (MHC) powder supplied by *Abhilash Chemicals Pvt. Ltd* and has been used as received for the experiments. Organic solvents such as 1-butanol (99.5% pure from *Merck Chemicals Ltd,* India) and 1-propanol (99.0% pure from *Merck Chemicals Ltd,* India) were used as anti-solvent. Milli-Q water is used for making the aqueous solution of metformin hydrochloride (MHC). These chemicals have been used without any further purification. Histidine was purchased from *HiMedia Laboratories Pvt. Ltd.* India Company and used as it is.

5.2.2 Batch LASP of MHC

Batch experiments were conducted in 30 mL glass vials. Aqueous solutions of MHC at different concentrations were prepared as mentioned in Table 5.1. The antisolvent mixture was prepared by mixing isopropanol and n-butanol in 50% v/v proportion kept at desired temperature using a temperature bath (Julabo, Germany). A glass vial containing 15 mL of antisolvent was partially submerged into an ultrasound bath (Equitron, India) operating at 53 KHz, 100% power at room temperature. 1 mL of 85% saturated solution of MHC was immediately injected into antisolvent with continuous sonication. A drop of the precipitate obtained after a minute was

placed on a glass slide for determination of particle sizes. To measure particles size, the precipitate was dispersed in four equivalent volumes of n-butanol to capture an image having less aggregated particles on the glass slide. The precipitate was separated by vacuum filtration using Whatman paper 1 and dried at room temperature. (Length of particles considered as size.)

Table 5.1. Solute (MHC) concentration in water

Sr. No.	Solute concentration(%)	Solublity of MHC (gm/10 mL)
1	100	4.120
2	95	3.914
3	90	3.708
4	85	3.502
5	80	3.296
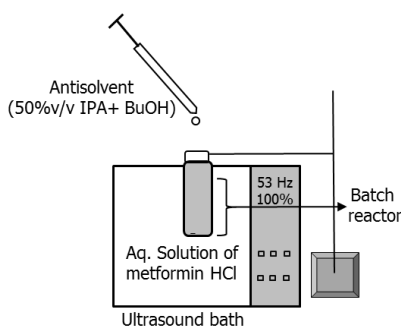
Figure 5.1: Schematics batch setup for LASP.

5.2.3 Continuous LASP in flow

5.2.3. A) Continuous flow LASP of MHC in Co-capillary

Continuous LASP experiments were carried out using co-capillary, schematic of the experimental setup is shown in figure 5.2. The inlet joint was made of two coaxially aligned cylindrical glass capillary tubes (outer diameter of 3.8 mm and the inner diameter of 0.55 mm).

The antisolvent was used as the outer phase, and the MHC solution was used as the inner phase. The flow rate of the MHC solution and antisolvent is maintained at 0.72 mL/min and 10.79 mL/min respectively, keeping an antisolvent to solution flow rate ratio of 15. A glass capillary of 3.8 mm diameter and 49 cm length was used, which provided a residence time of 30.5 s. The co-capillary outlet is connected to a filtration assembly which consisted of a Whatman filter paper 1, Büchner funnel and a vacuum pump (Buchi V-100, Switzerland). After a few seconds of mixing white coloured precipitated was observed into capillary and precipitate was filtered using a vacuum pump and dried at room temperature.
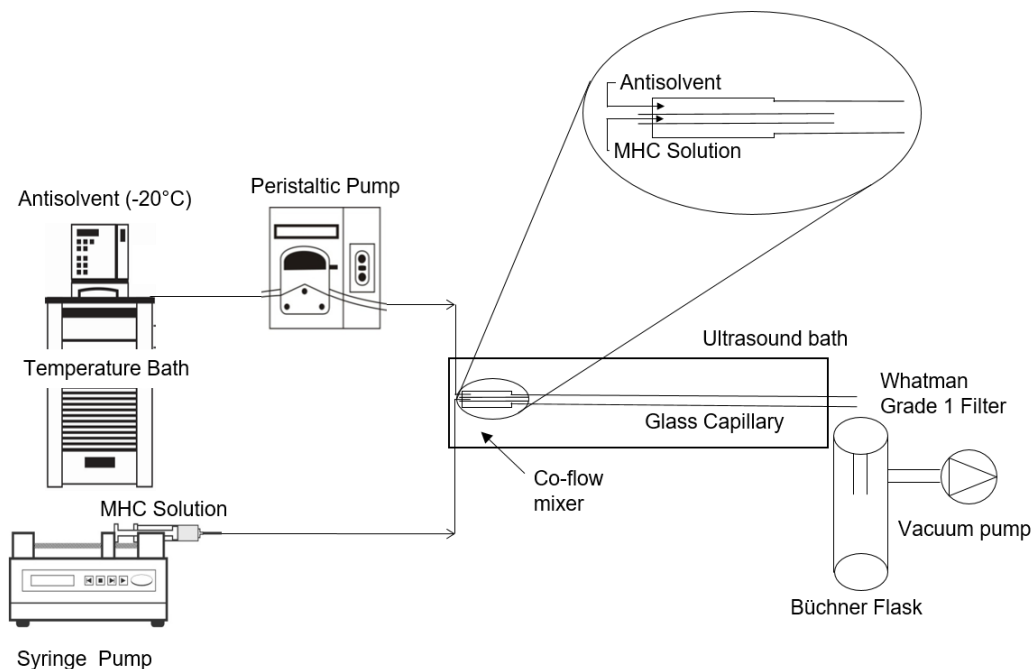
Figure 5.2: Schematic of co-capillary experimental setup for continuous flow precipitation of MHC.

5.2.3 B) Continuous flow LASP of MHC in the inverted jet reactor

Inverted impinging jet reactor (IIJR) was immersed in an ultrasound bath as shown in the schematic representation of the experimental setup in figure 5.3. Bell shaped IIJR having three

inlets of 1 mm I.D. has been used for continuous precipitation. Two inlets were directed opposite to each other, and the third inlet was perpendicular to two opposing inlets from the bottom of the reactor. Two peristaltic pumps were used to flow the antisolvent (isopropanol: n-butanol, 50% v/v) through two side inlets of IIJR using insulated silicon tubing at a flow rate of 15 mL/min. A syringe pump (Longer Pumps, China) was used to flow the metformin hydrochloride solution from the central inlet of the reactor. These two streams of antisolvent along with the third stream of MHC solution undergo rapid mixing (at a flow rate of 1mL/min) under sonication.

Figure 5.3: Schematics of the experimental setup for continuous flow synthesis of MHC particles.

5.3 Results and Discussion

Our exploration for the preparation of MHC particles started with a selection of a favorable solvent and antisolvent for precipitation. Key features to obtain ultrafine API particles by LASP are i) antisolvent should be miscible with solvent and ii) API should have minimum solubility into antisolvent. In this work, water is chosen as a solvent because of the high solubility of MHC in water and a mixture iso-propanol : n-butanol (50% v/v) is used as antisolven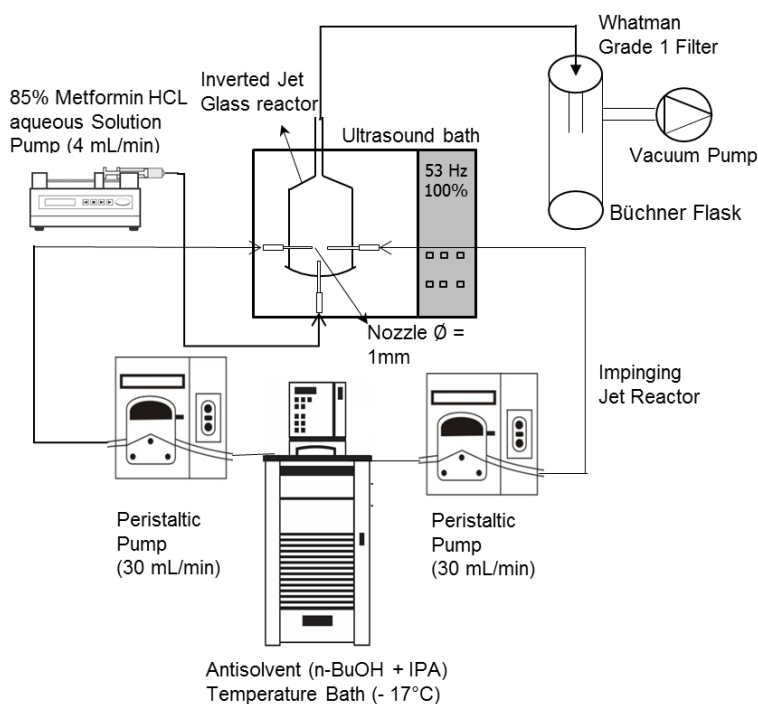t. Various polar organic solvent is miscible with water such as alcohols, THF, acetone, acetonitrile, etc. IPA : n-butyl alcohol 50% v/v mixture were used to for reprecipitation or LASP of MHC. When an aqueous solution of MHC injected into IPA and n-butanol mixture, the white coloured precipitate was observed almost instantaneously. Here, we would like to summarize that mixture of IPA : n-butanol (50% v/v) act as antisolvent due to increase in hydrophobic nature that causes precipitation of MHC.

5.3.1 Effect of MHC solution saturation

The driving force for precipitation is the supersaturation created by mixing the API solution and the antisolvent.[10] The level of supersaturation depends upon the concentration of solute and the amount of antisolvent. In this section, we studied the effect of concentration of solute on the particles size of MHC at the fixed antisolvent amount. From a standard 100% solute concentration solution of MHC, 95 % to 80 % solute concentration solution was made and injected into the 15 mL antisolvent with under sonication. After the solvent exchange, precipitate yielded smaller size MHC particles. Figure 5.4 displays optical microscope images of MHC particles clearly depicting elongated and cubic morphology. A large number of bigger sized rods shaped particles were observed at 95% solute concentration compared to all other concentration

(see figure 5.4d). MHC particles precipitated at 85% solute concentration was found to be small size cubes, rods and needle-shaped (see figure 5.4b).
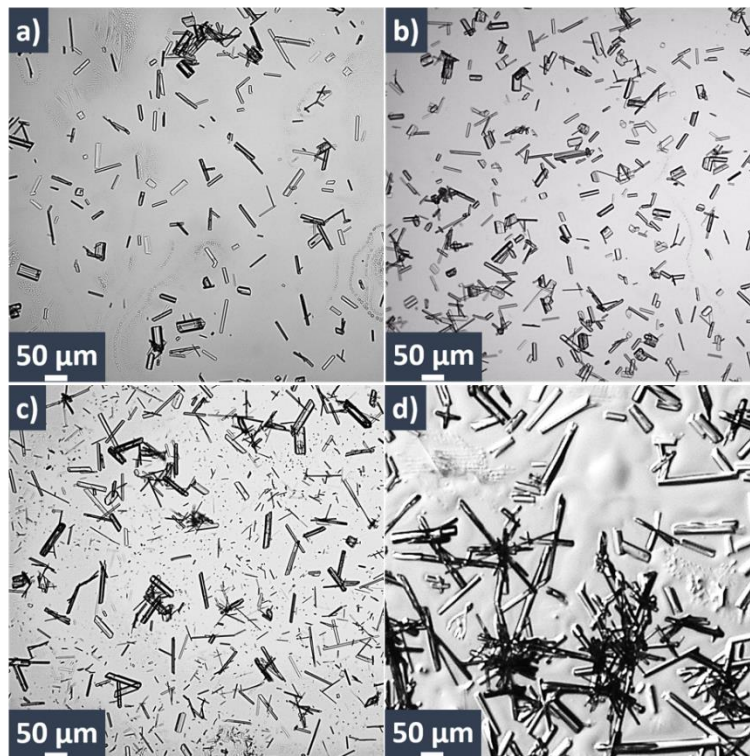
Figure 5.4: Optical micrographs of MHC particles prepared at different % solute concentration (Solution Temperature 25°C, Ultrasound Bath); (a) 80%, (b) 85%, and (c) 90%, (d) 95%.

To measure average size of particles, randomly 300 particles were selected for size (length) measurement. It was expected that increase in the solute concentration of MHC would yield smaller particles due to reaching higher supersaturation ratio. In contrary to our assumption, the particle size of MHC is found to be larger for high MHC concentration (95%, 65 μm) compared to the low MHC concentration (80%, 44 μm) (see the Figure 5.5). Variation in size and shape depends upon both events - nucleation and growth. At a higher concentration, a larger number of nuclei formed immediately after mixing of the solute and the antisolvent, as well as larger number of monomers were also present in solution. Though a larger number of

nuclei is formed higher concentration of solute leads to enhanced growth of those nuclei. With lowering the solute concentration (85%), sufficient number of nucleis were formed due to a very high antisolvent ratio but due to less number of monomer present into the solution for growth significantly decreses. This results into smaller size of MHC particles (35.75 μm). For further reduction of concentration (80%) the nucleation rate decreases significantly and lesser number of nucleis are formed. Despite reduction in concentration, sufficient number of monomers were present in solution for lesser number of nucleis. This resulted in an increase in the size of MHC particles. To conclude this section, 85% MHC solution gives a large number of nuclei which reflects a smaller size of MHC particles and is used for further experiments as optimum solute concentration.

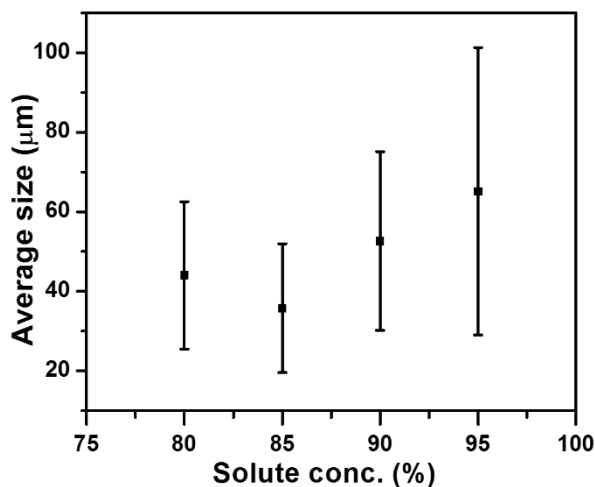**Figure 5.5: Effect of solution saturation on the MHC particle size.**

5.3.2 Effect of antisolvent to solvent (AS/S) ratio

Effect of antisolvent to solvent (AS/S) ratio on particles size was studied at room temperature, and it was observed that AS/S to ratio plays a vital role and deciding MHC particle size. Figure 5.6 shows the change in the particle size with AS/S ratio due to variation in the

degree of supersaturation. As the AS/S ratio increases from 5 to 15, particles of MHC becomes smaller in size (see Figure 5.6a). Here, AS/S ~ 15 yields smaller size particle having an average size 26.10 μm. This is due to the higher degree of supersaturation, producing a large number of smaller nuclei at increased AS/S ratio up to 15. At the AS/S ratio of 15, the maximum amount of MHC forms nuclei, which as a result leaves fewer MHC dissolved in the solution that is available for further growth. This results in smaller size MHC particles. The high degree of supersaturation also resulted into narrow particle size distribution (PSD) at AS/S ratio 15 (see Figure 5.6b). On the other hand, a further increase in AS/S ratio from 15 to 25 reflected into an slight increase in particle size which is quite unpredictable.
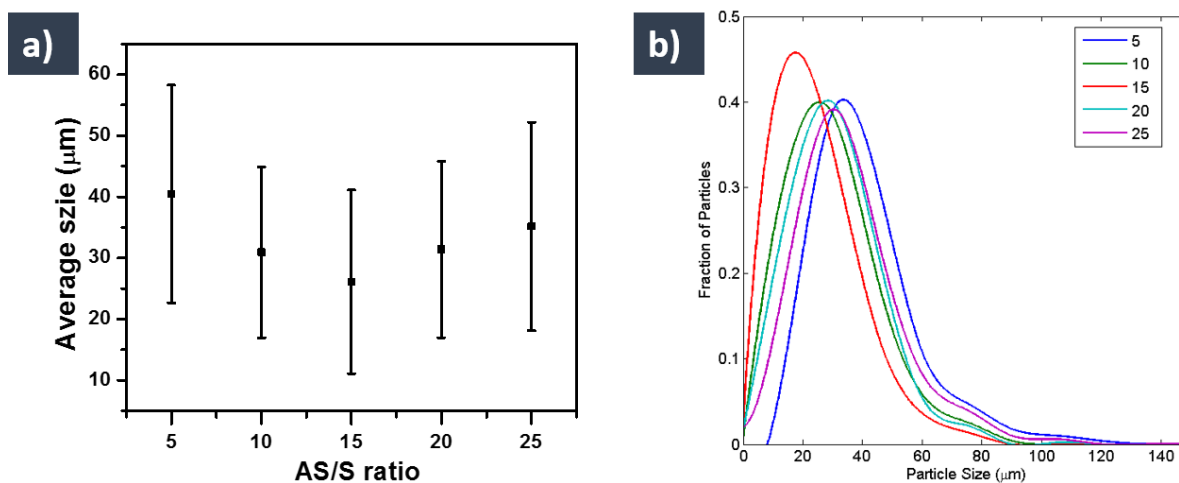
Figure 5.6: a) Particle size measurement b) Particle size distribution.

Optical microscopy images display the morphology of MHC particles (see the Figure 5.7). MHC particles prepared using different AS/S exhibits anisotropic structure such as needle, rods and cubes. In most of the cases, the MHC particles grow along the length which can be attributed to the monoclinic crystal structure of MHC, which leads to needle and rod shape growth. At AS/S ratio 5, the shape of particles is decided by the growth of the specific planes and hence the particles grow into needle shape (see Figure 5.7 a).

Figure 5.7: Optical micrographs of MHC particles prepared at different AS/S ratios (Solution Temperature 25°C, Ultrasound Bath); (a) AS/S = 5, (b) AS/S = 10, (c) AS/S = 15, (d) AS/S = 20, and (e) AS/S = 25.

When AS/S ratio was increased from 5 to 15, particle shapes started changing from needles to the rod and eventually to cubes. This change in shape of MHC particles can be attributed to the relative rates of nucleation (viz. in burst nucleation, less amount of MHC monomer available for growth process at 15 AS/S ratio in comparison to 10 and 5 AS/S ratio). With further increase in the AS/S ratio from 15 to 30, the concentration of MHC in total volume decreased when injected into antisolvent (AS) that causes slow nucleation and growth leading to large size anisotropic particles involving rods and cubes (see Figure 5.7 c-e).

5.3.3 Effect of antisolvent temperature

In reprecipitation, the driving force in attaining supersaturation is the antisolvent addition as well as temperature reduction. At room temperature, the choice of antisolvent and AS/S ratio was optimised. Here, we have systematically investigated the effect of temperature on particle size. A significant reduction in precipitation is observed with the decrease in AS temperature. It was noted that 24 s, 32 s, 35 s, and 51 s were the precipitation time required at -20˚C, -15˚C, -10˚C and -5˚C respectively. As a consequence of lowering temperature, precipitation occurs relatively faster when compared to a higher temperature which could produce small size particles.
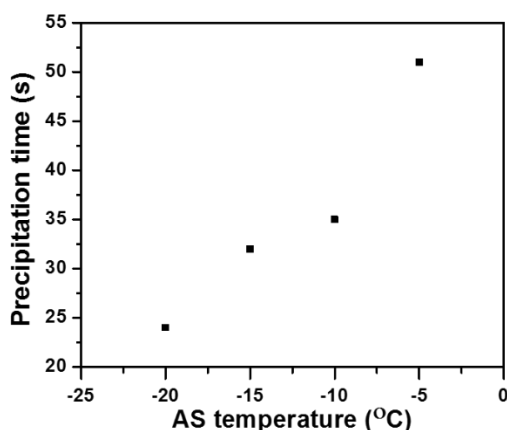
Figure 5.8: Effect of temperature on precipitation time of MHC particles.

The temperature of the antisolvent was reduced to increase the degree of supersaturation by LASP. Optical microscope images depict the change in particle size and morphology as the temperature of antisolvent decreases from -5ºC to -20ºC (see Figure 5.9). Majority of the particles obtained at -5ºC are found to be rod shapes (see Figure 5.9a). However, particle obtained at -20ºC found to be a mixture of smaller sized cubes as well as rod shape (see Figure 5.9d). Due to a technical limitation of thermostat we could not experiment below -20ºC temperature. From optical images, size and aspect ratio of MHC particles are determined.
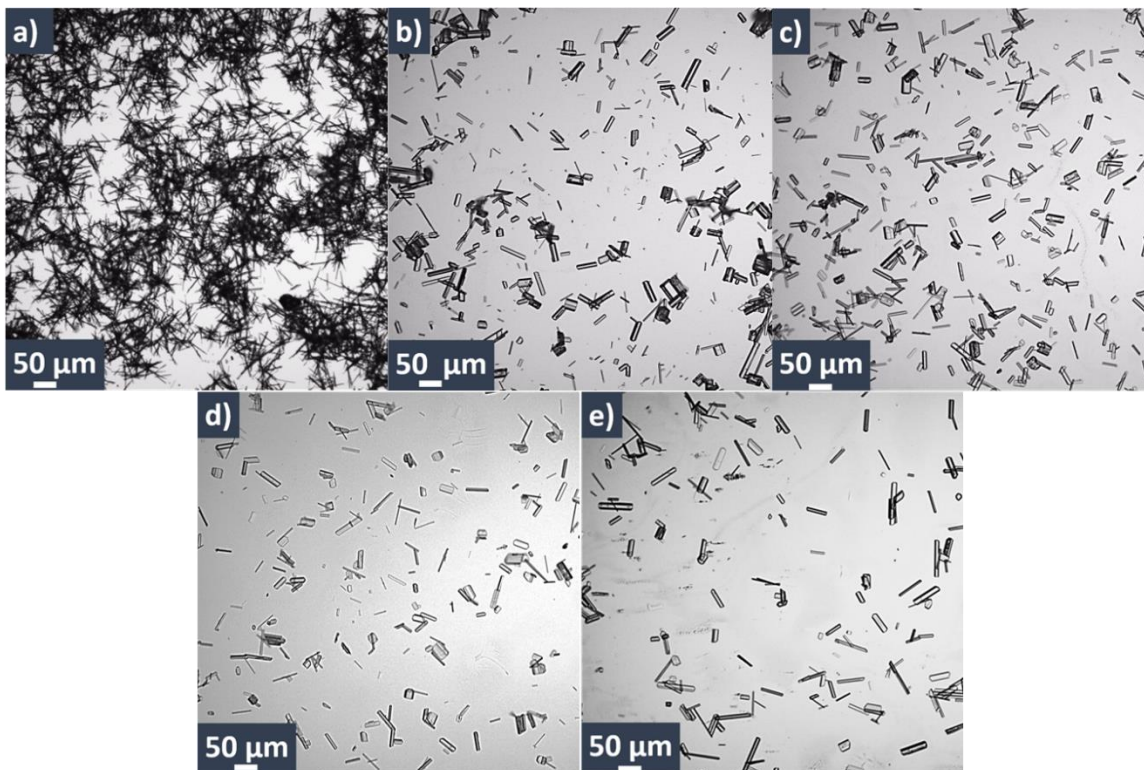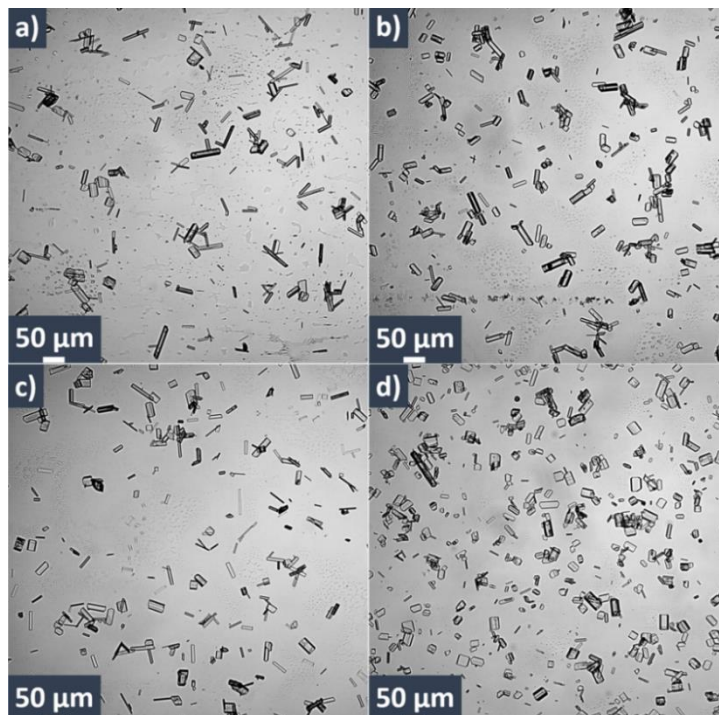
Figure 5.9: Optical micrographs of MHC particles prepared at different temperatures (Solution Temperature 25°C, Ultrasound Bath); (a) -5°C, (b) -10°C, (c) -15 °C, and (d) -20°C.

From figure 5.10a, it can be observed that the reduction in the antisolvent temperature results in more uniform and smaller size MHC particles (-20 ˚C, 19.79 µm). The aspect ratio of the precipitated particles was also observed to reduce with decreasing antisolvent temperature (see Figure 5.10b).
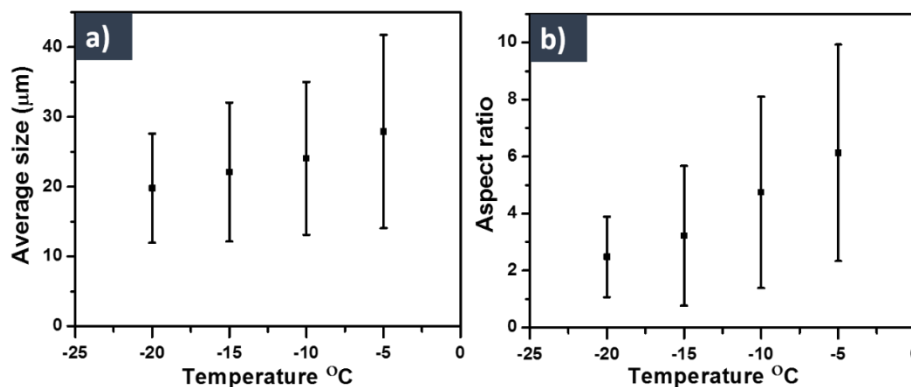
Figure 5.10: Effect of antisolvent temperature on A) particle size, and B) aspect ratio
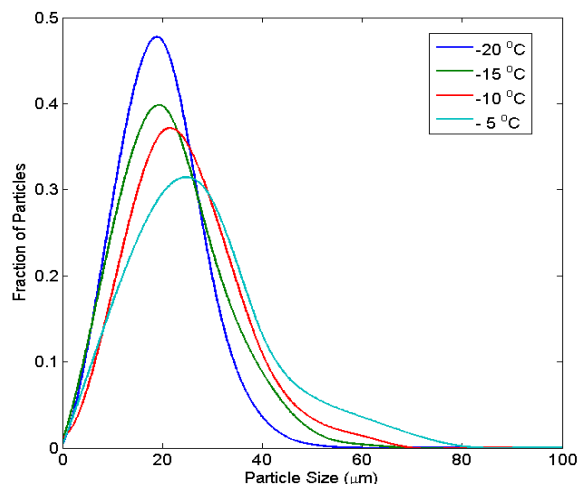
Figure 5.11: Effect of antisolvent temperature on particle size distribution.

In figure 5.11, particle size distribution curve shows the effect of temperature on the degree of supersaturation that results in narrow PSD. The rise in the peak height and movement of peaks to the smaller particle size were observed with decreasing temperature (see Figure 5.11). The main reason behind this is lowering of the antisolvent temperature that results in higher supersaturation ratios leading to the formation of larger number of smaller size nuclei. On the other hand, precipitation of MHC is diffusion limited phenomenon. Due to a decrease in the temperature, the viscosity of antisolvent increases which results in the slow diffusion of smaller nuclei/particle. Hence, further particle growth is not possible at low temperature by coalescence and aggregation because of the slow diffusion. Antisolvent temperature plays an important role to achieve a high degree of supersaturation which limits the growth of nanoparticles due to increase in viscosity. Finally, -20 °C is selected as the optimum AS temperature producing smaller size MHC particles having 19.88 μm average size and 2.48 aspect ratio.

5.3.4 Continuous precipitation

Initial continuous flow experiments were performed in a co-flow capillary reactor as the optimised antisolvent to solution ratio for the batch experiments. Parallel flow is observed for a different range of flow rates which was not able to provide adequate mixing performance for precipitation. Submerging the co-capillary system into an ultrasound bath resulted in better mixing leading to precipitation but the particle size observed was quite high (~55 μm) compared to the optimum batch conditions (see Figure 5.12a). This was due to severe growth of the particles at the stable interface between the two phases in parallel flow.

A novel inverted impinging jet reactor having three inlets has been developed to attain better mixing between antisolvent and solvent. Experimental parameter optimised for LASP in batch at -20˚C were considered for continuous flow LASP in the inverted jet reactor. Optical microscope image of MHC particles displays that MHC particles are rod and cube shape (see Figure 5.12b). The particles size is determined from optical image was 20 μm which is smaller than particle obtained in batch (22.2 μm) and co-capillary (55 μm). Reduction in size using inverted jet reactor is attributed to efficient mixing. Although, mixing of antisolvent and solvent play important role to achieve faster supersaturation that ensued small sized MHC particles, addition of additive would inhibit growth of MHC particles during LASP. To arrest growth of particle, 1 mass % histidine was added while preparing MHC solution. A further reduction in the particle size is observed with the addition of histidine (see Figure 5.13) though the particle morphology remained the same (see Figure 5.12c). The particle sizes obtained in various experiments conditions are compared in figure 5.13. Above result could be shortly described as continuous inverted jet reactor LASP process yield small size MHC particles due to efficient mixing and addition of additive hinder the growth of MHC particle lead to small size particles.

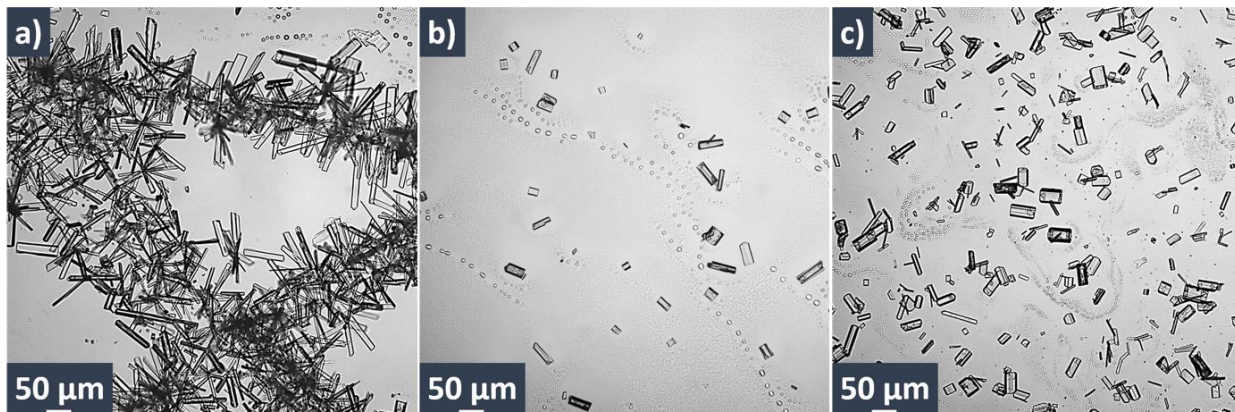**Figure 5.12: Optical microscope images of MHC particles prepared in flow a) without additive in co-capillary reactor (Average particle size, 55µm), (b) without additive in inverted jet reactor (Average particle size, 20 µm), and (c) with additive in inverted jet reactor (Average particle size, 15.8 µm).**
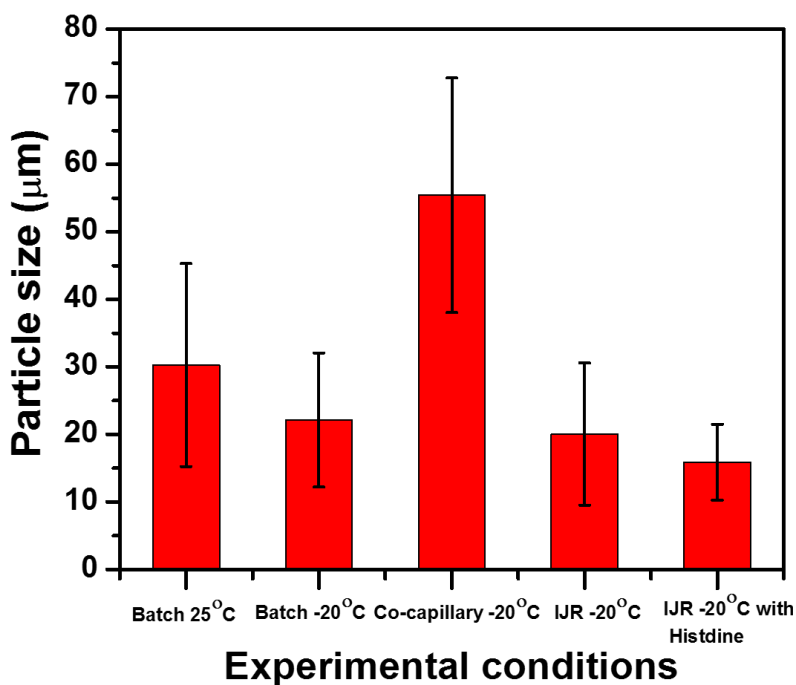

Figure 5.13: Particle size of MHC by LASP from different experimental conditions.

5.4 Conclusions

We have systematically investigated the effect of AS/S ratio, the concentration of solute, temperature and mixing on LASP to get small sized MHC particles. At -20 C, AS/S 15 and 85% solute concentration is best optimized condition produced small sized (19.79 μm) MHC particles. Adoption of batch LASP process into continuous flow process successfully achieved using IIJR. Continuous flow process was adopted to produce small-sized MHC particles in large quantity in a reproducible manner. We can obtain 15 μm sized MHC particles at -20 ˚C by continuous flow LASP in the inverted impinging jet reactor due to the efficient mixing.

5.5 References

1.   Ghosh Chaudhuri, R.; Paria, S. *Chem. Rev.* **2011,** 112, 2373-2433.

2.   Silva, A. S.; Tavares, M. T.; Aguiar-Ricardo, A. *J. Nanopart. Res.* **2014,** 16, 2602.

3.   Sanguansri, P.; Augustin, M. A. *Trends Food Sci. Technol.* **2006,** 17, 547-556.

4.   Kawashima, Y.; Cui, F.; Takeuchi, H.; Niwa, T.; Hino, T.; Kiuchi, K. *Powder Tech.* **1994,** 78, 151-157.

5.   Khadka, P.; Ro, J.; Kim, H.; Kim, I.; Kim, J. T.; Kim, H.; Cho, J. M.; Yun, G.; Lee, J. *Asian J. Pharm.* **2014,** 9, 304-316.

6.   Müller, R.; Böhm, B.; Grau, M. *Pharm. Ind* **1999,** 61, 175-178.

7.   Freitas, C.; Müller, R. H. *Eur. J. Pharm. Biopharm.* **1998,** 46, 145-151.

8.   Komai, Y.; Kasai, H.; Hirakoso, H.; Hakuta, Y.; Katagi, H.; Okada, S.; Oikawa, H.; Adschiri, T.; Inomata, H.; Arai, K. *Jpn. J. Appl. Phys.* **1999,** 38, L81.

9.   Silva, A.; González-Mira, E.; García, M.; Egea, M.; Fonseca, J.; Silva, R.; Santos, D.; Souto, E.; Ferreira, D. *Colloids Surf. B* **2011,** 86, 158-165.

10.   Zhao, H.; Wang, J.-X.; Wang, Q.-A.; Chen, J.-F.; Yun, J. *Ind. Eng. Chem. Res.* **2007,** 46, 8229-8235.

11.   Khan, S.; Matas, M. d.; Zhang, J.; Anwar, J. *Crys. Growth Des.* **2013,** 13, 2766-2777.

12.   Wu, W.; Zu, Y.; Wang, L.; Wang, L.; Li, Y.; Liu, Y.; Wu, M.; Zhao, X.; Zhang, X. *RSC Adv.* **2017,** 7, 54379-54390.

13.   Horn, D. *Macromol. Mate. Eng.* **1989,** 166, 139-153.

14.   Beck, C.; Sievens-Figueroa, L.; Gärtner, K.; Jerez-Rozo, J. I.; Romañach, R. J.; Bilgili, E.; Davé, R. N. *Powder Tech.* **2013,** 236, 37-51.

15.   Thorat, A. A.; Dalvi, S. V. *Chem. Eng. J.* **2012,** 181, 1-34.

16.   Matteucci, M. E.; Hotze, M. A.; Johnston, K. P.; Williams, R. O. *Langmuir* **2006,** 22, 8951-8959.

17.   Heyer, H. *Angew. Chem. Int. Ed.* **1965,** 77, 745-745.

18.   Horn, D.; Rieger, J. *Angew. Chem. Int. Ed.* **2001,** 40, 4330-4361.

19.   Hartman, R. L.; McMullen, J. P.; Jensen, K. F. *Angew. Chem. Int. Ed.* **2011,** 50, 7502-7519.

20.   Setter, S. M.; Iltz, J. L.; Thams, J.; Campbell, R. K. *Clin. Ther.* **2003,** 25, 2991-3026.

Chapter 6

Conclusions

Conclusions

The chapter first highlights increase in demand for nanomaterial due to its applications in consumer products. Scale-up of nanomaterial faces many limitations and challenges to realize industrial usage of nanomaterials. Integration of flow process with microwave or ultrasound showed potential to realize scalable production. We have adopted flow process for various nanomaterial including inorganic nanoparticles and organic particles.

In chapter 2, rapid and novel process were developed for the synthesis of monocrystalline CuO and Cu_2O nanoparticles using microwave-assisted synthesis. pH of reaction solution determined the phase purity of copper oxide. We found that at acidic pH, benzyl alcohol acted as reducing and obtained Cu_2O nanoparticles. Adoption of the batch to continuous flow process was successfully conducted by understanding reaction parameters in a batch process. Integration of continuous flow synthesis with microwave used to synthesize CuO nanoparticles up to production rate of 61 g/day maintaining particle size < 5 nm. Semiconducting nature of copper oxide was exploited for detection of hydrazine hydrate which showed CuO could be used as gas sensing material. Nanofluids of CuO in ethylene glycol which showed 9% thermal conductivity enhancement at 4% volume fraction of CuO nanoparticles.

In chapter 3, nickel and Pd/ Ni nanoparticles have been successfully synthesized using a microwave -assisted method in which benzyl alcohol acts as a solvent as well as reducing agent. In the presence of oleylamine, nickel nanoparticles could be obtained in a very short time of 4 min. We could extend this procedure to prepare nickel supported palladium nanocomposite via both the batch processes and continuous flow manner. This resulted in a reproducible synthesis protocol for these bimetallic nanoparticles. The Ni supported Pd

nanomaterial was found to be an active catalyst for the hydrogenation of alkene, alkyne, and aryl nitro compounds. The catalyst used could be easily retrieved by applying an external magnet. The flow synthesis approach reported here is easy to scale-up and can be used for other supports such carbon, metal oxide, and polymer.

In chapter 4, benzyl alcohol route was used to prepare bimetallic alloy of NiPt nanoparticles. The initial molar concentration of $Ni(ac)_2$ and $Pt(acac)_2$ was varied to obtain NiPt alloy with a different composition of Ni and Pt content. Batch synthesis parameters were considered to carry out flow synthesis which also produced a similar product as obtained in batch. NiPt alloy nanoparticles synthesized at 140 mg/h production rate. Evaluation of the electrocatalytic activity of 20 wt % loading of NiPt alloy nanoparticles on carbon for electrochemical HER showed that $Ni_{50}Pt_{50}/C$ shows higher efficiency for hydrogen evolution.

In Chapter 5, we explore rapid reprecipitation reaction in continuous flow process to obtain small size metformin nanoparticles. Fast mixing was realized using inverted impinging jet reactor and ultrasound. This fast mixing helped to attain a higher degree of supersaturation very rapidly which caused a reduction in the size of nanoparticles.

Our work in this thesis may inspire many researchers across the world to exploit the flow process for the production of nanomaterial in a large quantity.

Appendix – I

Instruments Used

UV-vis-NIR spectrophotometer: UV-Visible-NIR spectral measurements were carried out using JASCO V-570 model UV-Visible spectrophotometer with a resolution of 1 nm

X-ray Diffreaction: The diffractograms were recorded on a PAN analytical Xpert promachine using a CuKα (λ= 1.54 Å) source and operating conditions of 40 mA and 30 KV at different scan rates depending upon sample.

Transmission Electron Microscopy: Sample were characterized with Technai T-20 transmission electron microscope operated at 200 kV. For high resolution images Technai T-30 instrument operated at 300 kV was used. TEM samples were prepared by coating drop casting the samples on TEM grid and allowed to dry under ambient conditions.

Scanning Electron Microscopy: SEM images of samples were recorded using FEI Quanta environmental SEM operated at 20kV.

Surface Area Analysis: BET surface area of the samples measured using Quantachrome autosorb instrument.

Chromatography: Product of hydrogenation reaction were analysized on Thermo Fischer trace GC Ultra instrument (Column HP-5, I.D. = 0.25 mm, L =30 m).

Atomic Absorption Spectroscopy: Elemental analysis was done by using Agilent technology 240FS instrument.

Optical microscopy: A drop of the solution containing precipitate place on glass slide and examined under stereo-microscope on Zeiss Primo Star.

Appendix -II

List of abbreviations

CSTR	Continuous stirred tank reactor
I.D.	Inner diameter
O.D.	Outer diameter
R_e	Reynolds numbers
μ	Viscosity
V	Velocity of fluid
Dh	Hydraulic diameter
CTAB	Cetyltrimethylammonium bromide
PXRD	Powder X-ray diffraction
JCPDS	Joint committee on powder diffraction standards
TEM	Transmission electron microscope
UV	Ultraviolet
DRS	Diffuse reflectance spectrometer
EDX	Energy dispersive X-ray
AAS	Atomic absorption spectroscopy
OAm	Oleylamine
LASP	Liquid antisolvent precipitation
IIJR	Inverted impinging jet reactor
MHC	Metformin hydrochloride

Appendix –III

List of publications

1. **Arun V. Nikam**, Arulraj Arulkashmir, Kothamdam Krishanmoorthy, Amol A. Kulkarni and B. L. V. Prasd, pH dependent single step rapid synthesis of CuO and Cu2O nanoparticles from the same precursor, *Cryst.Growth Des.*, **2014**,14, 4329-4334.

2. **Arun V. Nikam**, Amol A. Kulkarni, and B. L. V. Prasad, Microwave-assisted batch and continuous flow synthesis of Palladium supported on magnetic Nickel nanoparticles and their evaluation as reusable catalyst, *Cryst. Growth Des*. **2017**, 17, 5163-5169.

3. **Arun V. Nikam**, Amol A. Kulkarni, and B. L. V. Prasad, Controlled Synthesis of Metal Oxide Nanoparticles, (**Review article - In preparation**).

4. **Arun V. Nikam**, Vijay Chaudhari, Amol A. Kulkarni and B. L. V. Prasad, Batch and continuous microwave assisted synthesis of NiPt nanoalloy and their evaluation as electro-catalyst for HER, (**Research article – In preparation**).

5. **Arun V. Nikam**, Arun Dadwal, Pattayil A Joy. Amol A. Kulkarni and B. L. V. Prasad, Flow synthesis of CuO and Cu_2O nanoparticles and their use as nanofluids, (**Research article – In preparation**).

6. **Arun V. Nikam**, Sayan Pal, Amol Kulkarni, B. L. V. Prasad, Preparation of small size metformin hydrochloride particles using integration of flow synthesis and ultrasound, (**Research article – In preparation**).

7. Yachita Sharma, **Arun V. Nikam**, and Amol A. Kulkarni, Telescopic integration of exothermic and endothermic reactions in multistep flow synthesis. **(Under revision).**
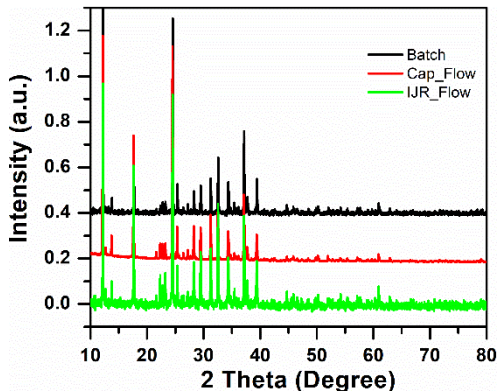
ADDENDUM

I would like to thank examiners for their valuable suggestions. Examiners have brought out some mistakes to my notice. I have modified the thesis taking these suggestion into consideration and incorporated correction as an addendum.
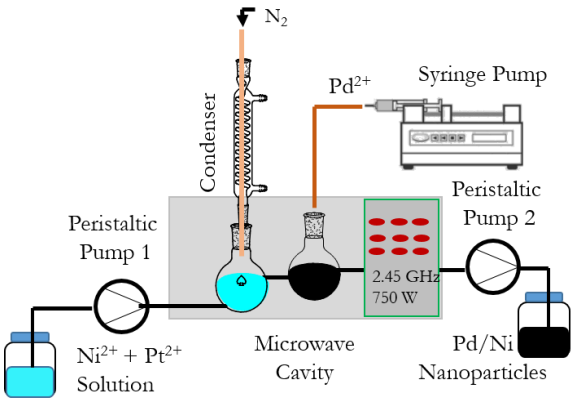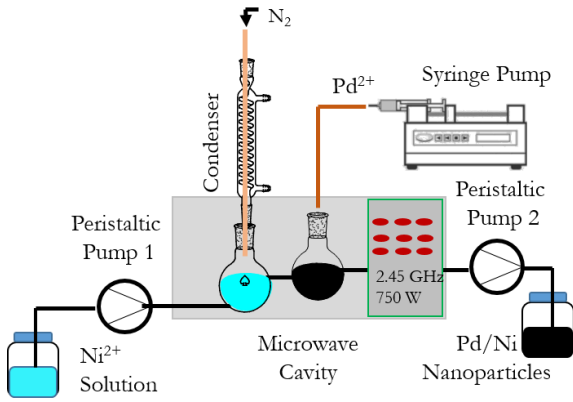
Examiner -1

Recommendation: The thesis is acceptable in the present form for the award of the Ph.D. degree

Examiner -2

The thesis is acceptable and the correction, modifications and improvements suggested by me would be incorporated in the thesis to satisfaction of the oral board.

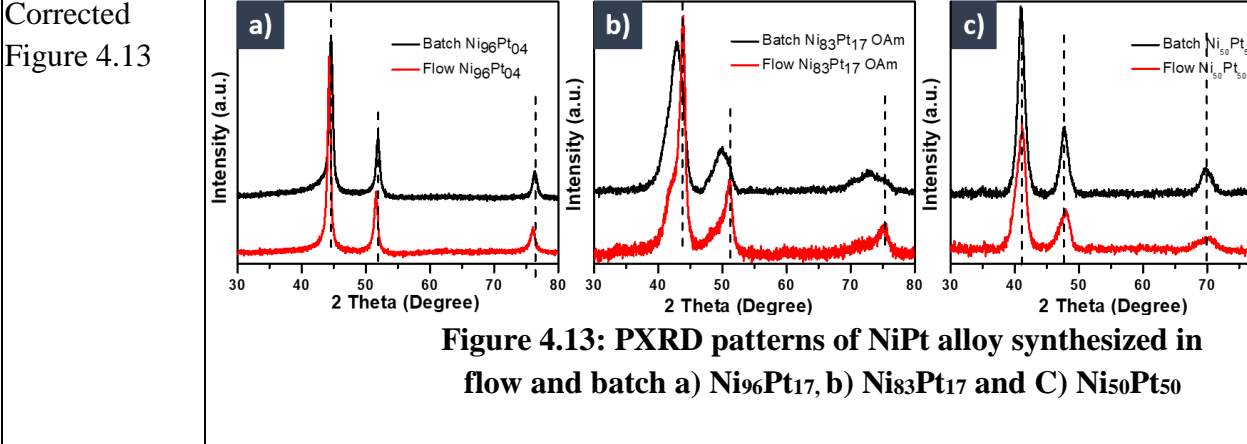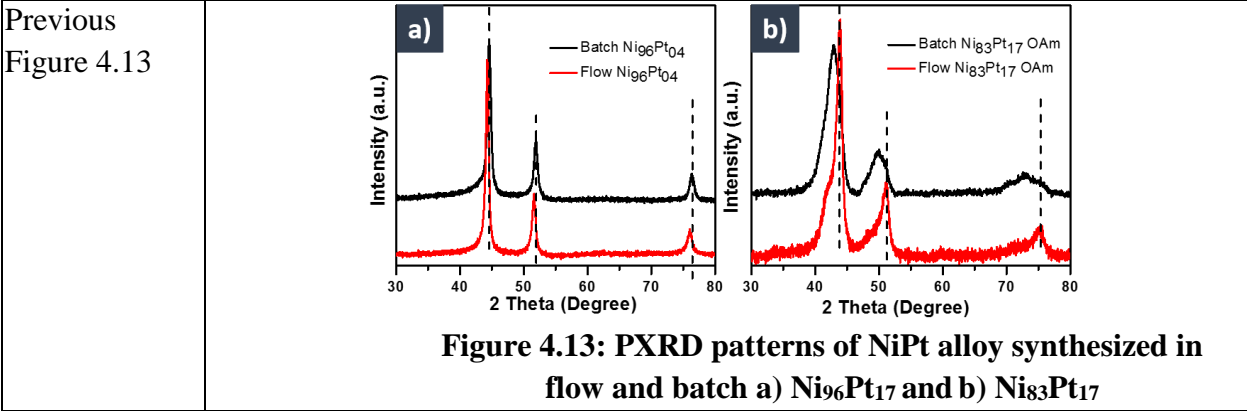| **Major Comments:**	
Comment 1.	Please include advanced characterization details like XRD for organic nanoparticles in Chapter 5.
Answer:	We have recorded the XRD patterns of the samples. **Figure A1: PXRD patterns of MHC particles produced using batch and (capillary reactor and IIJR) flow synthesis**. Although, particles prepared by changing experimental conditions shows different morphology but the PXRD patterns are exactly matching. MHC particles prepared using batch and (capillary reactor and IIJR) flow processes show simillar PXRD patterns and peaks from each patterns exactly match with each other. Hence, PXRD analysis clearly reveals that no other crystal structure or polymorphs are present in MHC particles sample prepared using different reactor or by changing precipitation condition.
Minor comments:	
Comment 1.	- Reference can be cited for classification of nanomaterials. Also, hybrid nanomaterials can be described in the text shortly

Page. Section	Page 4, Section 1.2
Answer:	Nanomaterials can be classified as inorganic nanomaterial or macromolecular nanomaterial or low molecular weight organic nano-material based on their chemical composition [a1] (see Figure 1.2). On the other hand, a material whose size is in nanometer scale and is made up of inorganic/organic or inorganic/polymeric combination regarded as a hybrid nanomaterial. For example: Pd–Polysiloxane Nanoconjugates 1. H Al-Kayiem, H.; Chun Lin, S.; Lukmon, A. *Nanoscience & Nanotechnology-Asia* **2013,** 3, (1), 60-71.
Comment 2.	Sentence is incomplete. 'As mentioned in an earlier section that 5 million tons nanomaterial required by 2025'. Or it can be merged with next line accordingly.
Page No., Section, Line	Page 6, Section 1.3, Line-1
Answer:	As mentioned in an earlier section that 5 million tons of nanomaterials required to satisfy growing demand in the industry by 2025.
Comment 3.	exposure time is mentioned 3 min in figure legends while in fig title, it is 4 min. Please correct.
Page No., Section, Figure,	Page 52, Section 2.4.1, Fig. 2.19
Answer:	The time in Figure 2.19 should be considered as 4 min.
Previous Figure	Corrected Figure

Comment 3.	Shows Ni^{2+} and Pt^{2+} precursor solution at start for Pd/Ni nanoparticle synthesis. It should be Ni^{2+} solution only.

Page No., Section, Figure,	Page 77, Section 3.3, Figure. 3.9	
Answer:	Suggested correction is incorporated in Figure 3.9.	
Previous Figure		Corrected Figure

Comment 3.	In Fig 3.8 and 3.10 titles (a-e) need to be corrected and should also include batch and flow process respectively.	
Page No., Section, Figure,	Page 76, Section 3.3, Figure. 3.8 Page 78, Section 3.3, Figure. 3.10	
Answer:	Previous Caption	Corrected Caption
	Figure 3.8: a) and b) TEM images of Pd/Ni NPs synthesized in batch under microwave irradiation for 4 min. EDX mapping of elemental distribution for c) Ni and d) Pd for Pd on Ni prepared in batch in the presence of OAm.	Figure 3.8: a) PXRD, b-c) TEM images, and d-e) EDX mapping of elemental distribution for (d) Ni and (e) Pd respectively for Pd/Ni NCs prepared using microwave assisted batch process in the presence of oleylamine.
	Figure 3.10: a) and b) TEM images of Pd/Ni NCs synthesized by microwave-assisted flow synthesis. And EDX mapping of elemental distribution for c) Ni and d) Pd for Pd on Ni prepared in flow in the presence of OAm.	Figure 3.10: a) PXRD, b-c) TEM images, and d-e) EDX mapping of elemental distribution for (d) Ni and (e) Pd respectively for Pd/Ni NCs prepared using microwave assisted flow process in the presence of oleylamine.
Comment 6.	Conclusion indicates better durability of $Ni_{50}Pt_{50}$, while the results of the same by continuous process have not been presented. Any specific reason or problem confronted during continuous process? That can be mentioned otherwise. These	

	results seem essential as it is claimed to be durable alloy composition in the results part of the section.
Page No., Section, Figure,	Page 109, Section 4.3.2, Figure 4.13 Page 109, Section 4.3.2, Figure 4.14
Answer:	We have synthesized $Ni_{50}Pt_{50}$ using flow methods and results are included in this addendum.
Previous Figure 4.13	 **Figure 4.13: PXRD patterns of NiPt alloy synthesized in flow and batch a) $Ni_{96}Pt_{17}$ and b) $Ni_{83}Pt_{17}$**
Corrected Figure 4.13	 **Figure 4.13: PXRD patterns of NiPt alloy synthesized in flow and batch a) $Ni_{96}Pt_{17}$, b) $Ni_{83}Pt_{17}$ and C) $Ni_{50}Pt_{50}$**
Previous Figure 4.14	Previous Figure 4.14

Figure 4.14: TEM images of NiPt alloy nanoparticles synthesized in flow a) and b) Ni$_{96}$Pt$_{04}$ (Average size, 16 nm) and c) and d)Ni$_{83}$Pt$_{17}$ (Average size, 17 nm).

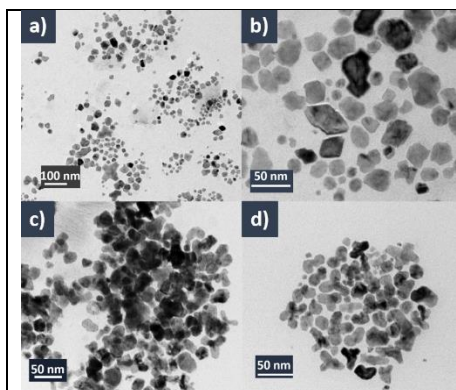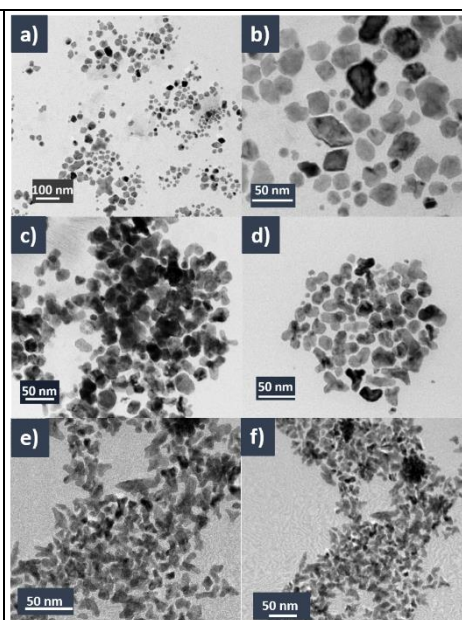**Figure 4.14: TEM images of NiPt alloy nanoparticles synthesized in flow a) and b) Ni$_{96}$Pt$_{04}$ (Average size, 16 nm) and c) and d)Ni$_{83}$Pt$_{17}$ (Average size, 17 nm), and e) and f) Ni$_{50}$Pt$_{50}$ (Average size 16 nm).**

Ni$_{50}$Pt$_{50}$ synthesized by flow technique shows almost similar PXRD features to these synthesized by batch process (Figure 4.13c). Based on PXRD, we can conclude that Ni$_{50}$Pt$_{50}$ alloy nanoparticles prepared in flow process have similar features as these synthesized by bath process and produced at 110 mg/h. TEM image shows that the nanoparticles synthesized by flow method are anisotropic in shape and average size of the nanoparticles was found to be 16 nm (Figure 4.14). Production rate of NiPt alloy nanoparticles using flow process was further enhanced up to 1 g/hr by optimizing the process parameters using 100 mL CSTR.

Comment 7.	Along with schematic representation of experimental setup Figure 5.3, the actual setup image can be provided for clear understanding of the intricacies of the setup.
Page No., Section, Figure,	Page No. 119, Section 5.2.3. B), Figure 5.4
Answer:	

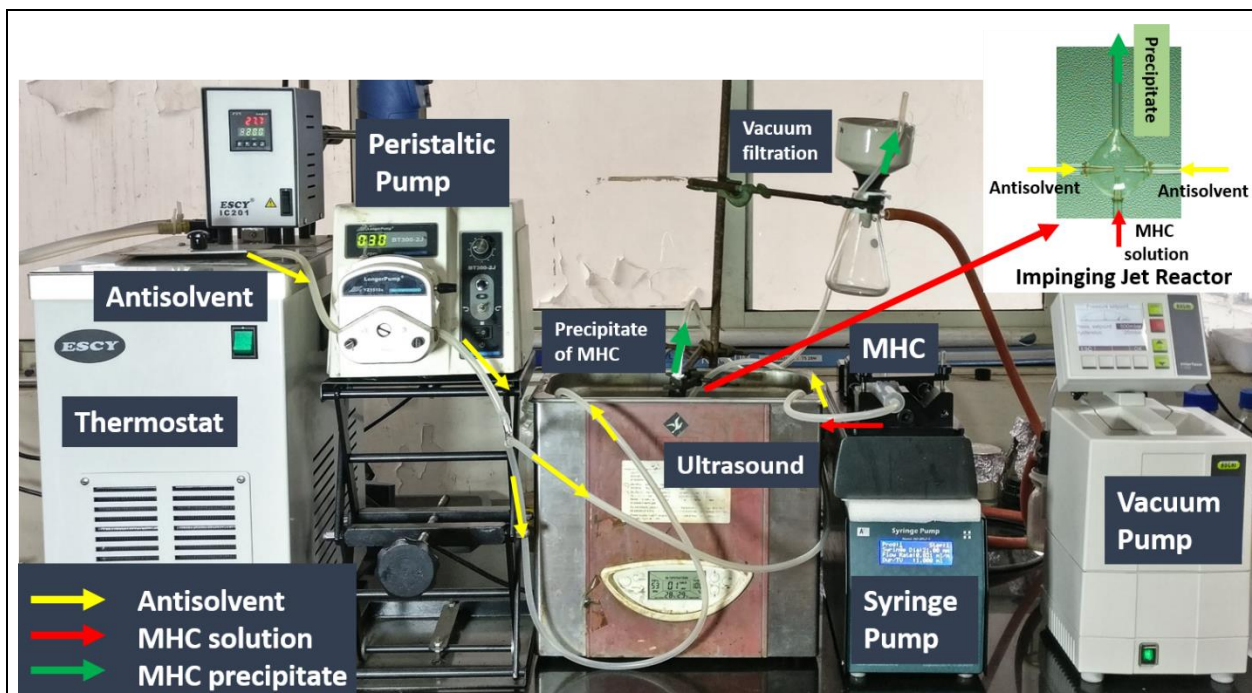**Figure A5.3):** **Photographic image of the experimental setup for continuous flow synthesis of MHC particles.**

Comment 7.	Overall conclusion mentions formation of metformin nanoparticles. However, the results and conclusion of chapter 5 mention formation of particles (small/micrometer), not the nanoparticles. Please confirm
Page No., Chapter	Page 134, Chapter 6
Answer:	

Previous Sentence	Corrected Sentence
In Chapter 5, we explore rapid reprecipitation reaction in continuous flow process to obtain small sized metformin nanoparticles. Fast mixing was realized using inverted impinging jet reactor and ultrasound. This fast mixing helped to attain a higher degree of supersaturation very rapidly which caused a reduction in the size of metformin nanoparticles.	In Chapter 5, we explore rapid reprecipitation reaction in continuous flow process to obtain small sized metformin particles. Fast mixing was realized using inverted impinging jet reactor and ultrasound. This fast mixing helped to attain a higher degree of supersaturation very rapidly which caused a reduction in the size of metformin particles.